A Viscosity-Dependent Affinity Sensor for Continous Monitoring of Glucose in Biological Fluids

THÈSE N^{O} 5324 (2012)

PRÉSENTÉE LE 5 AVRIL 2012

À LA FACULTÉ DES SCIENCES ET TECHNIQUES DE L'INGÉNIEUR
LABORATOIRE DE PRODUCTION MICROTECHNIQUE 2
PROGRAMME DOCTORAL EN SYSTÈMES DE PRODUCTION ET ROBOTIQUE

ÉCOLE POLYTECHNIQUE FÉDÉRALE DE LAUSANNE

POUR L'OBTENTION DU GRADE DE DOCTEUR ÈS SCIENCES

PAR

Christophe BOSS

acceptée sur proposition du jury:

Prof. H. Bleuler, président du jury
Prof. P. Ryser, directeur de thèse
Dr H. Knapp, rapporteur
Prof. S. Mougiakakou, rapporteur
Prof. Ph. Renaud, rapporteur

ÉCOLE POLYTECHNIQUE
FÉDÉRALE DE LAUSANNE

Suisse
2012

Abstract

For fifty years, tremendous efforts have been directed towards the development of glucose sensors for tight glycemic control of diabetic patients. Today, millions of diabetics test their blood glucose level daily, making glucose the most commonly tested analyte. Recently, subcutaneous implantable needle-type sensors became commercially available for continuous glucose monitoring. However, these devices require frequent calibrations and are lacking accuracy and reliability. They are based on electrochemical detection, which is strongly affected by the biological environment in which the sensor is placed. In addition, an accurate and reliable continuous glucose sensor would also be of great interest for tight glycemic control in intensive care units of hospitals. However, despite the many impressive breakthroughs, the development of clinically accurate continuous glucose sensors remains a challenge.

In this context, alternative approaches to overcome the limitation of electrochemical methods have been actively investigated. Among these, affinity sensing should offer several intrinsic advantages for *in vivo* monitoring. In this thesis, we investigate a novel viscosity-dependent affinity sensor for continuous monitoring of glucose in biological fluids such as blood and plasma. The sensing principle relies upon the viscosity variation of a sensitive fluid with glucose concentration. The sensitive fluid is based on the competitive binding of glucose and dextran with a glucose-specific binding protein, Concanavalin A. Basically, the sensor is filled with the sensitive fluid, and includes both an actuating and a sensing piezoelectric diaphragm as well as a flow-resistive microchannel. In addition, a nanoporous alumina membrane completely retains the sensitive fluid within the sensor whilst allowing glucose permeation through the membrane.

The sensor was extensively tested in isotonic saline solution for physiological blood glucose concentrations between 2 and 20 mM, demonstrating

an excellent accuracy, reversibility and stability for up to 3 days. In addition, the response time was close to the 10 minutes required for medical applications. However, despite the excellent short term stability, a progressive loss of sensitivity was observed for long term measurements. Concanavalin A retention by the alumina nanoporous membrane was assessed by ultraviolet absorbance spectrometry. Small leakage through the membrane was detected, which at least partly explains the sensitivity reduction over several days. Finally, the adequacy of the sensor for measurement in human blood serum and plasma was checked. Physiological glucose levels were successfully monitored, meaning that the chemical stability of the sensitive fluid and biofouling of the nanoporous alumina membrane were not an issue for short term applications. Moreover, interferences from biomolecules were limited and the sensitivity was still high enough for glucose monitoring. These results suggest that the combination of the ConA-based sensitive fluid and the microviscometer is a promising sensing principle for continuous glucose monitoring in blood.

Keywords: Diabetes, Glucose monitoring, Glucose sensor, Affinity sensor, Micromechanical sensor, Chemico-mechanical sensor, Viscosity, Concanavalin A, Dextran, Nanoporous membrane, Alumina membrane.

Résumé

Depuis cinquante ans, d'importants efforts ont été consentis pour développer des capteurs de glucose permettant un contrôle optimal de la glycémie des patients diabétiques. Actuellement, des millions de diabétiques mesurent quotidiennement leur glycémie, ce qui fait du glucose la substance la plus fréquemment testée. Récemment, des systèmes de mesure du glucose en continu utilisant l'insertion d'une aiguille sous-cutanée ont été commercialisés. Cependant, ces dispositifs nécessitent une calibration fréquente et manquent de précision et de fiabilité. Ils sont basés sur une détection électrochimique qui est fortement affectée par l'environnement biologique dans lequel le capteur est placé. En outre, un capteur de glucose permettant une mesure continue qui soit précise et fiable aurait aussi un grand intérêt pour le contrôle de la glycémie dans les unités de soins intensifs. Cependant, malgré les avances technologiques importantes, le développement d'un système permettant une mesure continue du glucose suffisamment précise reste un défi majeur.

Dans ce contexte, des approches alternatives qui permettraient de surmonter les limitations des méthodes électrochimiques ont été investiguées. Parmi ces dernières, les méthodes utilisant l'affinité spécifique de certains composés pour le glucose devraient offrir certains avantages pour les mesures *in vivo*. Dans cette thèse, nous investiguons un nouveau principe de détection pour la mesure continue du glucose dans les liquides biologiques tels que le sang et le plasma. Le principe de mesure repose sur la variation de la viscosité d'une solution sensible avec la concentration de glucose. La solution sensible est basée sur la compétition entre le glucose et le dextran pour lier la Concanavalin A, une protéine ayant une affinité spécifique pour le glucose. Plus précisément, le capteur est rempli avec la solution sensible, et comprend deux diaphragmes piézoélectriques ainsi qu'un micro-canal permettant de mesurer la viscosité. De plus, une membrane d'alumine nanoporeuse confine la solution sensible dans le capteur tout en permettant

la perméation du glucose à travers la membrane.

Le capteur a été testé dans une solution saline isotonique pour des concentrations physiologiques de glucose entre 2 et 20 mM, démontrant une excellente précision, réversibilité et stabilité jusqu'à 3 jours. De plus, le temps de réponse est proche des 10 minutes requises pour des applications médicales. Cependant, malgré l'excellente stabilité à court terme, une perte progressive de sensibilité a été observée pour des mesures à long terme. La rétention de la Concanavalin A par la membrane d'alumine nanoporeuse a été évaluée par spectrométrie d'absorption ultraviolette. De petites fuites ont été détectées, expliquant au moins partiellement la réduction de sensibilité observée sur plusieurs jours. Enfin, la capacité du capteur à fonctionner dans le sang et le plasma humain a été vérifiée. Différentes concentrations physiologiques de glucose ont été mesurées avec succès dans le plasma humain, ce qui signifie que la stabilité chimique de la solution sensible et l'encrassement biologique de la membrane d'alumine nanoporeuse n'est pas un problème pour les mesures à court terme. Par ailleurs, les interférences dues aux biomolécules du plasma étaient limitées et la sensibilité était encore suffisamment élevée pour permettre une mesure précise. Ces résultats suggèrent que la combinaison de la solution sensible basée sur la Concanavalin A et du micro-viscosimètre est un principe prometteur pour la mesure continue du glucose dans le sang.

Mots clé : Diabète, Mesure du glucose, Capteur de glucose, Capteur d'affinité, Capteur micromécanique, Capteur chimico-mécanique, Viscosité, Concanavalin A, Dextran, Membrane nanoporeuse, Membrane d'alumine.

Acknowledgments

This PhD thesis represents a significant work that would not have been possible without the constant support, encouragement, help and motivation from my colleagues, friends, and family.

Foremost, I express my gratitude to Professor Peter Ryser who offered me the opportunity to work at the Laboratory of Microengineering for Manufacturing.

I deeply thank Eric Meurville for the supervision of this research work. He continuously provided extremely valuable support, enthusiasm, ideas, and motivation to guide me throughout my thesis.

I owe special thanks to Dr Nao Takano, Dr Simon Kuenzi and Dr Antoine Barraud for their help in starting my thesis. Their expertise in glucose sensing, their laboratory experience, and their own research work were extremely valuable.

Many thanks to the team involved in the multi-analyte detection project funded by the Swiss Innovation Promotion Agency (CTI). I especially thank Dr Frédéric Schmitt for the fruitful collaboration.

I thank Dr Jean-Michel Sallèse for his valuable advices and his help for the publication of the two journal articles related to this thesis.

I also thank Dr Léandre Bolomey and Giancarlo Corradini for their help in electronics and precision assembly.

Finally, I wish to thank all my friends and family for their support and the good times during these years at EPFL. I especially thank my parents for their constant support and encouragement, and my siblings David, Aline et Antoine for the great moments together.

Contents

Chapter 1

Introduction

1.1 Glucose-sensing function of pancreas

Glucose concentration in blood is mainly regulated by insulin, which is a vital hormone secreted by the beta cells of the pancreas (Fig. 1.1). Insulin makes possible to assimilate nutrients, by triggering the glucose storage as glycogen in cells of the liver, muscles and fat tissues. The peak secretion of insulin coincides therefore with meals, when a high amount of glucose is absorbed by the body. By allowing the passage of glucose into the cells, insulin allows energy storage while preventing hyperglycemia after a meal. Insulin secretion in response to glucose is extremely rapid, occurring within one minute after the glucose concentration increase. When the glucose concentration is back to a normal level, the insulin secretion stops, thus avoiding a swing in the opposite direction that would lead to hypoglycemia. This mechanism, known as glucose-controlled insulin secretion, is normally regulating the glycemia. However, if the glucose concentration drops to dangerous levels, e.g. after an extended period without eating, the alpha cells of the pancreas release glucagon, an other hormone. Its effect is opposite that of insulin. This is a safety mechanism which acts to restore the glucose concentration in the physiological range. The glucagon triggers the conversion of the glycogen of the liver cells into glucose, which is subsequently released into the blood. The antagonist effects of insulin and glucagon keep the blood glucose concentration within very narrow limits (80–120 mg/dl or 4.4–6.6 mM)[1] in healthy persons in spite of the fact that

[1] Both units are commonly used for the glucose concentration (1 mM = 18 mg/dl).

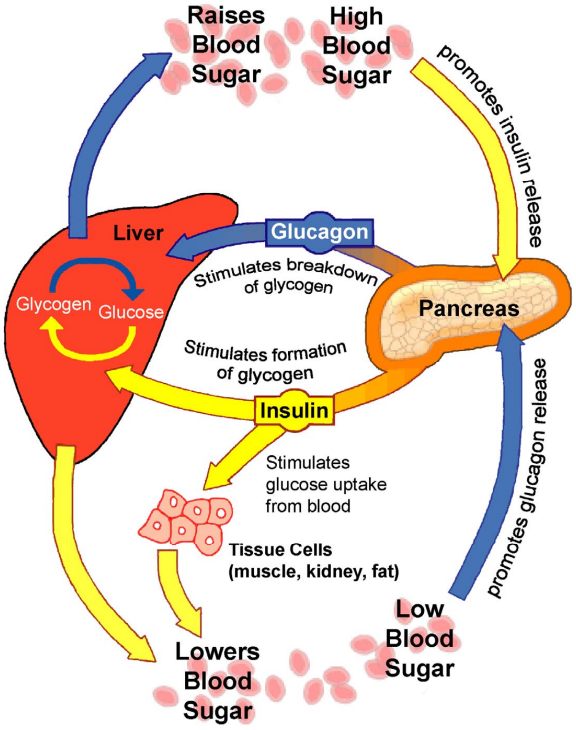

Figure 1.1: Regulation of the body glycemia: insulin and glucagon have opposite effects on liver and other tissues for controlling the blood glucose concentration. (Reprinted from http://health.howstuffworks.com.)

various amounts of carbohydrates are consumed both during and between meals.

1.2 Glucose monitoring for diabetes mellitus

In diabetes mellitus, this feedback homeostasis of blood glucose concentration is lost. This results in hyperglycemia and glucose intolerance due to insulin deficiency, impaired effectiveness of insulin action, or both. In type 1 diabetes, the autoimmune destruction of the pancreatic beta cells leads to severe insulin deficiency, which in the absence of insulin replacement, would lead to death because of the inability to assimilate nutrients. Fortunately, since the discovery of insulin in the early 1920s, patients were able to survive by injecting insulin themselves two to four times a day. In Type 2 diabetes, the glycemia regulation is impaired due to a combination of defective insulin secretion and a reduced insulin sensitivity. It is often

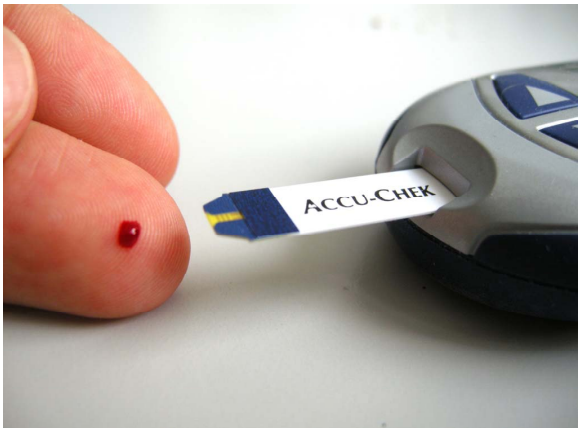

Figure 1.2: Procedure for self-monitoring of blood glucose: a drop of blood is applied on a test strip inserted on a handheld glucose meter.

associated with obesity, which itself can cause insulin resistance and lead to chronic high blood glucose levels. Type 2 diabetes is often managed by increasing exercise, dietary modification and routinely monitoring glucose levels. However, it may require insulin in case of persistent hyperglycemia.

Diabetes is one of the leading cause of death and disability in the world. Serious long term complications are related to chronic hyperglycemia, including higher risks of heart disease, kidney failure, or blindness [1]. Such complications were thought to be greatly reduced through stringent personal control of blood glucose, and since the early 1980s, blood glucose levels have been self-monitored. The test involves pricking a finger with a lancet device to obtain a small blood sample, and applying a drop of blood onto a dry chemical test strip inserted in a handheld meter for determining the glucose concentration (Fig. 1.2). Self-monitoring of blood glucose allows the improvement of glycemic control by collecting detailed information about blood glucose levels throughout the day. It helps diabetic patients to adjust their dietary intake, physical activity, and insulin doses in response to blood glucose values. The effectiveness of self-monitoring was confirmed by measuring the glycosylated hemoglobin, which is a marker of metabolic control over the previous 3–4 months. In general, studies support the evidence that self-monitoring of blood glucose is effective in improving glycemia [2]. The advent of self-monitoring is therefore considered as a major advance in diabetes management.

Today, millions of diabetics test their blood glucose levels daily, making

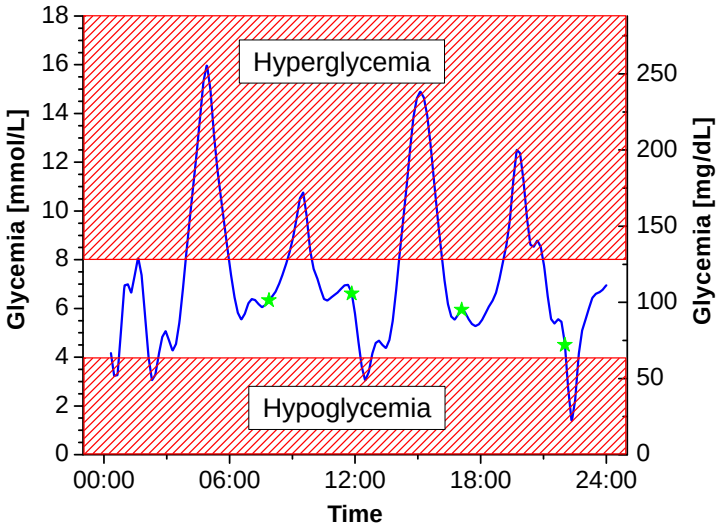

Figure 1.3: Glycemia evolution of a diabetic over one day. The green points represent the points-in-time monitoring obtained with finger-stick measurements, and the blue curve the real glycemia. (Reprinted from [3].)

glucose the most commonly tested analyte. However, conventional glucose monitoring is a discontinuous process that tells the patient about blood glucose concentration only at the moment it is performed. The fluctuations occurring between two measurements are not recorded. As the feedback homeostasis is lost, rapid fluctuations can occur, particularly after a meal or after insulin injection (Fig. 1.3). Hypo- and hyperglycemic episodes are therefore commonly happening in spite of frequent monitoring. Moreover, to avoid hypoglycemic episodes which could lead to unconsciousness, patients often regulate their blood glucose above the normal range. As a consequence, despite intensive insulin therapy, diabetic patients generally have their level of glycosylated hemoglobin over the normal range. This is a great concern regarding the long term complications associated with elevated blood glucose.

1.3 In vivo continuous glucose monitoring

1.3.1 Subcutaneous needle-type glucose sensor

The limitations of intermittent glucose monitoring were early recognized and a lot of effort was put towards the development of continuous glucose

Figure 1.4: Example of commercially available subcutaneous implantable needle-type glucose sensor (Guardian REAL-Time System from Medtronic).

meters [4]. In fact, continuous glucose monitoring (CGM) would provide maximal information about shifting blood glucose levels throughout the day and would therefore facilitate the making of optimal treatment decisions for the diabetic patient. Moreover, the sensor could be part of an alarm system to inform the patient about glucose concentrations outside the normal range, especially in the direction of hypoglycemia. The ultimate goal would of course be an artificial pancreas, consisting of a closed-loop insulin delivery system.

In the early 2000s, subcutaneous implantable needle-type glucose sensors became commercially available (Fig. 1.4). Such devices track glucose levels by measuring the glucose concentration in the interstitial fluid of the subcutaneous tissue. They are commonly inserted into the subcutaneous tissue in the abdomen or upper arm. Today, CGM devices are used to better understand the glycemia pattern of difficult-to-control diabetes and to facilitate adjustments in therapy. For instance, the impact of lifestyle modifications or mealtime insulin bolus changes can be assessed using a CGM device. This is therefore a very efficient tool for patient education. However, the limited accuracy is hindering a more routine use of these devices [5]. In fact, currently available CGM devices require up to four finger-stick blood glucose measurements per day for calibration. Moreover, they are

not sufficiently accurate to make therapeutic decisions and a finger-stick blood glucose measurement has always to confirm the CGM value. Finally, they do not measure the glucose concentration in the whole blood, but instead in the interstitial fluid, which introduces a lag time [5].

As methods for minimally invasive continuous monitoring advance, it appears likely that CGM devices will eventually become a routine part of diabetes management. However, in spite of the many impressive breakthroughs in the design and use of glucose biosensors, the promise of tight diabetes management has not been fulfilled. There are still major challenges in achieving clinically accurate continuous glycemic monitoring systems. Undesirable interactions between the surface of the implanted device and biological medium cause deterioration of the sensor performance upon implantation and proved to be the major barrier to the development of reliable *in vivo* glucose probes [6].

1.3.2 Limitations of electrochemical devices

The vast majority of glucose sensors used for *in vivo* applications are based on electrochemical detection. Basically, the measurement relies on a glucose oxidase (GOx) coated electrode. This enzyme catalyzes a chemical reaction between glucose and oxygen, which generates an electroactive product measured by common working electrodes. With such a detection method, other oxidizable constituents of biological fluids can compromise the selectivity and hence the overall accuracy of measurement [6, 7]. Considerable effort was devoted to minimizing the interference of coexisting electroactive compounds. Major improvements were realized by coating the electrode for minimizing the access of these constituents and decreasing the operating potential. Oxygen consumption by the oxidase-based reaction was an other major limitation for *in vivo* measurements. In fact, physiological oxygen concentrations are about one order of magnitude lower than the glucose level. This limitation, known as oxygen deficit, was addressed by using mass-transport-limiting films for increasing the oxygen/glucose permeability ratio. However, despite these technological improvements, challenges for achieving a reliable and accurate *in vivo* electrochemical sensor remain. In particular, these include long term stability of the enzyme and transducer, oxygen deficit and surface biofouling (the adhesion of biomolecules to surfaces) of the electrode.

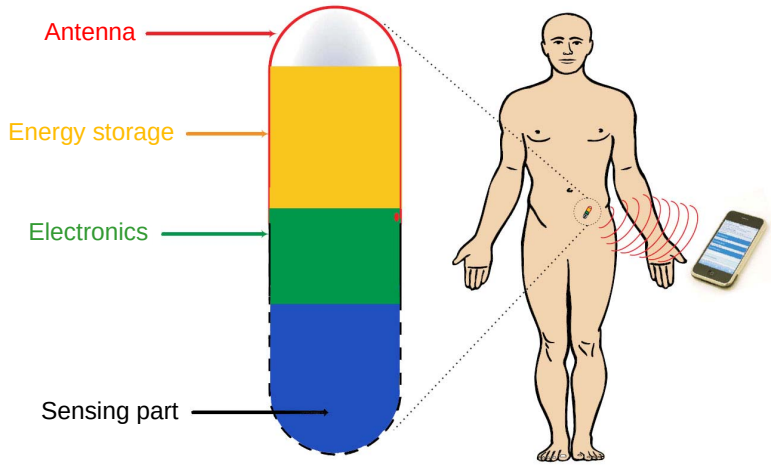

Figure 1.5: Concept of long term implantable autonomous glucose sensor.

1.3.3 Long term implantable glucose sensor

A minimally invasive, long term implantable glucose sensor would be an interesting alternative to achieve tight glucose control for diabetic patients. Such a sensor would be implanted in the subcutaneous tissue and would wirelessly transmit the glucose measurements to an external handheld device, like the patient's smartphone (Fig. 1.5). The signal from the sensor would be sent to the external device via radiofrequency and the power necessary for the sensor operation would be transmitted via inductive power telemetry. The wearable patient control unit would display real-time glucose levels updated every few minutes as well as the glucose level trends based on the past 20–30 minutes. The sensor would be implanted in the physician's office using a minimally invasive procedure (using a trocar for example) and would operate for up to 12 months.

Compared to existing transcutaneous needle-type sensors, a long term implantable sensor would eliminate the need to wear an external cumbersome device and to regularly change the needle. Moreover, a stable sensor-tissue interface would be established, whereas the recent implantation of a transcutaneous sensor generates a local inflammation. This is expected to decrease the frequent calibrations generated by a changing local environment.

However, the development of a long term implantable sensor is a challenge with many functional requirements. The implantable sensor should

have a very small size allowing minimally invasive implantation. The detection method and control electronics should therefore allow extreme miniaturization. In addition, the sensor should operate for up to 12 months after implantation with infrequent recalibration. This requires a glucose detection method which is stable and reliable for *in vivo* long term operation. Finally, the sensor-tissue interface is probably the most critical aspect for the long term sensor function. After typically 2–3 weeks, the sensor is encapsulated by a fibrotic capsule, which significantly hinders the glucose diffusion and leads to an increased response time. The sensor-tissue interface must therefore be coated with a biocompatible material promoting neovascularization within the matrix of the coating material.

Despite the considerable effort devoted to the development of an implantable glucose sensor, the technological challenges for long term *in vivo* monitoring have not been solved, and to date no product was brought to commercial realization.

1.4 Critically ill patients monitoring

In critical care, aberrant respiratory, cardiovascular, and other parameters are generally restored to physiologic levels in the belief that such maneuvers would confer a survival benefit. Glucose homeostasis is often dysregulated in critically ill patients, resulting in hyperglycemia, even those who have not previously had diabetes. Recently, clinical studies have demonstrated that maintenance of normoglycemia with intensive insulin therapy can reduce morbidity and mortality in critically ill patients [8, 9, 10, 11]. It is hypothesized that hyperglycemia or relative insulin deficiency may confer a predisposition to complications such as severe infections or multiple-organ failure.

Today, tight blood glucose control are performed in certain intensive care units (ICU), by taking and analyzing blood samples every 30–60 minutes. Several glucose monitoring handheld devices providing quantitative glucose measurement of capillary, venous and arterial blood are FDA[2] approved for the ICU. However, tight glycemic control increases the nursing

[2]The Food and Drug Administration (FDA) is an agency within the U.S. Department of Health and Human Services protecting the public health by assuring the safety, effectiveness and security of a wide variety of products. In particular, medical devices are regulated by FDA's center for Devices and Radiological Health.

workload and its implementation may prove to be a challenge as it requires a change in practice and an adequate education of the nursing staff. A continuous glucose sensor would likely facilitate the implementation of tight blood glucose control, and would also provide alarm signals for impending glycemic excursions.

Several pilot studies of continuous glucose monitoring and closed-loop control have been performed using subcutaneous needle-type glucose sensors [12, 13, 14, 15]. However, commercially available CGM devices are not accurate and reliable enough for implementing a truly closed-loop control, and blood glucose measurements are still required. Moreover, capillary blood values obtained by finger stick, or measurements in the interstitial fluid do not appear to be reliable in the ICU setting [16, 17].

There is therefore a strong need for a continuous glucose sensor monitoring accurately and reliably in arterial blood. In 2008, Edwards Lifescience, a leader in the monitoring of critically ill patients, and DexCom, a developer of continuous monitoring systems for diabetic patients, entered into a collaboration agreement to develop a continuous sensor for monitoring blood glucose levels for critically ill patients. This emphasizes the growing interest for tight glycemic monitoring in the ICU. However, there is currently no commercially available product, which indicates that electrochemical methods encounter difficulties in accurately and reliably monitoring glucose levels in blood.

1.5 Affinity sensing as an alternative method

1.5.1 Advantages of affinity sensing

The development of glucose sensor for *in vivo* applications that allows for long term reversibility and stability remains a challenge. In this context, alternative approaches to overcome the limitation of electrochemical methods have been investigated. Research groups focused on affinity sensing based on either glucose-specific protein concanavalin A (ConA) [18, 19, 20, 21, 22, 23] or acid boronic-based artificial glucose-specific receptors [24, 25, 26]. Independent of the type of receptor, affinity sensing offers several intrinsic advantages for *in vivo* monitoring. The absence of an electrode-based system eliminates its related issues, like potential interfer-

ences of electroactive components or the dependence upon oxygen tension. Furthermore, the binding reaction in affinity-based sensors is equilibrium driven, resulting in a signal sensitivity that is independent on the rate of glucose diffusion into the sensor. This is an advantage when compared to electroenzymatic sensors, which consume glucose and therefore depend on its diffusion rate. In particular, biofouling which degrades the sensitivity and stability of electrochemical measurements should only increase the response time of the affinity sensor. For these reasons, investigations on affinity binding sensors have been undertaken using various technologies, such as fluorescence [20, 21, 22, 25] or viscosity-based [19, 27, 28] principles. In particular, Roche (Disetronic) worked on the development of a subcutaneous implantable needle-type glucose sensor relying on monitoring glucose-induced changes in the viscosity associated with binding to ConA [29, 30].

1.5.2 A novel viscometric affinity biosensor

We propose a novel chemico-mechanical concept which aims at detecting viscosity changes of a solution featuring a selective affinity for glucose. The innovation relies in the viscosity detection method, which is based on the measurement of the flow resistance of a microchannel upon piezoelectric diaphragm actuation. This piezoelectric-based measurement should provide a very accurate and low-power viscosity detection controlled with basic electronics. In addition, the sensor topology would allow its realization using microfabrication technology, thus allowing the required miniaturization. These characteristics, combined with the intrinsic advantages of affinity sensing for *in vivo* monitoring, make this sensor particularly well suited for long term implantable applications. Beside that, microfabrication technology may allow batch manufacturing, and therefore disposable sensors for *in vivo* and *ex vivo* applications could also be envisioned.

In this thesis, after a brief state-of-the-art of glucose measuring technologies, the sensor principle and modeling are presented in detail, including the viscosity detection method, the glucose sensitive fluid and the sensor-body interface. The glucose sensor demonstrator and the experimental test setup are then presented, followed by the viscosity detection method and model validation using viscosity reference standards. Next, the glucose sensor demonstrator was extensively characterized in isotonic

saline solution of varying glucose concentrations, investigating the sensor reversibility, reproducibility and stability. The long term performance of the demonstrator was further evaluated regarding its potential application as a long term implantable sensor. Finally, the glucose sensor demonstrator was assessed in human blood serum and plasma for checking its adequacy to detect glucose in biological fluids. Special attention was paid to biofouling of the sensor-body interface and to potential interferences from other biomolecules present in blood.

Chapter 2

Glucose measuring technologies

2.1 First glucose sensors

The initial dominant detection technology for glucose sensors was based on a reflectometer invented by Anton Clemens in 1971, whose work led to the launch of the first blood glucose measurement system, the Ames Reflectance Meter. The intrument measured the reflected light from a strip covered with a chemical reagent whose color was changing with the addition of a drop of blood. Even if the original Ames Reflectance Meter was large and expensive, it was a success and led to a variety of products.

In 1975, Yellow Spring Company (YSI) launched the first commercial electrochemical glucose analyzer for direct measurement of glucose in 25 μL whole blood samples. The measurement relied on the enzyme glucose oxidase (GOx) which catalyzes a reaction between glucose and oxygen producing gluconic acid and hydrogen peroxide (H_2O_2):

$$\text{glucose} + O_2 \xrightarrow{\text{GOx}} \text{gluconic acid} + H_2O_2$$

In this original device, glucose oxidase was immobilized between two membrane layers. An outer polycarbonate membrane confined the enzyme whilst allowing glucose to diffuse. It also reduced the interferences by preventing large biomolecules present in the blood from entering into the device. In presence of the enzyme, glucose was oxidized, producing hydrogen peroxide. This latter diffused through a cellulose acetate membrane

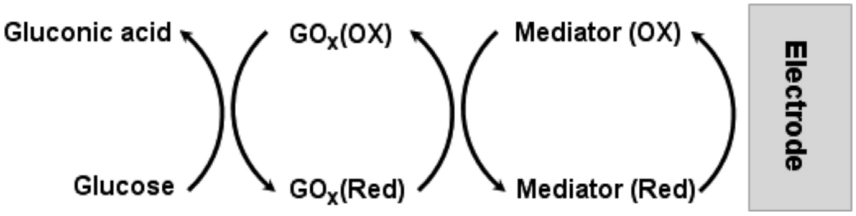

Figure 2.1: Sequence of events that occur in mediator-based electrochemical glucose sensors. (Reprinted from [6].)

and was amperometrically measured by a platinum electrode. The second membrane acted as a further size exclusion barrier preventing many other electroactive compounds from reaching the electrode surface. Since then, the YSI device and its successors have become a standard for clinical diagnostics used in many hospitals and laboratories.

2.2 Electrochemical test strips

During the 1980s, considerable efforts were devoted to the development of electrochemical glucose sensors for home testing. Oxygen was replaced with a nonphysiological (synthetic) electron acceptor for catalyzing the glucose oxidation (Fig. 2.1). This facilitated the electrons transfer to the electrode surface, which no longer depended on the local oxygen concentration. Moreover, this allowed to decrease the operating potential, thus reducing the interferences from other electroactive compounds and consequently enhancing the sensor performance. The electrochemical technology was further adapted to disposable test strips by using screen-printing technology which allowed inexpensive and reproducible test strips manufacturing. Screen-printing was widely used in the electronics industry, allowing the deposition of patterned thick-films in a simple and rapid way. The screen-printing technology involves printing patterns of conductors and insulators onto the surface of planar (plastic, ceramic, metal) substrates based on pressing the corresponding inks through a patterned mask. This process was one of the major reasons for the commercial success of electrochemical glucose sensors.

In 1987, Medisense launched the first glucose sensor for self-monitoring of blood glucose based on electrochemical test strips. Glucose was amper-

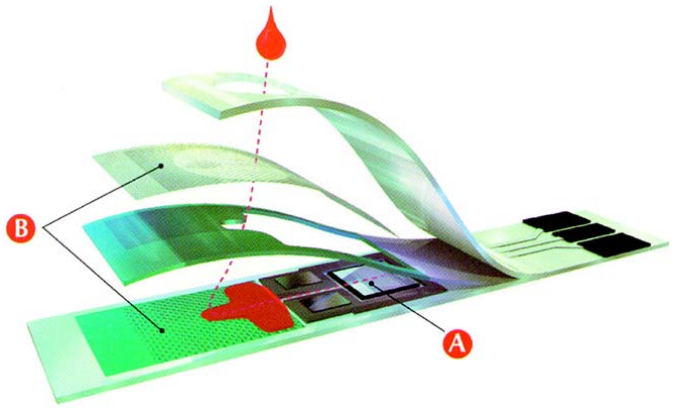

Figure 2.2: Cross section of a commercial strip for self-testing of blood glucose (based on the Precision biosensor manufactured by Abbott Inc.): (A) electrode system; (B) hydrophobic layer (drawing the blood). (Reprinted from [6].)

ometrically measured using a GOx electrode and a ferrocene mediator [31]. Ferrocene and its derivatives were in fact shown to rapidly shuttle electrons from GOx to electrodes [32]. Various improvements have been incorporated since the launch of the original device, but the concept has remained unaffected. Commercial blood glucose self-testing meters commonly rely on the use of ferricyanide or ferrocene mediators [6]. A strip is typically a plastic substrate containing the printed working and reference electrodes, with the working one coated with an enzyme, a redox mediator and other reagents (Fig. 2.2). A small volume capillary chamber ($\sim$1 μL) is formed over the electrodes by means of an adhesive spacer and a cover layer. In addition, various membranes are often incorporated in the test strips to separate the blood cells and minimize interferences for other biomolecules.

Today, over 40 different commercial strips and pocket-size monitors have been introduced for self-testing of blood glucose [33]. However, over 90% of the market is dominated by four major diagnostics compagnies, including Roche Diagnostics, Abott, Bayer and Lifescan (Table 2.1). The recent glucose meters utilize capillary fill which allow sampling small blood volumes (0.3–4 μl), thus allowing to decrease the needle size and to reduce the pain associated with finger pricking. In addition to fast response (5–30 s), good accuracy (5–10% rms error compared to laboratory standards) and automatic fill detection, modern glucose meters have extended memory capacity, automatically storing results along with times and dates. Some de-

Table 2.1: Characteristics of leading commercial blood glucose self-testing meters.

	Accu-Chek Performa	FreeStyle Lite	ContourTS
Company	Roche diagnostics	Abbott	Bayer
Sample size	0.6 μL	0.3 μL	0.6 μL
Test time	5 s	5 s	8 s
Memory	500 tests	450 tests	250 tests
Operating temp.	14–40˚C	10–50˚C	5–45˚C

vices have also features such as computer downloading capabilities which, combined with data management systems, allow to quickly review and analyze the results. Test strips are produced in high volume ($\sim$6 billion total electrochemical strips/years in 2007), at high manufacturing yield, low cost (<5 cents/test strip), with a defect rate of less than 0.1% [7]. Overall, the attractive performance of modern blood glucose monitors reflects significant technological advances along with major fundamental developments.

2.3 Continuous glucose monitoring

2.3.1 Major commercial developments

The development of continuous glucose sensors was initiated with the hope that this new glucose measurement tool would enable significant improvements in diabetes management. The early 1980s saw the appearance of an important symposium on potentially implantable glucose sensors, which included several important contributions from many of the leaders in the field [34]. However, developing reliable *in vivo* glucose sensors was an enormous technical challenge, and this is only in 1996 that the first continuous glucose sensor (MiniMed, Northridge, CA), based on a subcutaneous amperometric electrode, moved from the laboratory bench to clinical trials. The MiniMed CGMS was FDA approved in 1999 and became the first commercial CGM system [35, 36]. However, this system was not FDA approved to provide real-time glucose measurements, and thus the results had to be downloaded in a physician's office. It will be in 2005 that a continuous glucose sensor displaying real-time glucose values, the Medtronic Guardian RT system, was approved by the FDA [37]. Following a 2 hours warm-up period, this system displays updated glucose values every 5 minutes and

sounds an alarm when glucose levels become too high or too low. Since then, two other companies received FDA approval for their real-time CGM systems based on similar electrochemical technologies. The STS glucose monitor from DexCom, Inc. (San Diego, CA) and the FreeStyle Navigator glucose monitor from Abbott Diabetes Care (Alameda, CA) were respectively approved in 2006 and 2008.

An alternative to implanted electrodes is to use microdialysis as an interface between the body and the biosensor. In 2002, Menarini Diagnostics (Florence, Italy) received the CE[1] approval and since then, commercializes the GlucoDay, a glucose monitor based on a microdialysis technique. Clinical trials showed good correlation with blood glucose measurements [38, 39, 40]. However, it was not approved for real-time monitoring and is therefore used by professionals for the retrospective analysis of glucose trends. A hollow dialysis membrane (in regenerated cellulose) is subcutaneously inserted and perfused with an isotonic fluid, in which glucose from the interstitial fluid diffuses. The isotonic fluid is pumped (with a flow rate of 15–100 μL/min) outside the body, where the glucose is detected using an amperometric enzyme electrode [41, 42]. As the electrode is outside the body, this eliminates the issue of subcutaneous oxygen deficit. This is also advantageous regarding biofouling which cannot interfere with the measurements. However, as the isotonic fluid has to be pumped to the sensor, a lag time into the measurements is introduced, which could be of concern regarding real-time monitoring.

Beside the currently available needle-type CGM devices, alternative detection methods led to commercial developments. The GlucoWatch Biographer developed by Cygnus, Inc. (Redwood, CA), was approved by the FDA in 2001 for real-time display of glucose values. It employed reverse iontophoresis, in which a small current is applied and brings subcutaneous fluid through the skin by attraction of ions [43, 44]. The extracted fluid, which is characterized by a glucose concentration proportional to the subcutaneous fluid, is collected in a hydrogel pad and the glucose is detected electrochemically. The device is worn like a wristwatch and provides glucose measurements every 10 minutes. Despite the FDA approval and clinial trials [45, 46], it was never widely accepted in the market-place. Sweating,

[1] "Conformité Européenne", certification required for medical devices in the European Union.

rapid temperature changes, cold skin or excess movement precluded glucose measurements and led to frequent skipped readings. In 2007, Animas Corp. which purchased Cygnus one year earlier, decided therefore to stop selling the GlucoWatch Biographer system.

Unlike all the other continuous glucose monitoring devices, the Pendra developed by Pendragon Medical Ltd. (Zurich, Switzerland), was truly noninvasive. It operates by impedance spectroscopy, generating a small electromagnetic field across the skin in the frequency range of 1–200 MHz. Sodium and potassium transport over the erythrocyte membrane, which is related to changes in glucose levels, results in a change of impedance detected with the Pendra device. Initial evaluations of the device were promising [47, 48], and the Pendra was CE approved for the European market in 2004. However, post-market evaluations indicated poor accuracy and the device also suffered from unsuitability for large number of patients due to strong varying skin and subcutaneous properties [49]. Like most non-invasive methods, the changes in impedance measured by the device was likely suffering from interferences due to the complexity of biological tissues. As a consequence, the device was withdrawn from commercial distribution and Pendragon Medical filed for bankruptcy in 2005.

2.3.2 Subcutaneous amperometric technology

All commercially available real-time continuous glucose sensors rely on a subcutaneous glucose oxidase (GOx) electrode, a technology which benefited from the previous developments of home blood glucose monitors. In electrochemical test strips, the enzyme and mediator are typically applied to the working electrode as a solution and deposited by solvent evaporation. However, such a straightforward technique was not compatible with continuous *in vivo* monitoring, as the enzyme and mediator would dissolve in the subcutaneous fluid and diffuse away form the electrode. For a sensor to successfully operates *in vivo*, the enzyme and mediator have therefore to be immobilized onto the electrode surface. A variety of techniques for immobilizing enzymes exists, like adsorption onto insoluble particles, covalent linking to an insoluble polymer matrix, or enzyme entrapment with a porous polymer membrane. However, the enzyme immobilization remains a key factor for *in vivo* continuous monitoring and the methods used in commercial sensors are often proprietary and protected as trade secrets.

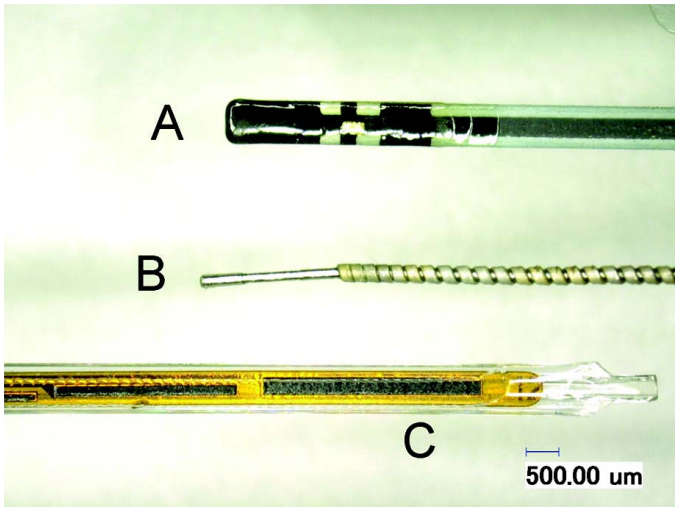

Figure 2.3: Commercially available transcutaneous sensors. (A) FreeStyle Navigator; (B) Dexcom STS; (C) Guardian RT. (Reprinted from [7].)

Transcutaneous amperometric sensors consist of a thin, sub-1 mm diameter, flexible sensor having a working electrode with an immobilized enzyme (GOx) and an Ag/AgCl reference electrode (Fig. 2.3) [7]. The electrooxidation of glucose is mediated by either oxygen, or by an immobilized redox mediator. Due to potential leaching and toxicity of the mediator, most *in vivo* devices (Guardian RT, Dexcom STS) are mediatorless [50]. However, when using oxygen as electron acceptor, the low physiological oxygen concentration is an issue regarding to the electrochemical reaction. Both sensors addressed the oxygen deficit limitation using a block copolymer membrane, which consists of a hydrophobic polymer highly permeable to oxygen and impermeable to water and thus glucose, and of a hydrophilic polymer enabling glucose flux. By varying the ratio of the two polymers, the oxygen and glucose flux are adjusted to an optimal value for the redox reaction.

The last approved device (FreeStyle Navigator) is based on an alternative mediator substituting for oxygen, using the enzyme wiring technology. The enzyme is wired to the electrode surface with a long hydrophilic polymer backbone having a dense array of covalently linked redox polymers. An advantage of the wired enzyme is a lower operating potential, thus reducing the electroactive interferences. However, although the wired enzyme is not subject to the subcutaneous oxygen deficit, the enzyme con-

Table 2.2: Characteristics of the three FDA approved real-time continuous monitoring devices [51].

	Guardian RT	DexCom STS-7	FreeStyle Navigator
Company	Medtronic	DexCom	Abbott
FDA Approval	2005	2006	2008
Enzyme	GOx	GOx	GOx
Mediator	Oxygen	Oxygen	Redox mediator
Life time	3 days	7 days	5 days
Calibration	Every 12h	Every 12h	At 10, 12, 24 and 72h
Test freq.	5 min	5 min	1 min

centration that can be immobilized on the surface of an electrode is low and saturated at very low glucose levels. A glucose limiting membrane is therefore still required.

2.3.3 Performance of commercial devices

The three commercial real-time devices have similar characteristics (Table 2.2) [51]. Initially, a suitable break-in period of 1–10 hours has to be observed, both to equilibrate the sensor with its tissue-environment and to normalize the insertion-wound perturbed site. After the initial stabilization period, the sensor has to be calibrated because of the variability of the subcutaneous environment. The calibration procedure is performed by testing the capillary blood glucose concentration using a glucose test strip. The *in vivo* calibration process has to be repeated during the implantation to correct the sensor output drift, due to the ever-changing wound healing environment and biofouling of the system. The glucose concentration is measured and displayed in real-time every 1–5 minutes, and depending on the model, the subcutaneous sensor has to be replaced every 3–7 days. Finally, the precision of CGM devices is very much dependent on the calibration. In fact, as there is a lag time between the blood and interstitial fluid glucose concentration, a calibration performed while the glycemia is fluctuating results in poor precision.

The frequent calibrations and the lack of accuracy and reliability are the major drawbacks of all approved continuous sensors [52]. At low glucose (below 80 mg/dL), all of the sensors have lower accuracy than they do at higher levels [53], which is critical because the low regions are by far the

most important. However, these sensors are accurately and reproducibly measuring glucose on the bench with no need for calibration, which indicates that the main source of sensor inaccuracy comes from the biological environment in which the sensor is placed. In particular, the high variability of glucose and oxygen in the wound healing site is thought to be responsible for calibration changes [7]. Biofouling of the device is also likely changing the rate-dependent signal of the enzyme electrode. Now that the fundamental measurement principle has been demonstrated, improvements in accuracy and reliability will likely be achieved by ingenious technological and manufacturing improvements. A better understanding of the factors causing sensitivity-variation would also help in improving *in vivo* sensor performance.

2.4 Affinity sensing technology

2.4.1 Fluorescence affinity sensors

Due to the problems encountered by the amperometric enzyme electrode for *in vivo* sensing, new approaches to glucose sensing have been actively explored. Amongst these, affinity sensing received particular attention as it is thought to offer several intrinsic advantages for *in vivo* monitoring. The affinity detection principle was inspired by immunoassays developed in the 1950s, which consist in measuring the concentration of an antigen in blood using its affinity for a specific antibody. In 1982, early developments on affinity sensing were reported by Schultz et al., based on the competitive binding of glucose and dextran with a glucose-specific binding protein, Concanavalin A (ConA) [18]. The specific affinity of ConA with polysaccharides was previously investigated by Goldstein et al., which reported that ConA was interacting with the nonreducing chain ends of the dextran molecule [54]. In the sensor described by Schultz et al., ConA was immobilized on the inside surface of a hollow dialysis fiber containing a high-molecular-weight dextran labeled with fluorescein isothiocyanate (FITC) (Fig. 2.4). The molecular weight cutoff of the dialysis fiber was low enough to completely retain dextran within the fiber lumen while glucose was freely permeating through the membrane. Glucose entering from the external medium displaced dextran from ConA and increased the fluores-

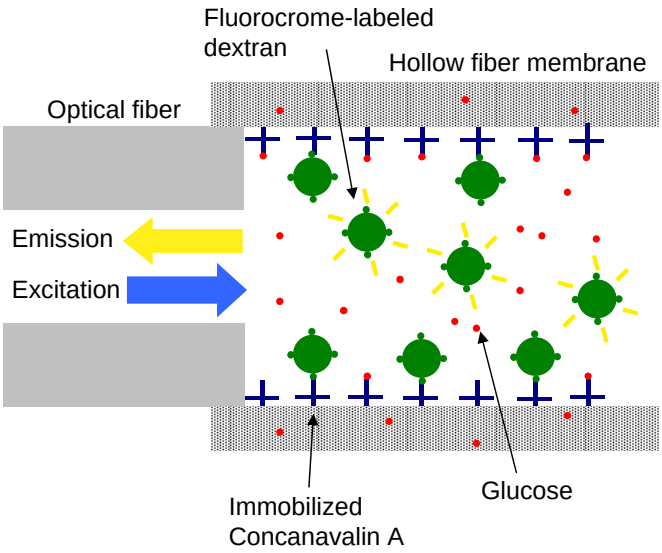

Figure 2.4: Schematic view of the original fluorescence affinity sensor based on a hollow dialysis fiber proposed by Schultz et al. in 1982 [18].

cence intensity in the lumen, which was recorded using an optical fiber. Preliminary tests of the sensor indicated the feasibility of the approach.

This concept was later adapted by the same laboratory so that measurements were based on Fluorescence Resonance Energy Transfer (FRET) [55]. FRET relies on the distance-dependent transfer of energy from a fluorescent molecule which absorbs the incident radiation (donor molecule) to an other fluorescent molecule to which the energy is subsequently transferred (acceptor molecule). The transfer of energy leads to a reduction in the donor's fluorescence intensity and an increase in the acceptor's emission intensity. In this new fiber-optic sensor, FITC-dextran and rhodamine-ConA were respectively the donor and acceptor molecules. When glucose is added to the solution, FITC-dextran and rhodamine-ConA move further apart, which lead to a decrease in energy transfert and consequently an increase in the donor fluorescence. The glucose concentration is therefore directly related to the FITC fluorescence. The working range of the solution was adjuted to physiological glucose concentration with a good sensitivity up to 200 mg/dL. However, the stability of the solution was quite poor, ConA precipitating and forming aggregates over periods of hours. Chemical procedures were subsequently developed to prevent the ConA aggregation and the solution was shown to be stable over several days

[56]. Moreover, the ratio ConA-dextran was optimized to achieve glucose detection up to 1600 mg/dL. The sensor was further improved by using FITC-dextran, rhodamine-dextran and unmodified ConA in an attempt to avoid chemical modifications of the protein which are time-consuming and can affect its binding activity [57]. The sensor stability was also enhanced, showing a good measurable fluorescence signal over 11 days.

Ballerstadt and co-workers have further investigated various concept of fluorescence affinity sensors. In 2000, to avoid the risk of bacterial infection related to needle-type sensors, they proposed a concept of subcutaneous implantation relying on the illumination and fluorescence measurement through the skin [21]. To ensure that the fluorescence emission was sufficiently high to be measurable through skin tissue, they increased the fluorescence response intensity by a factor 50, by using immobilized pendant glucose moities inside Sephadex beads. The long term stability of this sensor was investigated by continuously cycling glucose test solutions during 4 months, showing a decrease in fluorescence of 25% per month [20]. Aqueous ConA was considered the weakest link due to its involvement in precipitation reactions in response to protein-to-protein aggregation and protein/dextran-induced precipitation reactions [58, 57]. In an attempt to prevent these adverse precipitation reactions, and therefore increase the stability and lifetime of the sensor, ConA was immobilized within a macroporous bead matrix, which led to a remarkable long term stability of the sensor (6 months) [59]. They further successfully demonstrated *in vivo* performance of an implanted fluorescence affinity sensor over more than 16 days in a rodent model [60].

In conclusion, the technical feasibility of fluorescence affinity sensors has been clearly demonstrated. Significant improvements to the overall performance of the sensor have been made since the concept introduction in 1982. However, long term stability remains a challenge, due to inferior ConA stability and inadequate photostability of fluorescent dyes. Therefore, the search for an optimal sensor configuration that fulfills practical requirements such as a chemically and optically stable signal continues.

2.4.2 Viscosity-dependent affinity sensors

The change in viscosity of a glucose sensitive fluid was also extensively investigated as an alternative method to fluorescence for the signal trans-

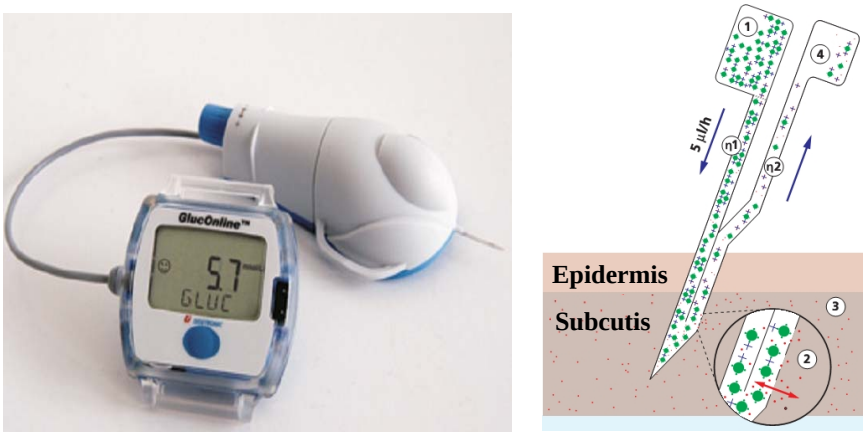

Figure 2.5: GlucOnline device prototype from Disetronic (left) and schematic view of the measuring principle (right): (1) reservoir and pump; (2) microdialysis through the semi-permeable membrane; (3) subcutaneous tissue; (4) collecting vessel. The viscosity is measured using the two pressure sensors η_1 and η_2.

duction of affinity sensors. In 1994, Ballerstadt and Ehwald demonstrated this variant by filling a hollow fibre of regenerated cellulose with a solution of dextran and ConA [19]. Air pressure pulses were used for generating oscillations of the fluid, the amplitude of which was measured with an ocular micrometer. They further investigated the viscosity response of different formulations of sensitive fluid based on dextran and ConA [61]. They suggested that high-molecular-weight dextran combined with a low value of basic viscosity were suitable regarding both the absolute and relative sensitivity. Next, the effect of frequency and shear stress on the rheological properties of the sensitive fluid was also assessed with a view to the sensor design [62].

The same laboratory, in collaboration with Disetronic Medical Systems (Burgdorf, Switzerland), developed a transcutaneous needle-type glucose sensor based on this viscometric principle [29]. The needle encloses a dialysis hollow fiber through which the sensitive fluid is continuously pumped with low rate ($\sim$5 μL/h). The viscosity is determined by measuring the pressure difference created by the flow at both ends of the fiber using two pressure sensors. The viscometric sensor showed a linear and stable dependence on the glucose concentration, with a response time of 5–10 min. This device was further developed by Disetronic under the trade name Gluc-

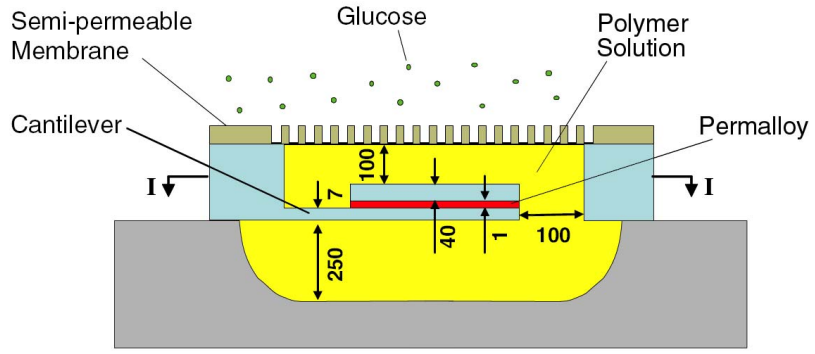

Figure 2.6: Schematic cross view of the MEMS viscometric glucose sensor proposed by Zhao et al. Dimensions indicated in micrometer. (Reprinted from [28].)

Online (Fig. 2.5). In 2004, the performance of the sensor was evaluated in a clinical pilot study on twelve type 1 diabetic patients [30]. An error grid analysis of the results showed that 98.9% of the values were within the clinically acceptable zone, but the residual values were clinically unacceptable. Disetronic was acquired by Roche in 2003, which further sold the GlucOnline project to Sensile Medical. This company was not able to enter the market with the GlucOnline concept.

The recent advance of microfabrication technolgies, allowing batch fabrication of miniaturized devices, led to the development of new sensors based on a viscometric sensitive fluid. In 2007, Zhao et al. reported a MEMS viscometric sensor based on a magnetically-driven vibrating microcantilever located in a microfluidic chamber filled with a dextran-ConA sensitive fluid [28]. The cantilever was realized by patterning a layer of SU-8, a commonly used epoxy-based photoresist, and the subsequent deposition of permalloy thin film strips at its free end (Fig. 2.6). The cantilever was actuated by applying a magnetic field to the permalloy strips, which induced a flow of the solution. The damping effect of the flow on the cantilever vibration, which was directly dependent on the solution viscosity, was recorded using an optical system. The glucose dependence of the cantilever vibration was demonstrated, although they did not show continuous and reversible measurement. They further developed a biocompatible boronic acid based polymeric sensitive fluid in order to address stability issues related to the dextran-ConA solution [26]. The device was also improved by fabricating the microcantilever from Parylene, a biocompatible

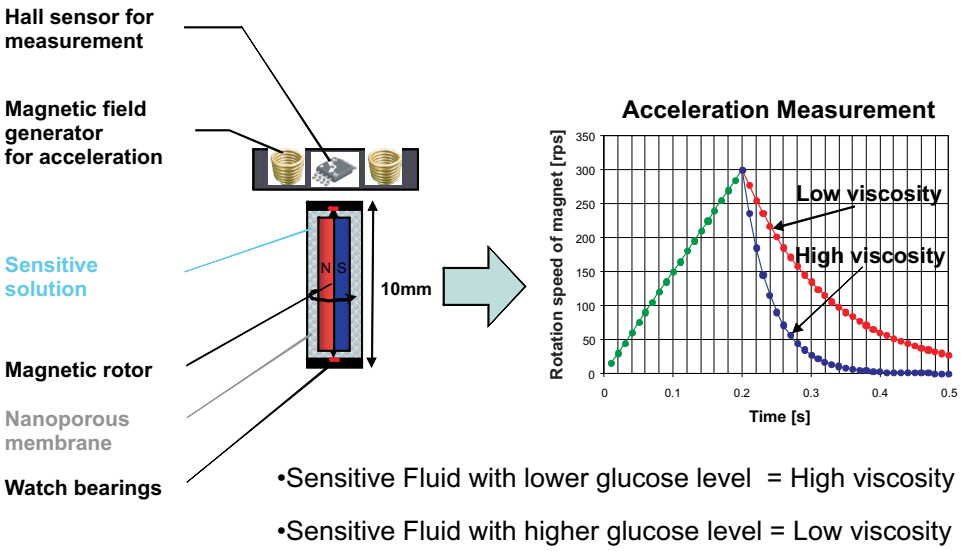

Figure 2.7: Measurement principle of the glucose sensor based on a concentric rotational microviscometer developed by Kuenzi et al. (Reprinted from [3].)

soft polymer, which decreased the resonance frequency of the cantilever to ∼30 Hz [27]. Short term (20 hours) continuous reversible measurements were reported. The last variant of the sensor consisted of a Parylene diaphragm, whose vibration was measured capacitively [63].

Since 2003, our laboratory has been investigating viscometric affinity sensors for continuous glucose monitoring. A concentric rotational microviscometer was developed and extensively characterized using viscosity reference standards [64]. A magnetic cylinder was actuated by a rotational magnetic field, and its angular position was recorded with Hall effect sensors (Fig. 2.7). The viscosity was measured by the viscous friction produced by the fluid on the rotating magnet. Although this measurement principle had a high accuracy, only few successful reversible glucose measurements were obtained [65]. Various low viscosity ConA-dextran solutions were also investigated using a glass Ubbelohde viscometer combined to a camera read-out [66]. The results showed that low-viscous mixtures, down to 5 mPas, are well suited for glycemic sensing applications. Further work studied the selective interface between the sensitive fluid and the analyzed solution, which has to retain dextran and ConA whilst being permeable to glucose [3]. Glucose diffusion and ConA retention properties of

nanoporous alumina membranes and nanoporous polyethylene films were characterized. A good ConA retention was achieved by coating 20 nm pores alumina membranes with poly(poly(ethylene glycol) methacrylate) (PPEGMA) brushes.

This work is a continuation of the efforts devoted to the development of a viscometric affinity sensor for continuous glucose monitoring. In an attempt to overcome the limitations encountered with the previous device, possibly due to the high shear stress generated by the high rotational speed of the rotor, a novel viscosity detection principle was investigated. This detection principle should provide a simple, accurate and low-power viscosity measurement.

Chapter 3

Sensor principle and modeling

3.1 Introduction

Presently, continuous glucose monitoring devices require frequent calibration and are lacking accuracy and reliability. They are based on electrochemical detection, which is strongly affected by the biological environment in which the sensor is placed. The development of clinically accurate continuous glucose sensors remains therefore a challenge. In this context, we propose an alternative method, based on affinity sensing, which aims at detecting viscosity changes of a solution with a selective affinity for glucose. The innovation relies in the viscosity detection method, based on an induced liquid flow in a microchannel upon piezoelectric diaphragm actuation. The sensitive fluid is based on the competitive binding of glucose and dextran with a glucose-specific binding protein, Concanavalin A (ConA). The sensitive fluid is very selective to glucose due to the properties of ConA, and particularly sensitive at low glucose concentration, which is crucial to prevent hypoglycemia.

Basically, the sensor is filled with the sensitive fluid, which is confined by a semi-permeable membrane completely retaining dextran and ConA within the sensor whilst allowing glucose permeation through the membrane (Fig. 3.1). The sensor includes both an actuating and a sensing piezoelectric diaphragm as well as a flow-resistive microchannel. In operation, the actuating diaphragm generates a flow through the microchannel which

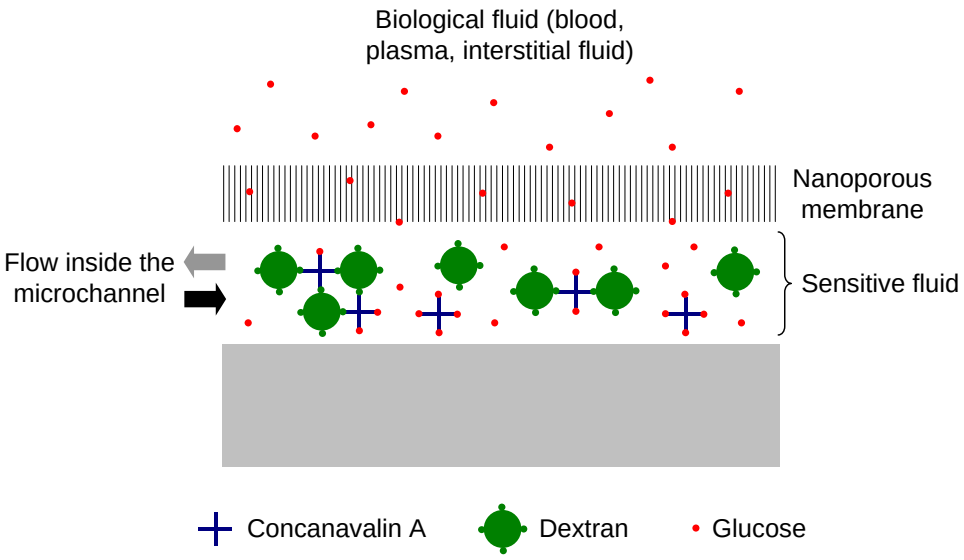

Figure 3.1: Sensor measurement principle: glucose diffuses through a nanoporous membrane in the sensitive fluid, the viscosity of which is measured by inducing a flow into a microchannel.

is recorded by the sensing diaphragm, while the microchannel exhibits a resistance to the flow which depends upon the viscosity.

This chapter presents in detail the three core technologies of the sensor: the sensitive fluid, the viscosity sensing principle and the semi-permeable membrane. The sensor modeling is also exposed to provide a better understanding of the principles involved in this glucose detection.

3.2 Sensitive fluid

3.2.1 Sensing principle

The sensitive fluid used within the sensor is the key element for glucose detection. This is based on the competitive affinity of two saccharides, namely glucose and dextran, to a specific saccharide-binding protein, Concanavalin A. The sensing principle was first demonstrated by optical measurement of glucose concentration using fluorescence-labelled dextran [18], and then from the change in the viscosity of an aqueous blend of dextran and ConA [19]. This competitive affinity process was shown to be reversible and highly sensitive.

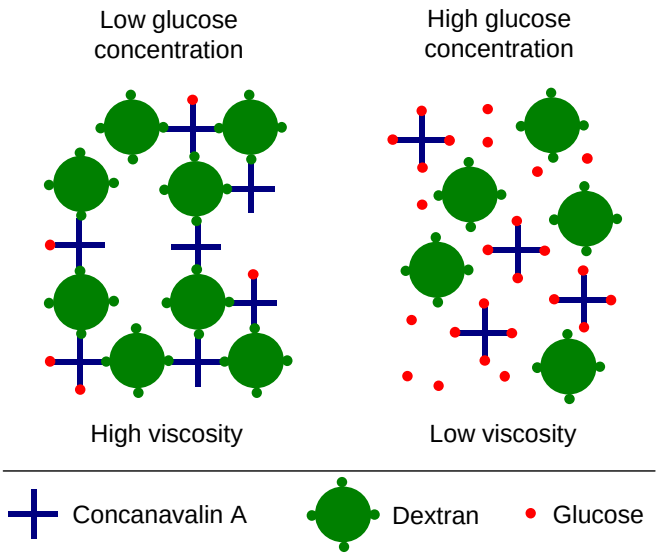

Figure 3.2: Principle of the glucose sensitive fluid: competitive binding of glucose and dextran on ConA in the case of low and high glucose concentrations.

This viscosity variation of a sensitive fluid using a high-molecular-weight dextran is actually the core of our sensor. At low glucose concentration, dextran molecules are cross-linked by binding to ConA, forming a viscous solution (Fig. 3.2). Next, when the glucose concentration increases, dextran molecules are partially replaced by glucose ones at the binding sites of ConA. As a result, the network ConA-dextran is weakened and the viscosity of the sensing solution decreases.

3.2.2 Rheological properties

The viscosity variations are especially strong in the human glycemic range (2–30 mM glucose). Indeed, changes in viscosity as high as one order of magnitude in the physiological relevant range were reported [66]. The sensitive fluid viscosity can also be tailored for the sensor of interest by modulating the proportions of dextran and ConA. We chose a low viscosity sensitive fluid which was characterized using a standard capillary viscometer (Fig. 3.3). It is worth noticing that the sensitivity of the fluid is particularly high in the hypoglycaemic range (2–4 mM), whereas it decreases in the hyperglycaemic range (7–30 mM). High accuracy in hypoglycaemic re-

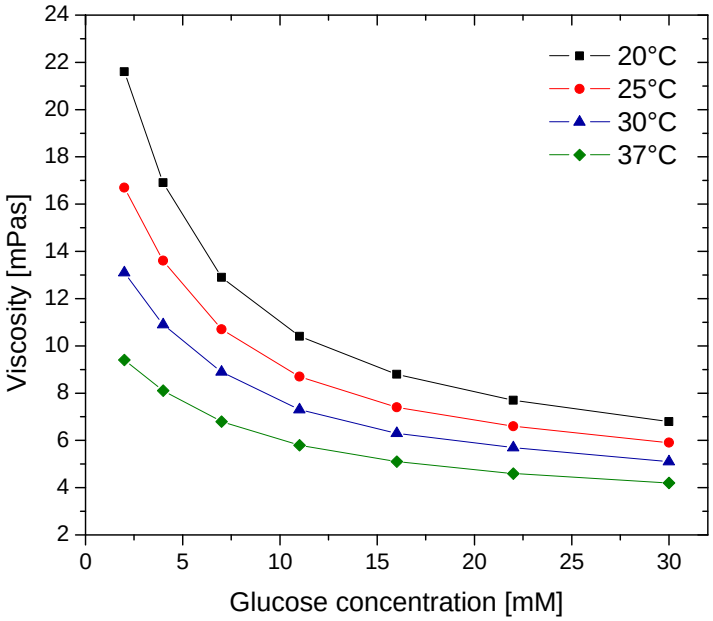

Figure 3.3: Characteristics of the low viscosity sensitive fluid used within the sensor. (Data from [3].)

gion is mandatory to make this sensitive fluid particularly well suited for patient monitoring. Beside that, the sensitive fluid viscosity is highly temperature dependent. When raising the temperature from 25 to 37°C, the sensitive fluid viscosity decreases on average by 38%. This dependance should therefore be taken into account through calibration when working in physiological conditions.

3.2.3 Concanavalin A properties

The affinity of ConA for glucose, mannose and their polysaccharides was firstly described by Goldstein et al. [54], and since then, has been extensively studied. The ConA monomer was reported to be a globular protein of overall dimensions $42 \times 40 \times 39$ Å [67]. In solution, ConA appears as dimer and tetramer configurations (two or four identical subunits) depending on pH. Below a pH of 5.5, ConA exists as a dimer, and for a pH ranging from 5.5–7.0, ConA is at an equilibrium state of dimer-tetramer [68]. At pH values higher than 7.0 the tetramer configuration is highly prevailing although some dimers seem to remain [69]. Each subunit of ConA has one specific carbohydrate-binding site [70], which implies that four bind-

ing sites are present in tetramer configuration. ConA dimer and tetramer have respectively a molecular weight of 52 and 104 kDa, and their hydrodynamic radiuses are respectively 3.3 and 4.4 nm [71].

The glucose binding site of ConA needs to be activated with two metal ions per monomer. When two ions are trapped, the protein undergoes a conformational change, forming a so-called locked form, which increases its affinity for glucose by a factor 1000 [72]. Several transition metals can bind the two binding sites of ConA, the most stable choice being Mn^{2+} and Ca^{2+}. The average concentration of Ca^{2+} in blood is 1.18 mM whereas Mn^{2+} only appears as a trace element. Calcium can also be used to activate the two binding sites, which has the advantage to be closer to *in vivo* conditions. However, the occurrence of precipitation after a substantial time was reported when using only Ca^{2+} [73]. Moreover, a high energy barrier separates the two conformations of ConA [74], the locked form should therefore be stable even in absence of Mn^{2+} in the measured fluid. As a result, we selected the most stable configuration (Mn^{2+} and Ca^{2+}).

ConA has been associated with a variety of toxicological effects in cell cultures and animals, which may be of concern regarding the implantation in human for *in vivo* glucose monitoring [75, 76, 77]. However, the majority of adverse biological effects observed in animals are the result of the administration of large doses of ConA. The small amount of ConA used in most glucose sensors (10 to 100 times less than dosage tested on animals) suggests that there would be little or no health risk associated with the sensor rupture [78].

3.3 Viscosity sensing principle

Basically, viscosity is obtained from the relationship between pressure and flow when the sensitive fluid goes through a channel. The sensor comprises two microchambers filled with the sensitive fluid that communicate through a microchannel and a rigid nanoporous semi-permeable membrane (Fig. 3.4). This membrane has two roles: it confines the sensitive fluid inside the sensor (large molecules cannot go through) and ensures that the glucose can pass through, meaning that the concentration in the sensor and in the liquid should be the same. Each chamber is composed of a flexible piezoelectric diaphragm which whether deflects under voltage (actuating

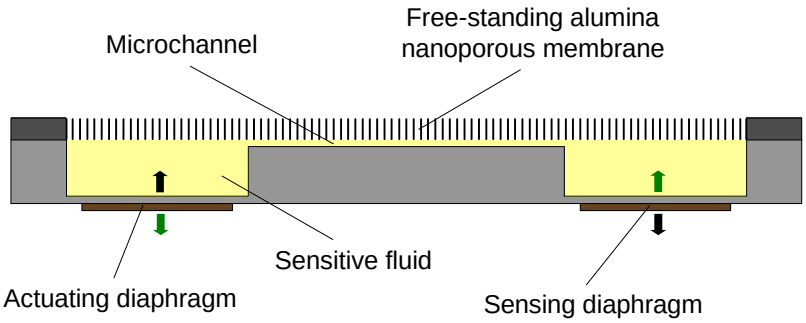

Figure 3.4: Schematic cross view of the glucose sensor.

diaphragm) or generates a voltage under some pressure load (sensing diaphragm).

These actuating and sensing piezoelectric diaphragms together with the microchannel are the basis for viscosity detection. When a voltage is applied on the actuating piezoelectric diaphragm, the latter deflects and tends to generate a flow through the microchannel. Due to its small section, the microchannel exhibits a resistance to the flow which depends on the fluid viscosity. Next, the flow through the microchannel is recorded using the voltage induced by the sensing piezoelectric diaphragm deflection.

Both transient and harmonic electric signals can be used to actuate the diaphragm (Fig. 3.5). The way viscosity is measured will depend on these waveforms. In transient mode, a constant voltage is suddenly applied to the actuating diaphragm for a given time, and then it is switched off. These states generate a strain in the piezoelectric membrane that in turn will create some pressure in the fluid. Due to its small cross section, the microchannel exhibits a resistance to the flow which depends upon the viscosity of the sensitive fluid. The system is characterized by a relaxation time that depends upon the viscosity of the sensitive fluid: the more viscous the sensitive fluid, the larger the relaxation time.

Conversely, under harmonic operation, a sinusoidal voltage is applied on the actuating diaphragm. This generates an alternative flow inside the microchannel which in turn generates a sinusoidal deflection and induced voltage of the sensing diaphragm. Since the amplitude and the phase shift between the applied and induced piezoelectric voltages characterises the viscosity, we have a simple tool to assess the fluid characteristics: the more viscous the sensitive fluid, the smaller the deflection and the larger the

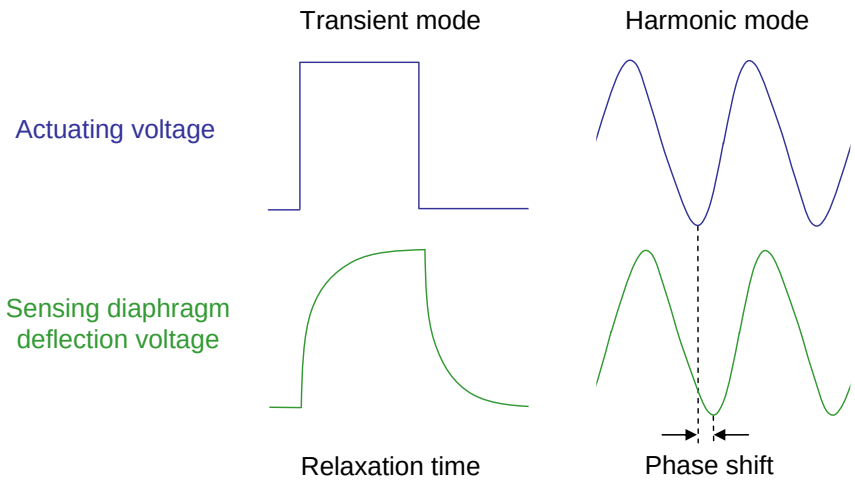

Figure 3.5: Description of the measurement methods for viscosity detection.

phase shift. In particular, we choose to measure the phase shift between 0 to 90 degrees, which revealed to be an accurate and robust measurement.

3.4 Semi-permeable membrane

3.4.1 Function and requirements

The role of the semi-permeable membrane is to retain the essential molecules of the sensitive fluid (ConA and dextran) inside the sensor whilst allowing glucose to diffuse freely in and out. For maintaining the rheological properties of the sensitive fluid constant, the semi-permeable membrane has also to prevent some of the biological fluid macromolecules (like peptides and proteins) to penetrate into the sensor. The main constituent molecules of the sensitive fluid and of a typical biological fluid (interstitial fluid) are sketched in Fig. 3.6. In particular, there may be glycosylated molecules which could competitively interfere with the glucose measurement. The semi-permeable membrane has therefore to act as a size-selective interface, allowing only the diffusion of molecules of size comparable to glucose. In addition, the interface material has to be biocompatible and has to minimize biofouling by preventing the non-specific adhesion of biomolecules.

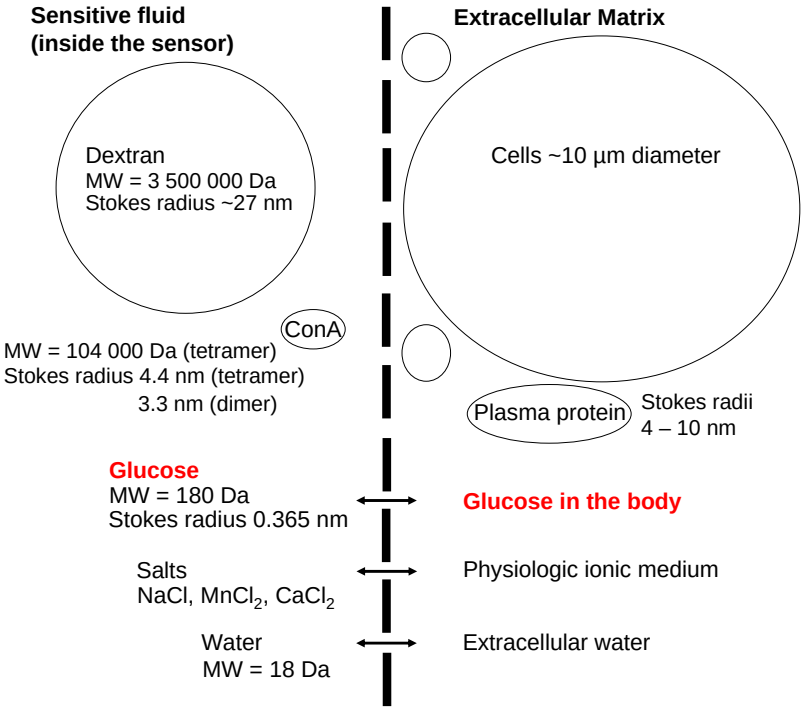

Figure 3.6: Illutration of the relative size of the molecules that the membrane has to select. MW is the molecular weight in Dalton. (Reprinted from [3].)

For small molecules like glucose, the intrinsic selectivity of the membrane is determined by the pore size distribution which defines the membrane molecular weight cut-off (MWCO). For larger biomolecules such as proteins, polymers or peptides, the molecule dimensions depend on the three-dimensional structure which itself depends on the chemical environment. When dealing with complex biomolecules, the selectivity of a membrane is therefore more likely to be compared by the Stokes radius[1] than the MWCO. In addition, the effective radius of a protein in the context of membrane separation can be considerably larger than the Stokes radius due to the presence of a diffuse ion cloud that surrounds the charged protein in aqueous solution [79]. For the size-selectivity to act correctly, one could simply choose a membrane with pores much smaller than the dimensions of the molecules to be retained. However, the size difference between glu-

[1]The Stokes radius, or hydrodynamic radius, is the radius of a hypothetical hard sphere that diffuses at the same rate as the molecule. It is indicative of the apparent size of the molecule, including hydration and shape effects.

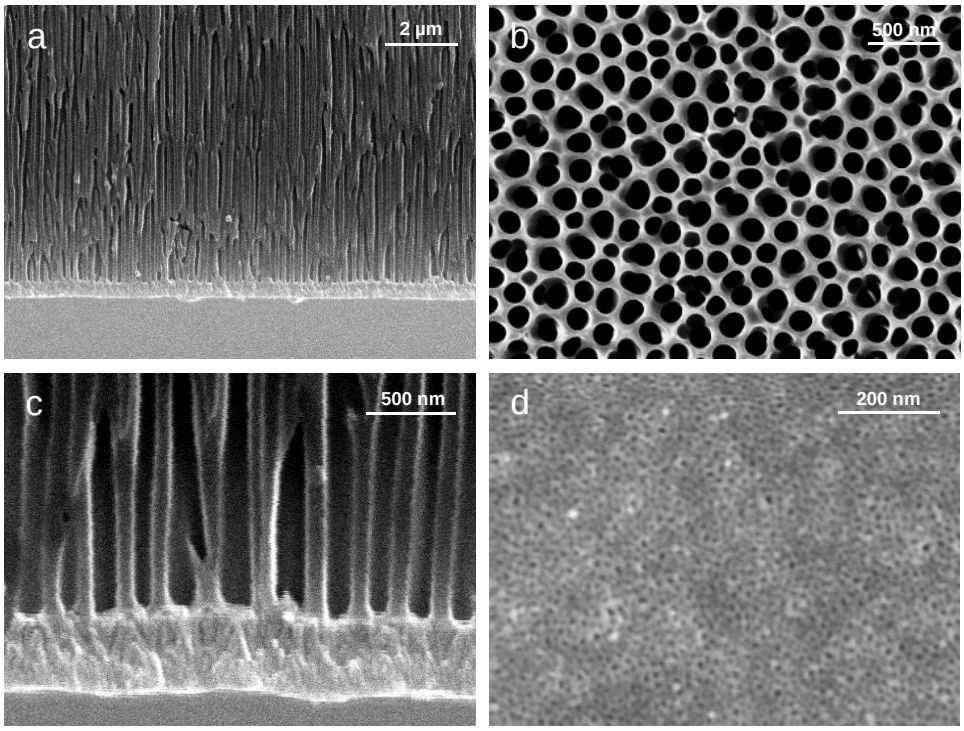

Figure 3.7: SEM pictures of a nanoporous alumina membrane with a bilayer structure: (a) cross section; (b) support layer with 200 nm pores; (c) zoom over the active layer cross section; (d) active layer with 2–4 nm pores.

cose and ConA dimer is only a factor 9 and thus we have to face the case where the molecule size and pore size are comparable. A semi-permeable membrane with a narrow pore size distribution (1–5 nm) is therefore required.

3.4.2 Nanoporous alumina membrane

Nanoporous anodic alumina membranes were selected as selective interface for the glucose sensor (Fig. 3.7). These membranes exhibit arrays of straight parallel pores of quasi-uniform shape and have the chemical properties of a ceramic. They are formed by an electrochemical process involving the oxidation of high purity aluminium sheets. For small pore sizes, anodic alumina membranes are generally prepared with a bilayer structure. These asymmetrical membranes have a thin active layer and a support layer with larger pores. Typically, the active layer is 0.5 μm thick with 10 nm pores and the support layer is 50 μm thick with 200 nm pores. This double

layer configuration ensures rigid membranes whilst allowing good diffusivity properties. The pore diameter is controlled with great precision and reproducibility, allowing narrow pore size distribution, which is hardly achieved by other type of membranes. Moreover, annealed anodic alumina membranes have excellent chemical resistance and long-term stability in aqueous solution. The smallest pore size commercially available is 2–4 nm from Synkera Technologies Inc., and they are currently moving towards manufacturing of nanofitration membranes with 0.5–1 nm pores. With the right selectivity (pore size and distribution), high permeance, long-term stability in aqueous solution and intrinsic biocompatibility, anodic alumina membranes seem therefore well-suited to act as size-selective interface on the glucose sensor.

3.5 Sensor modeling

3.5.1 Viscosity sensing principle

Modelling aspects of the device are quite important to optimize the sensor with respect to the expected variation of the sensitive fluid viscosity. A sketch of the sensor principle used for the derivation of the generic analytical solution is explained in Fig. 3.8.

Under quasi static conditions, the laminar viscous flow of a liquid through a circular channel with a length much greater than its diameter, is described by the Hagen-Poiseuille equation

$$Q = \frac{\pi D^4}{128 \eta L} \Delta P \tag{3.1}$$

where Q is the volumetric flow rate, D and L are respectively the channel diameter and length, η is the liquid viscosity and ΔP represents the pressure drop across the channel.

On the other hand, the deflection of the center of a piezoelectric diaphragm depends on the applied voltage and pressure load. Assuming small deflections, the relationship is linear and given by

$$x = \alpha V - \beta P \tag{3.2}$$

where x is the deflection of the piezoelectric diaphragm center, V the volt-

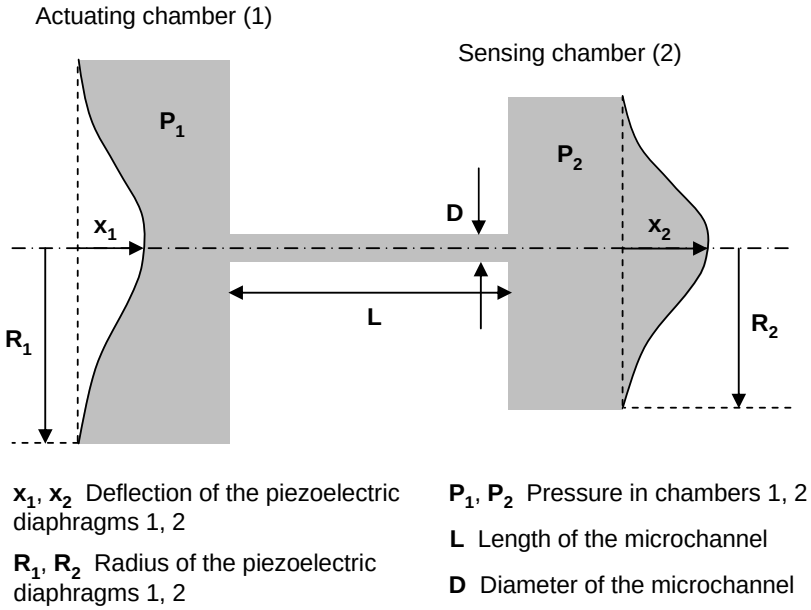

Figure 3.8: Schematic representation of the viscosity sensing principle with the used notations for the theoretical calculations.

age applied to the piezoelectric diaphragm and P the pressure acting against the diaphragm deflection. The coefficients α and β depend on the diaphragm geometry and material properties. For static deflections of a circular multi-layered piezoelectric diaphragm, their values are obtained from the model of Deshpande et al. [80]. As no external voltage is applied to the sensing piezoelectric diaphragm, its deflection only depends on the pressure load:

$$x_2 = \beta_2 P_2 \tag{3.3}$$

Next, the total volume displaced by a fixed-edge circular diaphragm under uniform load is given by

$$V = \frac{1}{3} x \pi R^2 \tag{3.4}$$

where x and R are respectively the deflection of the center and the radius of the diaphragm, (note that this equation was derived for a diaphragm under uniform pressure load and not for a multi-layered piezoelectric diaphragm, but we will nevertheless use it as a good approximation).

The volumetric flow rate through the channel is equal to the volume

change under the sensing piezoelectric diaphragm:

$$Q = \frac{dV}{dt} = \frac{\pi R_2^2}{3}\frac{dx}{dt} \tag{3.5}$$

Coupling the Hagen-Poiseuille flow through the channel with the piezoelectric diaphragms deflections, and considering a sinusoidal voltage $V_1 = V_1^0 \sin(\omega t)$ for actuation, we get the time dependent differential equation:

$$\frac{128\eta L R_2^2 \beta_1}{3D^4}\frac{dx_2}{dt} + \left(\frac{R_2^2\beta_2 + R_1^2\beta_1}{R_1^2\beta_2}\right) x_2 = \alpha_1 V_1^0 \sin(\omega t) \tag{3.6}$$

The solution of the differential equation is composed of a transient and a stationary part. Here, we are mainly interested in the stationary solution describing the deflection of the sensing piezoelectric diaphragm, which is given by:

$$x_2(t) = A\sin(\omega t - \phi) \tag{3.7}$$

with

$$A = \frac{R_1^2\beta_2}{R_2^2\beta_2 + R_1^2\beta_1}\frac{\alpha_1 V_1^0}{\sqrt{\tau^2\omega^2 + 1}} \tag{3.8}$$

and

$$\phi = \arctan(\tau\omega) \tag{3.9}$$

where τ is the relaxation time of the system. The relaxation time is proportional to the liquid viscosity with a constant coefficient depending only on the geometric and piezoelectric characteristics:

$$\tau = k\eta \tag{3.10}$$

with

$$k = \frac{128L}{3D^4}\frac{R_2^2 R_1^2 \beta_2 \beta_1}{R_2^2\beta_2 + R_1^2\beta_1} \tag{3.11}$$

This means that when a sinusoidal voltage is applied to the actuating piezoelectric diaphragm, the sensing diaphragm will also deflect harmonically, but its amplitude and phase shift will now depend on the relaxation time of the system which is proportional to the liquid viscosity. Next, these

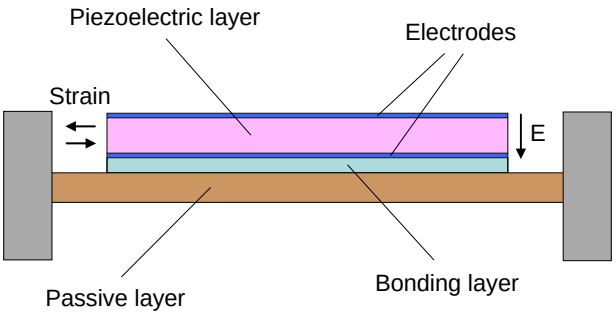

Figure 3.9: Cross-sectional schematic view of a typical piezoelectric diaphragm. The electric field (E) is applied vertically to the plane.

mechanical signals will generate electrical waveforms that will be used to extract the viscosity of the sensitive fluid.

Aside this analysis, since a time dependent sinusoidal voltage is applied to the actuating diaphragm, we can wonder if the flow can still be considered in steady state. When a high viscous liquid pulsates slowly in a narrow pipe, the instantaneous velocity distribution is given by a parabola as in the case of steady Poiseuille flow. Uchida demonstrated that the steady state criteria was still justified provided $\sqrt{\omega/\nu}\, D \ll 1$, where ω is the pulsation of the flow, ν the kinematic viscosity and D the diameter of the channel [81]. As the sensitive liquid viscosity is several times that of water and since the channel is only some micrometers in diameter, using $\omega = 10$ rad/s, $\nu = 70$ mm^2/s and $D = 100 \times 10^{-6}$ m, we find a typical value for the steady state criteria equal to 4.24×10^{-2}. Therefore, the quasisteady condition is satisfied and the Hagen-Poiseuille equation can be used.

3.5.2 Piezoelectric diaphragm deflection

For the sensing principle to operate properly, the deflection of the actuating diaphragm has to generate a sufficiently large flow for accurately detecting the viscosity. In addition, the deflection of the sensing diaphragm has to produce an amount of charges allowing the signal amplification. The actuating and sensing diaphragms are therefore key elements for the sensor design.

Basically, a piezoelectric diaphragm consists of a piezoelectric layer covering partially a passive layer (Fig. 3.9). With parallel electrodes below and

on top of the piezoelectric layer, the electric field is applied vertically to the plane and the transverse piezoelectric effect generates in plane strain. This strain in the piezoelectric layer induces an unimorph effect which produces a transverse deflection of the diaphragm.

A model describing the static deflections of a circular multi-layered piezoelectric diaphragm under voltage and pressure loads was developed by Deshpande et al. [80]. This model relies on the geometry and material properties of each layers, and applied when the piezoelectric layer covers the substrate layer only partially. In addition, the model was derived using the classical laminated plate theory, which implies in particular that small deflections are considered. The piezoelectric material was also assumed to be a polycrystalline film polarized along the axis normal to the surface. The model was validated both numerically via finite element analysis and experimentally via static deflections of a commercially available piezoelectric diaphragm. A good agreement was reported between the model, the finite element results and the experimental measurements.

This analytical model leads to a linear dependence of the piezoelectric diaphragm deflection upon voltage and pressure loads, which is given by

$$x(r) = \alpha(r)V - \beta(r)P \tag{3.12}$$

where $x(r)$ is the deflection of the piezoelectric diaphragm depending on the radial position r, and V and P are respectively the voltage and pressure loads. The coefficients $\alpha(r)$ and $\beta(r)$ depend on the piezoelectric diaphragm geometry and material properties in a complex manner. Their detailed expressions can be found in the article by Desphande et al. [80]. Note that the volume displaced by the diaphragm also depends linearly on the voltage and pressure loads.

The model was implemented in Mathematica and the deflection of a typical piezoelectric diaphragm under multiple voltage and pressure loads was investigated. The diaphragm was made of a 3 mm in diameter, 50 μm thick layer of lead zirconate titanate (PZT) onto a 3.5 mm in diameter, 10 μm thick brass layer. When applying a voltage to the diaphragm, a dome-like deflection is produced with the maximal deformation occuring in the center (Fig. 3.10). A voltage of 30 V generates a deflection of 2.7 μm of the diaphragm centre, which represents a displaced volume of 12 nl. This generates a flow over 1.2 mm in a typical 100×100 μm^2 section channel,

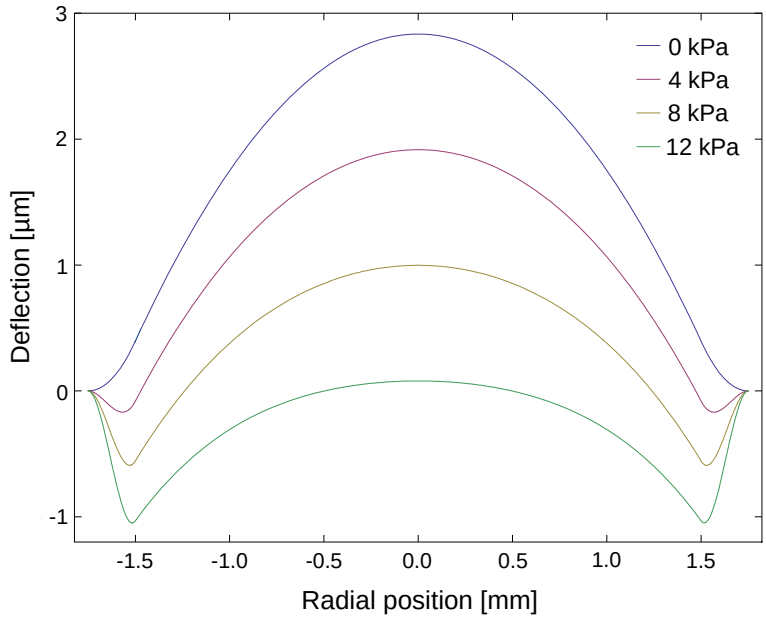

Figure 3.10: Deflections along a diameter of the piezoelectric diaphragm under a voltage of 30 V and multiple pressure loads.

which should enable precise viscosity sensing.

Generally, the piezoelectric layer covers the substrate layer only partially, which reduces the thickness at the edge and thus favours the diaphragm deflection. More precisely, the deflection depends upon the piezoelectric layer size which can be optimized to maximize the diaphragm deflection (Fig. 3.11). In this particular case, as the piezoelectric layer is largely thicker than the passive layer, a small reduction of the piezoelectric layer is sufficient to favour the diaphragm deflection. However, when the thickness of the piezoelectric and passive layer are closer, the optimal piezoelectric radius decreases. According to the model, the optimal ratio of the piezoelectric and passive layer radiuses mostly depends upon their respective thicknesses. It does not depend on the voltage or membrane size, and only slightly on the applied pressure. Note that an optimal piezoelectric layer size is of primary importance when strong forces are required given that in this case the deflection is strongly reduced when decreasing the piezoelectric layer size.

The piezoelectric and passive layers thicknesses also strongly influence the diaphragm deflection. Depending on the application, thin layers are used to produce large deflections whereas thicker structures are usefull to

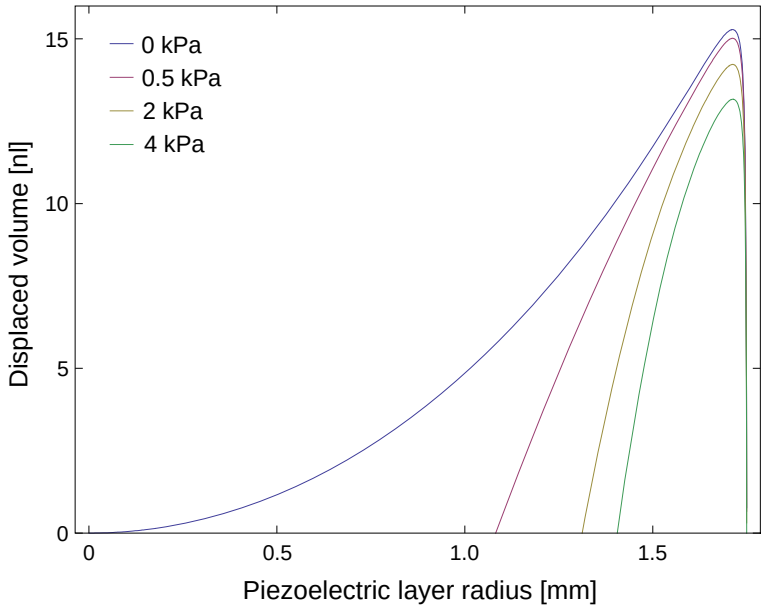

Figure 3.11: Deflection dependence upon the piezoelectric layer radius for a constant voltage (30 V) and multiple pressure loads.

generate strong forces. Under constant electric field, the diaphragm deflection depends on both the piezoelectric and passive layers thicknesses with optimal values maximizing the deflection (Fig. 3.12). Under pressure load, both the optimal piezoelectric and passive layers thicknesses increase: the thicker passive layer stiffens the structure while the thicker piezoelectric layer is required to generate stronger forces.

3.5.3 Fundamentals of diffusion

Diffusion describes the spread of particles through random motion from regions of higher concentration to regions of lower concentration. Diffusion is phenomenologically described by Fick's law, which relates the diffusive flux to the concentration by postulating that the flux goes from regions of high concentration to regions of low concentration, with a magnitude that is proportional to the concentration gradient. In one dimension, this is

$$J = -D\frac{\partial c}{\partial x} \tag{3.13}$$

where J is the flux (amount of particles per unit area per unit time), D is the

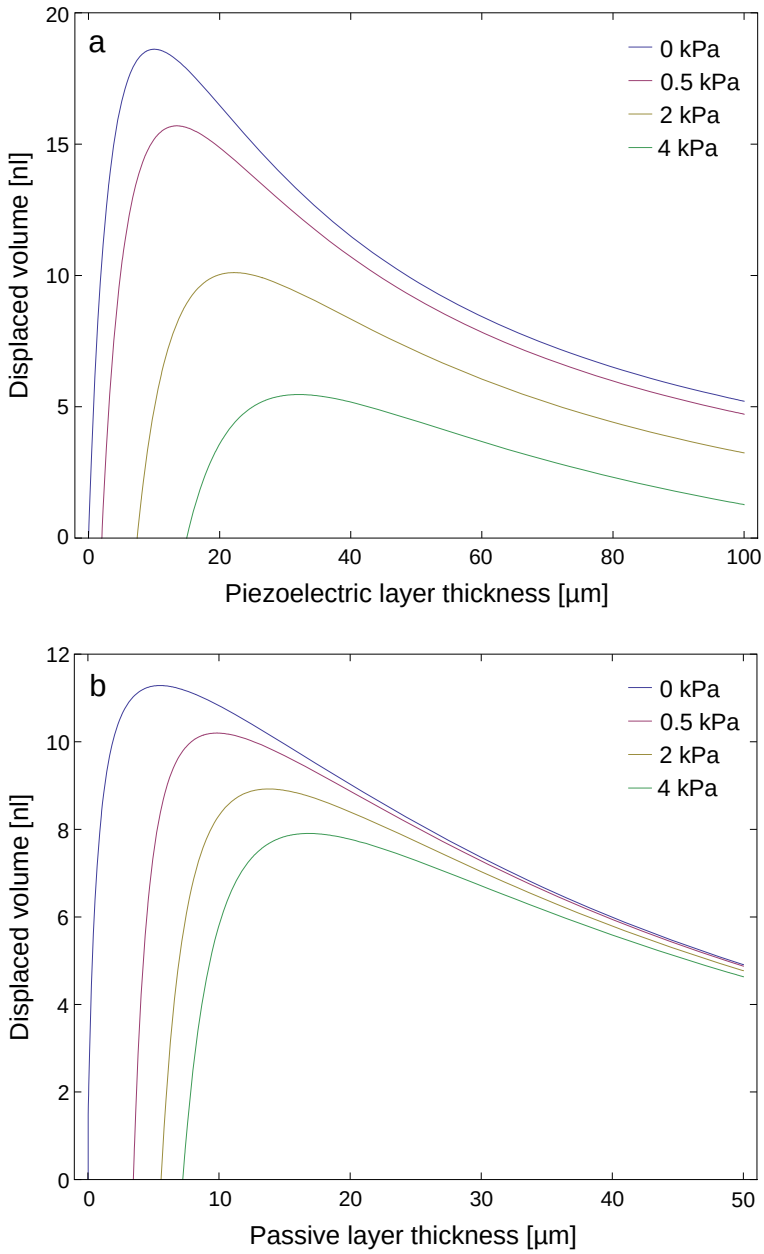

Figure 3.12: Deflection dependence upon the layers thickness for multiple pressure loads: (a) piezoelectric layer (constant electric field of 0.5 V/μm); (b) passive layer (constant voltage of 30 V).

diffusion coefficient, c is the concentration, and x is the position.
Combining Fick's law with the continuity equation which states that a change in density in any part of the system is due to inflow and outflow of material, we get the diffusion equation predicting how diffusion causes the concentration to change with time:

$$\frac{\partial c}{\partial t} = D\frac{\partial^2 c}{\partial x^2} \tag{3.14}$$

Eintein's theory of Browian motion relates the diffusion coefficient to the particle mobility as

$$D = \mu k_B T \tag{3.15}$$

where μ is the particle mobility, k_B is the Boltzmann's constant, and T is the temperature. The frictional coefficient (inverse of mobility) exerted on spherical particles with small Reynolds numbers (Re$\ll$1) in a viscous fluid is given by

$$\gamma = 6\pi\eta r \tag{3.16}$$

where η is the dynamic viscosity and r is the radius of the spherical particle. Combining (3.15) and (3.16), we get the Einstein-Stokes equation which expresses the diffusion coefficient of spherical particles through liquids with low Reynolds numbers:

$$D = \frac{k_B T}{6\pi\eta r} \tag{3.17}$$

3.5.4 Diffusion in membranes

A simple way of describing diffusion through membranes is to consider two well-stirred volumes separated by a membrane (Fig. 3.13). In particular, this diffusion cells configuration is used to characterize the diffusion properties of membranes. To achieve this, a chamber is filled with a solution of known concentration and the other chamber is filled with solvent. Next, the concentration is measured at regular intervals and the diffusion coefficient is extracted from the concentration dynamics. An exact solution to this problem is elaborate and unnecessary for practical use [82]. The useful approximate solution depends on the assumption that the flux

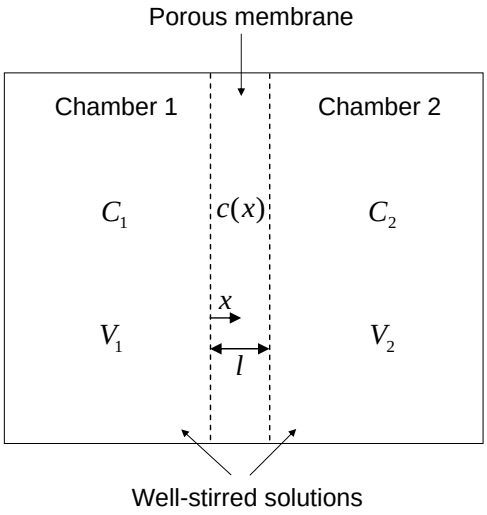

Figure 3.13: Diffusion through a porous membrane separating two well-stirred solutions. V_i and C_i are respectively the volume and concentration of the chamber i, and $c(x)$ is the concentration inside the membrane.

across the membrane quickly reaches its steady-state value [83], and that a steady-state flux is approached even though the concentrations in the two chambers are changing with time.

In the case of steady diffusion, each side of the membrane is a well-mixed dilute solution of fixed concentration. In these conditions, the concentration in the membrane does not change with time and the diffusion equation (3.14) becomes

$$\frac{d^2c}{dx^2} = 0 \tag{3.18}$$

where c is the concentration in the membrane depending on the position x.

The boundary conditions relating the concentration in the membrane to the fixed concentrations C_1 and C_2 of the dilute solutions are given by

$$\begin{aligned} c &= HC_1 \quad \text{for} \quad x = 0 \\ c &= HC_2 \quad \text{for} \quad x = l \end{aligned} \tag{3.19}$$

where H is the partition coefficient, which is the concentration in the membrane divided by that in the adjacent solution. The partition coefficient is an equilibrium property, which takes into account the relative solubility in

the membrane compared with that in the adjacent solutions. For porous membranes, it also includes the porosity which is the pores-to-membrane area ratio.

The concentration profile in the membrane is obtained by integrating the diffusion equation (3.18) using the boundary conditions (3.19):

$$c = HC_1 + H\left(C_2 - C_1\right)\frac{x}{l} \tag{3.20}$$

The solution is a linear change of concentration across the membrane which depends upon the membrane properties through the partition coefficient. The flux across the membrane is found by combining the concentration in the membrane (3.20) with Fick's law (3.13):

$$J = -\frac{HD}{l}\left(C_2 - C_1\right) \tag{3.21}$$

We next write an overall mass balance on the adjacent chambers, expressed by

$$V_1\frac{dC_1}{dt} = -SJ \tag{3.22}$$

$$V_2\frac{dC_2}{dt} = +SJ \tag{3.23}$$

where S is the membrane area. Coupling these mass balance equations with the flux equation (3.21), we obtain the differential equation for the concentration of the dilute solutions:

$$\frac{d}{dt}\left(C_2 - C_1\right) = -\frac{HDS}{l}\frac{V_1 + V_2}{V_1V_2}\left(C_2 - C_1\right) \tag{3.24}$$

The solution of this differential equation is given by

$$\left(C_2 - C_1\right) = \left(C_{2,0} - C_{1,0}\right)\exp\left(-\frac{t}{\tau}\right) \tag{3.25}$$

with

$$\tau = \frac{l}{HDS}\frac{V_1V_2}{V_1 + V_2} \tag{3.26}$$

This means that the concentration of two well-stirred solutions separated by a porous membrane evolves towards the equilibrium following an

exponential relation. The time constant of this diffusion process depends upon the diffusion coefficient, the membrane geometry and diffusive properties, and the size of both chambers. When considering two chambers with identical volumes and an effective diffusion coefficient, the time constant becomes

$$\tau = \frac{lV}{2D_{\text{eff}}S} \tag{3.27}$$

For nanoporous membranes, an effective diffusion coefficient is often considered, as many effects may restrict diffusion. In particular, the diffusion rate may be greatly slowed if the dimensions of the pores are comparable with those of the diffusing molecules. In fact, it was shown that the rates of diffusion of organic non-electrolytes through membranes with very small pores decrease, as a function of molecular size, far more rapidly than can be accounted for on the basis of the free diffusion coefficients of the test molecules [84]. It also appears that diffusion is severely restricted even when the pores are of the order of 20 times larger than the diffusing molecules [85]. The increased viscous drag in the pore and the particle-pore wall interaction could explain this diffusion reduction. A further restriction to diffusion may result from steric effects at the entrance to the pore, as the diffusing molecules can enter a pore only if they do not strike the edges [86].

With a factor 9 between glucose and ConA hydrodynamic radiuses, our sensor is characterized by a high solute-to-pore ratio, which means that the glucose diffusion through the nanoporous membrane will likely be reduced compared to diffusion in solution.

3.5.5 Free diffusion

For the glucose concentration to be in equilibrium with the surrounding environment, glucose molecules have first to diffuse across the nanoporous membrane, and then in the sensitive fluid. This is a free diffusion which can be approximately described by the diffusion in a semi-infinite slab (Fig. 3.14). The slab initially contains a uniform concentration of solute. At time $t = 0$, the concentration at the interface is suddenly increased, which is described by the following boundary conditions:

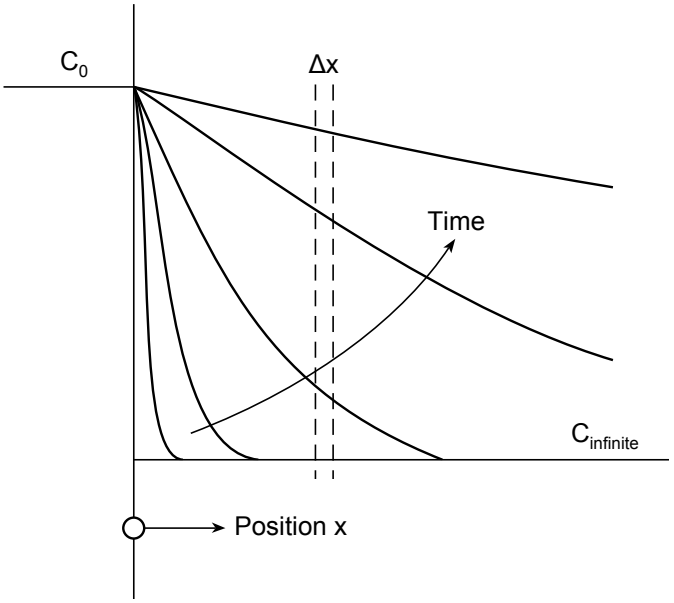

Figure 3.14: Free diffusion in a semi-infinite slab. The concentration at the left is suddenly increased to a higher constant value, which induces diffusion in the region to the right. (Reprinted from [87].)

$$\begin{aligned} c(x) &= C_\infty \quad \text{for all } x \text{ at } t = 0 \\ c(x=0) &= C_0 \quad \text{at } t > 0 \\ c(x=\infty) &= C_\infty \quad \text{at } t > 0 \end{aligned} \tag{3.28}$$

The concentration at $x = \infty$ is constant because it is so far from the interface as to be unaffected by events while the concentration at $x = 0$ is kept constant by adding material at the interface.

The solution is found by solving the diffusion equation (3.14) with the boundary conditions (3.28) using the definition of the variable $\xi = x/\sqrt{4Dt}$, (the detailed resolution of this problem can be found in [87]):

$$\frac{c(x,t) - C_0}{C_\infty - C_0} = \text{erf}\left(\frac{x}{\sqrt{4Dt}}\right) \tag{3.29}$$

where

$$\text{erf}(\xi) = \frac{2}{\pi}\int_0^\xi \exp\left(-s^2\right) ds \tag{3.30}$$

is the error function.

The expression $\xi = x/\sqrt{4Dt}$ completely determines the concentration at the position x and time t, which means that the same diffusion level is achieved for ξ constant. The length $\sqrt{4Dt}$, called the diffusion length, provides a measure of how far the concentration has propagated at time t. It is worth noticing that the diffusion time depends quadratically upon the distance and linearly upon the diffusion coefficient. This implies that the sensor has to be as small as possible to minimize the diffusion length and thus reduce the response time. A good diffusion coefficient is also useful to favour the diffusion process. According to the Eintein-Stokes relation (3.17), the diffusion constant decreases with the fluid viscosity due to an increased viscous drag slowing the particle movement. A low-viscosity sensitive fluid is therefore also required for rapid measurement.

3.6 Conclusion

In this chapter, we described and modeled the sensing principle relying on the viscosity variation of a ConA-based sensitive fluid. With a hydrodynamic radius of 3.3 nm, the confinement of ConA require a nanofiltration membrane with a narrow pores size distribution. Nanoporous alumina membranes were selected as they are characterized by a rigid structure, a narrow pores size distribution, and a long term stability in aqueous solution. Concerning the sensor modeling, we showed that when applying a sinusoidal voltage the system oscillates harmonically with amplitude and phase shift which depend on the sensitive fluid viscosity. The use of piezoelectric diaphragms was also validated by simulation, showing that small diaphragms can produce significant deflections. Finally, we expose a simple exponential model for glucose diffusion in membranes, which allows to experimentally determine the diffusion constant using diffusion cells.

Chapter 4

Sensor development and assessment

4.1 Introduction

The sensor topology was designed to allow its realization in microelectromechanical system (MEMS) technology. Its flat and stack-based structure is in fact especially well-suited for microfabrication batch processes like etching, thin film deposition, and patterning. The two chambers and the microchannel could be etched in silicon using existing microfabrication processes (Fig. 4.1). Such structures are commonly fabricated in silicon for lab-on-a-chip applications. Piezoelectric thin films and their integration in MEMS technology have also been subject to intensive research, and a number of devices based on PZT (lead zirconate titanate) thin films were successfully fabricated [88]. However, piezoelectric thin film fabrication is still a complex technology which is mastered by a limited number of research groups. Moreover, MEMS technology often brings miniaturization issues, especially for microfluidic devices. For these reasons, we chose to demonstrate the sensing principle using macroscopic technologies. The sensor was realized in stereolithography, also known as 3D printing, which allows to create plastic objects using laser-induced polymerization of a photo-curable resin. The object is created by successively printing thin layers of ultraviolet curable material on top of each other. Stereolithography allows rapidly creating prototypes with high accuracy.

In this chapter, the development and assessment of the sensor in iso-

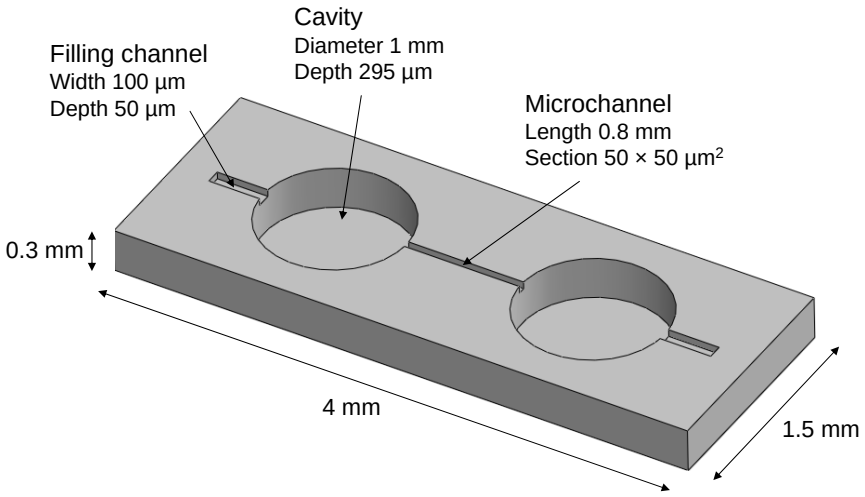

Figure 4.1: Schematic view of the MEMS sensor concept with optimal dimensions.

tonic saline solution are presented.

4.2 Sensor design

4.2.1 Sensor structure

According to the sensor model, a microchannel of about 50–100 μm was required to detect viscosity with a small size sensor. Such a microchannel is not feasible by standard stereolithography; with layers thickness of 50 μm, the smallest achievable channel is 300 μm. A glass capillary was therefore integrated in the stereolithography housing (Fig. 4.2). In addition, the actuating and sensing chambers were both defined by circular apertures in the stereolithography housing and sealed by circular piezoelectric diaphragms and nanoporous membranes. Two filling channels were also included on both sides of the stereolithography housing. Finally, the thickness of the chambers was minimized in order to keep a small diffusion length and hence a good response time.

4.2.2 Actuating piezoelectric diaphragm

For accurately detecting viscosity, the actuating diaphragm has to generate a large flow through the microchannel with sufficient pressure. A flow

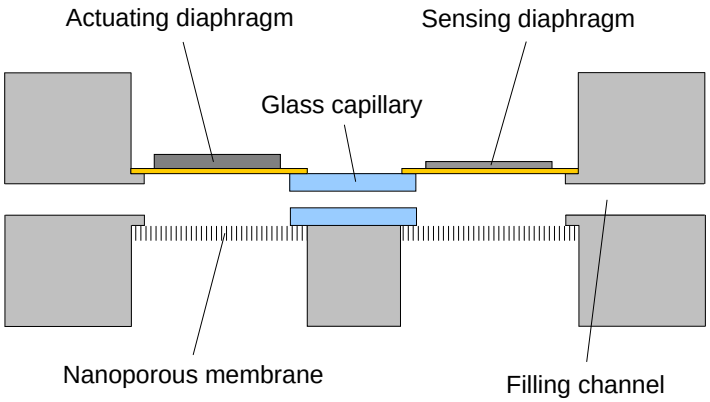

Figure 4.2: Schematic section view of the sensor design including a glass capillary as microchannel.

through the whole microchannel is also required to equilibrate the glucose concentration inside the microchannel. Piezoelectric ceramics generate strong forces and large excursions in bending structures and are therefore well suited for the actuating diaphragm. In particular, PZT is a ceramic perovskite material which exhibits outstanding piezoelectric properties. These properties make PZT-based compounds one of the mostly used piezoelectric ceramics. Important fields of application are actuators for micropositioning, sensors such as conventional vibration pickups, and ultrasonic transmitters and receivers, like automotive parking radars. Among these, piezoelectric diaphragm is a basic electronic sound component characterized by a simple structure, stable performance and high reliability. It is used for buzzers and alarms, as well as shock sensors in many sensitive equipments.

The smallest piezoelectric diaphragm commercially available is a 5 mm diameter, 50 μm thick PZT layer onto a 6.5 mm diameter, 50 μm thick brass layer (Audiowell electronics, Ltd.). As a quite small sensor was targeted, the handmade fabrication of smaller piezoelectric diaphragms was required. When decreasing the size of a piezoelectric diaphragm, its thickness must be reduced accordingly to maintain good bending properties. However, the minimum thickness of commercially available PZT layers is 50 μm, which limits the miniaturization of the diaphragm. The brass layer thickness was reduced to 10 μm, which allowed to decrease the diaphragm size to 3.5 mm (Fig. 4.3). The diaphragm deflection was characterized using a specular-reflective laser displacement meter (LC-2420 from Keyence)

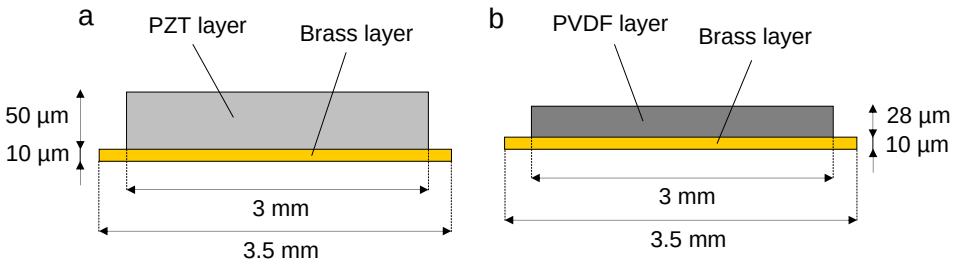

Figure 4.3: Dimensions of the actuating (a) and sensing (b) piezoelectric diaphragms.

(Fig. 4.4). The piezoelectric diaphragm model describes accurately the diaphragm deflection for small voltages. However, large deflections are underestimated by the model with a quite important deviation from the expected linear behaviour. This could be explained by an increase in polarization with the magnetic field, which would increase the piezoelectric effect. The model relies on a constant piezoelectric coefficient, and therefore this non-linear behaviour is not taken into account. However, the theoretical and experimental values are of the same order of magnitude, which allows to properly estimate the sensor response.

In operation, a voltage of 30 V was applied to the diaphragm, which generates a deflection of 2.7 μm of the diaphragm center and corresponds to a flow of 1.2 mm in the 100×100 μm^2 section channel. Such a high voltage was imposed by the sensor design, as a flow through the whole capillary is required to mix the sensitive fluid inside the microchannel. Since a high voltage is not compatible for *in vivo* applications, we can wonder whether a lower actuating voltage could also be used. The voltage could be reduced by decreasing the microchannel dimensions, as the flow required to mix the sensitive fluid would be reduced. For instance, a voltage of 5 V could be used with a 500 μm length, 50×50 μm^2 section microchannel. The voltage could also be reduced by decreasing the piezoelectric layer thickness, as an equivalent electric field would be produced with a lower voltage. However, as commercially available piezoelectric diaphragms have a minimum thickness of 50 μm, a dedicated fabrication would be required. In the case of MEMS fabrication, PZT thin-film diaphragms could be directly integrated in the device [89]. Finally, the need to produce a flow across the microchannel could be suppressed if glucose could directly diffuse into a mi-

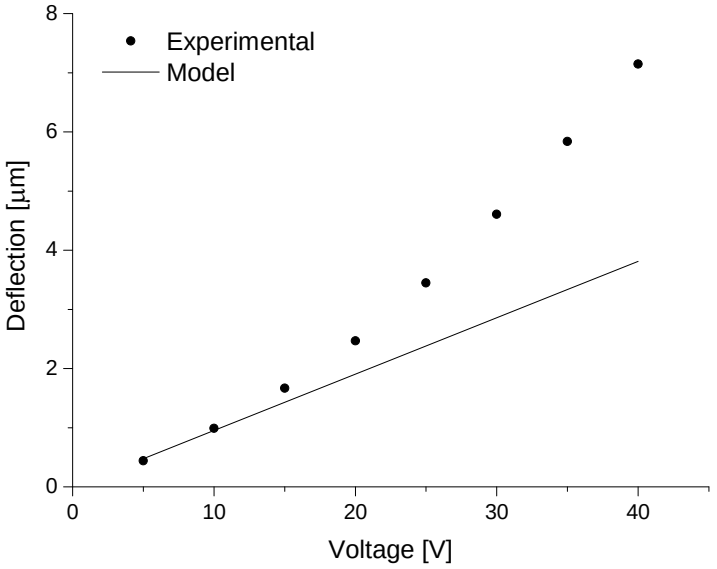

Figure 4.4: Deflection of the actuating piezoelectric diaphragm under voltage load.

crochannel with a porous side wall. For instance, the alumina nanoporous membrane could be used to seal an open microchannel. This would be the ideal case since the only remaining constraint on the deflection would be the detection of the sensing signal. Therefore, solutions exists to decrease the actuating voltage, but this was not the primary focus for this proof of concept sensor.

4.2.3 Sensing piezoelectric diaphragm

For the sensing principle to work properly, the sensing diaphragm has to bend more easily than the nanoporous membrane, otherwise the nanoporous membrane would deform instead of the sensing diaphragm and the flow would not be detected. According to the piezoelectric diaphragm model, the PZT diaphragm used as actuator is 1.7 times stiffer than the 50 μm thick alumina nanoporous membrane, implying that a more flexible structure has to be used for the sensing side. Polyvinylidene fluoride (PVDF) is a thermoplastic fluoropolymer which exhibits a large piezoelectric coefficient as well as a low elastic modulus. The piezoelectric properties of PVDF are used to manufacture tactile sensor arrays, inexpensive strain gauges and lightweight audio transducers. A 28 μm thick PVDF foil was

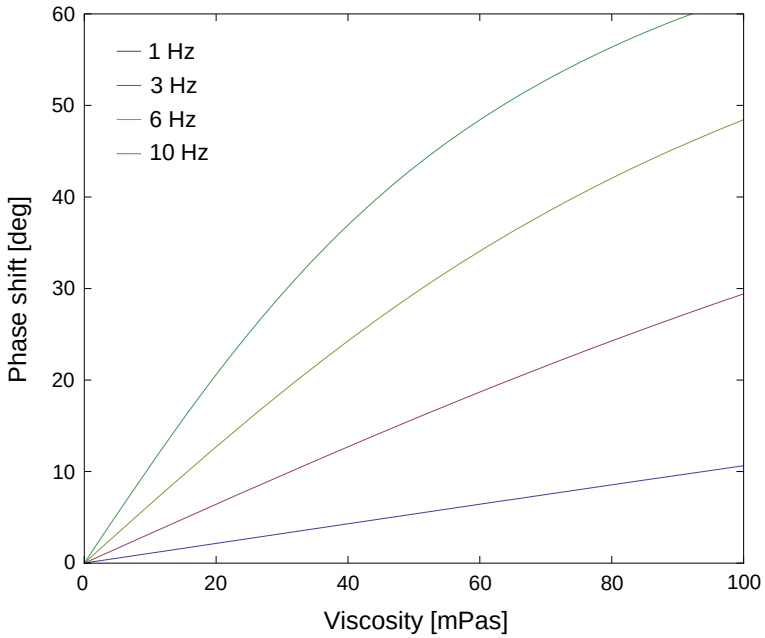

Figure 4.5: Theoretical phase shift of the sensor calculated using the sensor model (Eq. (3.9)).

therefore used as piezoelectric layer on the sensing diaphragm (Fig. 4.3). For practical reasons, a 10 μm thick brass foil was also used as passive layer and the size of the actuating and sensing diaphragms was the same. According to the piezoelectric diaphragm model, this brass-PVDF diaphragm is 16 times more flexible than the alumina nanoporous membrane, which makes it a well suited sensing diaphragm.

4.2.4 Measurement process

The actuating frequency may be tailored according to the sensitive fluid viscosity. The same phase shift is indeed maintained by increasing the actuating frequency when using a lower viscosity sensitive fluid. The higher measurable viscosity is defined by the lower possible frequency, which is limited by the instrumentation amplifier used to measure the piezoelectric signal. A minimum frequency of 1 Hz is required by most amplifiers. On the other hand, when using a lower viscosity, the frequency can always be increased and consequently no lower viscosity limit exists. However, a small channel with a high fluidic resistance provides a better measure-

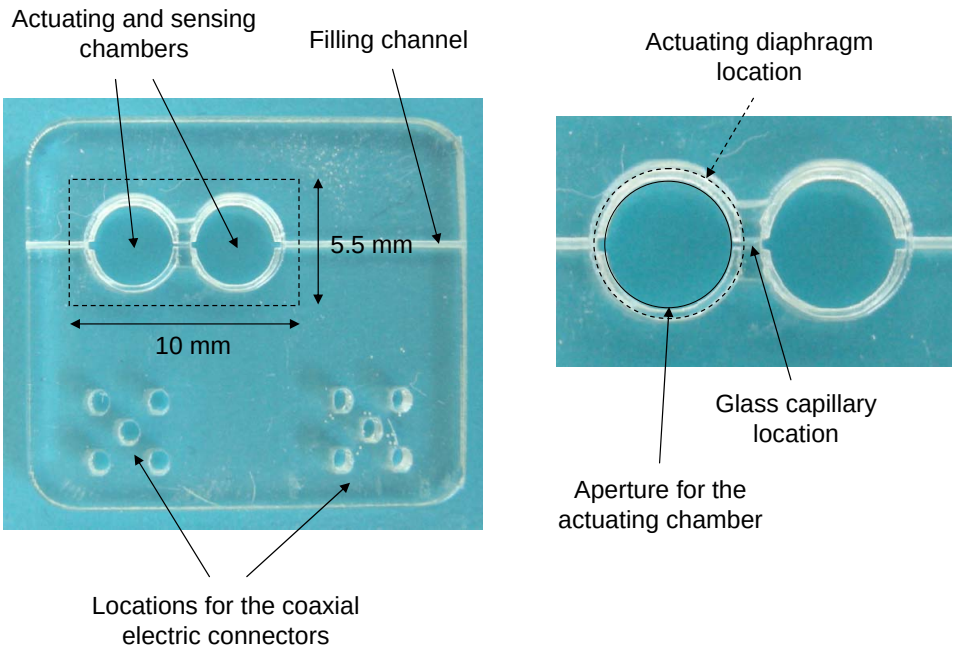

Figure 4.6: Picture of the sensor housing fabricated by stereolithography.

ment accuracy; it is therefore better to operate at low frequency. A viscosity measurement range has therefore to be defined, while the actuating frequency is used to tailor the phase shift. Our sensor was designed to measure low viscosity sensitive fluids (10–100 mPas) at low frequency (1–10 Hz) (Fig. 4.5).

4.3 Experimental section

4.3.1 Sensor fabrication

The piezoelectric diaphragms were prepared by cutting 4 mm diameter discs from a 10 μm thick brass foil (Goodfellow) using laser ablation (LS-520G Nd:YAG 1064 nm from Laser Systems). A 3 mm diameter PZT disc was also cut by laser ablation from a 50 μm thick PZT layer provided by Audiowell Electronics. Next, a 3 mm diameter disc was punched in a 28 μm thick PVDF foil provided by Measurements Specialties. The piezoelectric diaphragms assembly was performed by gluing the PZT and PVDF discs onto brass discs using a low-viscosity epoxy adhesive (Loctite M-31CL). In

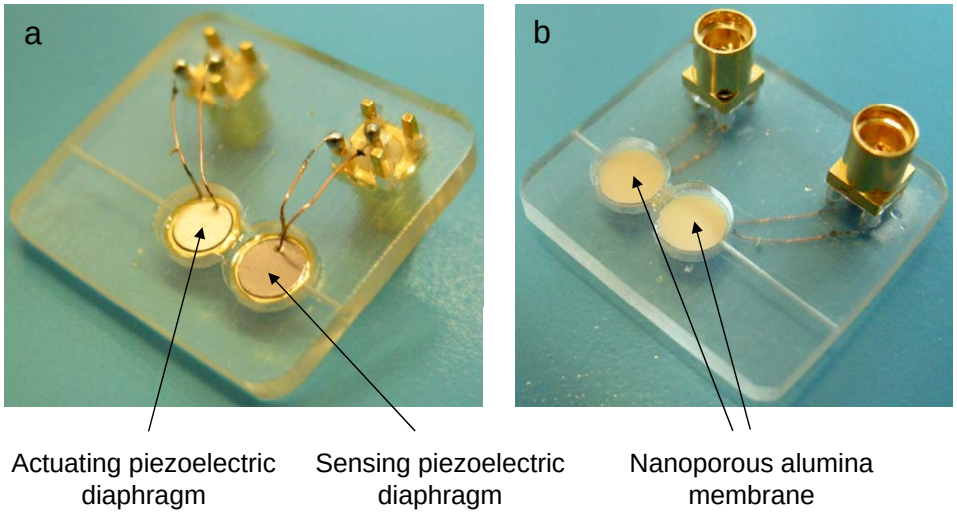

Figure 4.7: Pictures of the assembled sensor showing the actuating and sensing piezoelectric diaphragms (a) and the nanoporous alumina membranes (b).

addition, electric contacts were achieved by bonding 0.1 mm copper wires using a conductive adhesive epoxy (EPO-TEK E4110 from Epoxy Technology). Finally, the piezoelectric diaphragms were coated with 10 μm parylene C to prevent any corrosion caused by water contact. Such coating was chosen because parylene is a chemically very stable polymer deposited at room temperature.

The sensor housing was manufactured by stereolithography using a biocompatible medical-grade resin (Proform, Part. DSM XC11122) (Fig. 4.6). The housing included two 3.5 mm diameter circular apertures for the actuating and sensing chambers, two 0.3 mm diameter filling holes, as well as dedicated locations for the glass capillary, the piezoelectric diaphragms and the alumina membranes. The semi-permeable membrane was a 50 μm thick alumina nanoporous membrane with 2–4 nm diameter pores (Synkera Technologies, Inc.). In addition, a 1 mm length, 100×100 μm^2 section glass capillary was used for the microchannel (Vitrocom, Part. ST8510). The sensor assembly was realized using medical-grade adhesive epoxy (Loctite M-21HP) using a precision syringe dispenser and a stereoscopic microscope (Fig. 4.7). Finally, the sensor was 200 μm thick, which was imposed by the outer dimension of the glass capillary, and contained 4 μl of sensitive fluid.

4.3.2 Sensitive fluid characteristics

The sensitive fluid consists in 2% [w/w] dextran 3200 (PSS) and 0.4% [w/w] ConA (Sigma) in a buffered saline solution (10mM Tris base, 1mM $CaCl_2$, 1mM $MnCl_2$, 0.05% NaN_3, 0.15M NaCl). Two metal ions, Mn^{2+} and Ca^{2+}, were added to the solution to activate the glucose binding site of ConA. This conformational change strongly increases its affinity to glucose. The pH was adjusted to the physiological value (pH 7.4), which also ensures a maximal proportion of tetrameric ConA able to bind up to 4 glucose groups and form a large network. The saline concentration was set to its physiological value (0.15M NaCl) and NaN_3 was added as preservative. The viscosity of the sensitive fluid was characterised using a capillary viscometer. Its values were ranging from 5.9 to 16.7 mPas at 25˚C and from 4.2 to 9.4 mPas at 37˚C (Fig. 3.3).

4.3.3 Sensitive fluid preparation

To prepare the sensitive fluid, 3 stock solutions were necessary.

Stock solution 1 was prepared by dissolving 20 mM of Trizma buffer pH 7.4 (Sigma, Cat. T-7693), 0.1% [w/w] of sodium azide (Riedel-de Haen, Cat. 13412) and 4 mM D-(+)-glucose anhydrous (Fluka, Cat. 49138) in millipore water.

Stock solution 2 contained 2 mM calcium chloride dehydrate (Fluka, Cat. 21101), 2 mM manganese II chloride tetrahydrate (Riedel-de Haen, Cat. 31422) and 300 mM sodium chloride (Fluka, Cat. 71379).

Stock solution 3 was a 50 mM sodium hydroxide (Fluka, Cat. 71691) aqueous solution, which was used for the pH adjustment of the sensitive fluid.

The sensitive fluid was prepared by dissolving dextran (Polymer Standards Service, Cat. dxtb3m) in stock solution 1 and ConA (Sigma, Cat. C2010) in stock solution 2, as described below.

Solution A: Twice the concentration of the final preparation of dextran was dissolved in stock solution 1 and mixed at room temperature for at least 10 h.

Solution B: Twice the concentration of the final preparation of ConA was dissolved in stock solution 2. The pH was adjusted to 7.4 by carefully adding stock solution 3. Since this step is very critical, care was taken to

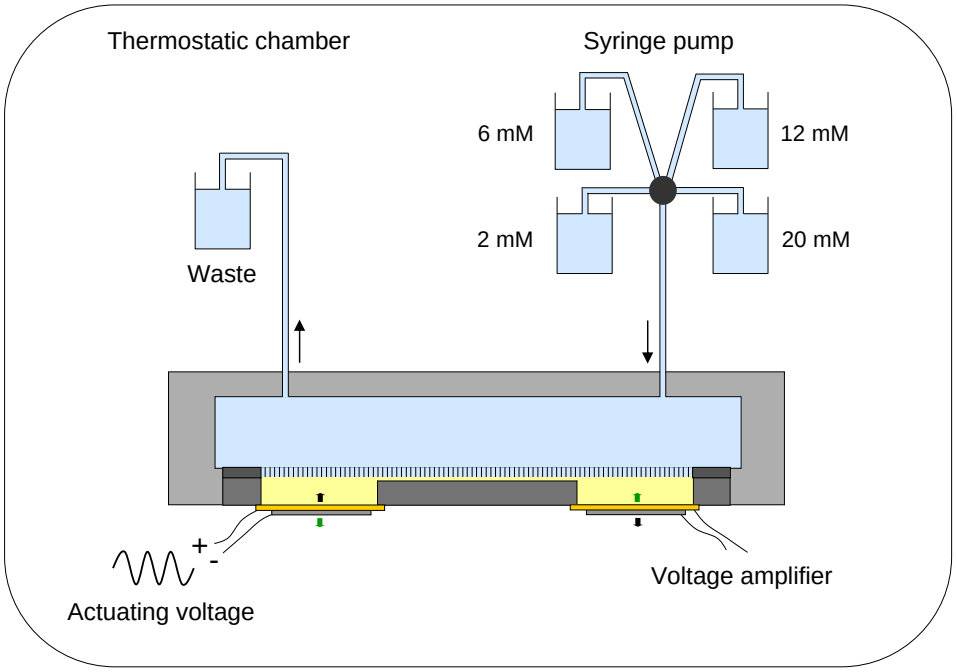

Figure 4.8: Experimental *in vitro* setup.

add the sodium hydroxide at a slow and controlled flow rate with constant mixing. If the transition is made too fast ConA tends to be denaturated and precipitates. However this process should not take too long either, because ConA has a tendency to precipitate in the absence of dextran. The solution was centrifuged at 4600 turns/min for 10 min.

One volume of solution A was put in a new recipient and the same volume of solution B (filtered through a Millex HV 0.45 μm syringe filter) was added. The obtained preparation was thoroughly mixed by shaking.

4.3.4 Experimental setup

As the viscosity of the sensitive fluid is temperature-dependent, the whole setup was located in a thermally regulated enclosure ($\pm$0.01°C) (Fig. 4.8). The temperature of the thermostatic chamber was monitored with a high precision thermometer (GMH 3710 from Greisinger GmbH) and was regulated using a Peltier element controlled by a PID (proportional-integral-derivative) algorithm implemented in LabVIEW.

The sinusoidal voltage generation and acquisition were performed us-

ing a multifunction data acquisition board (PCI-6052E from National Instrument). The actuating piezoelectric diaphragm was driven with a low-frequency sinusoidal voltage (1-5 Hz) amplified up to 30 V by means of a high voltage amplifier (WMA-02 from Falco Systems). The sensing voltage was amplified using an instrumentation amplifier (AD8661 from Analog Device). The voltage generation, acquisition and phase shift computation were performed using a LabVIEW interface. The phase shift was determined by fitting the sensing signal with a sinusoidal function using the least square regression method.

To evaluate the characteristics and response of the device, glucose measurements were performed in an isotonic saline solution which had the same composition as the sensitive fluid except dextran and ConA. This solution was characterized by physiological values of the pH and saline concentration. The two metal ions used to activate the glucose binding site of ConA, Mn^{2+} and Ca^{2+}, were added to the solution to ensure a good stability of the sensitive fluid. Sodium azide (NaN_3) was used as preservative, and concentrated (2M) D-glucose was added to increase the glucose concentration to the desired level.

The sensor was enclosed in a dedicated housing containing the solution to be measured. Glucose solutions of varying concentrations were pumped into the test cell using a computer controlled syringe pump (Tecan Cavro XCalibur). A 9-port ceramic valve was used for the evaluation of multiple test solutions.

4.4 Results and discussion

4.4.1 Demonstrating the viscosity sensing principle

Before implementing the glucose sensor, the viscosity sensing principle was first demonstrated using a system consisting of two piezoelectric diaphragms and a microchannel, which was filled with viscosity reference standards (Paragon Scientific, Ltd.). Phase shift measurements were performed with five different reference standards exhibiting dynamic viscosities ranging from 3.65–17.25 mPas (Fig. 4.9). As expected from the model, the tangent of the phase shift depends linearly upon the viscosity. The mean standard deviation was about 0.2%, which shows the potential ac-

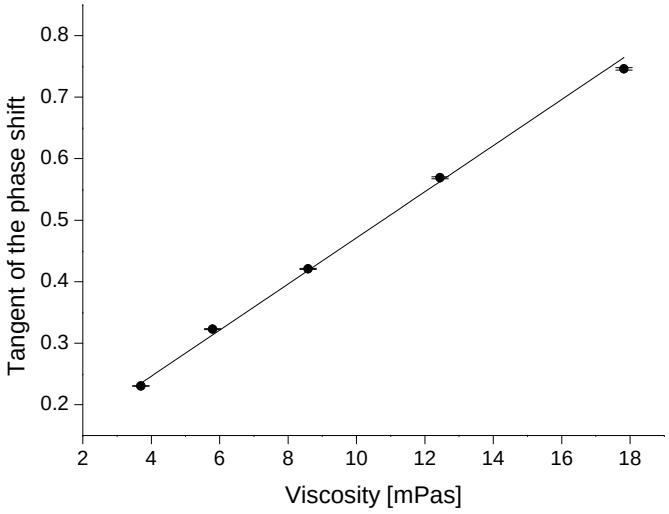

Figure 4.9: Phase shift measurements of different viscosity reference standards at 20˚C.

curacy of this detection method. Moreover, the deviation from the linear curve may be due to the need to open and change the viscosity reference standard, which may lead to systematic errors from one measurement to the other. This will not be the case for the glucose sensor, and we could therefore expect a much better reproducibility.

4.4.2 Sensor characterization at various temperatures

The sensor was characterized at 25 and 37˚C. Stepwise increasing levels of glucose concentrations (2-4-7-11-16 mM) have been used, followed by similar decreasing glucose concentrations (16-11-7-4-2 mM) (Fig. 4.10). The data indicates that the sensing principle is highly reversible; the phase shift characterizing a glucose level is the same after increasing or decreasing the glucose concentration.

The reversibility of the sensitive solution was expected since the reversibility of the ConA-saccharide binding was previously demonstrated. Nevertheless, the difficulty is the confinement of the sensitive fluid inside the sensor, provided that ConA is a small protein. The ConA hydrodynamic radius in tetramer configuration (highly prevailing at pH 7.4) is 4.4 nm whereas the nanoporous alumina membrane pores distribution was 2–4 nm. The high degree of reversibility obtained implies that ConA

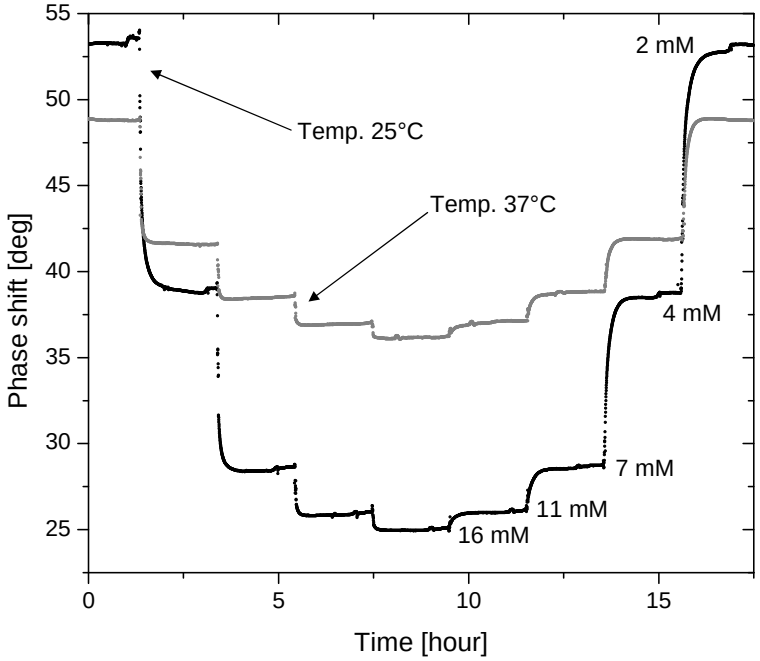

Figure 4.10: Phase shift response to stepwise increasing and decreasing glucose concentrations (2, 4, 7, 11, 16 mM) in isotonic saline solution at 25 and 37˚C.

molecules in tetramer configuration were well confined by the alumina membrane. Moreover, a good reversibility was also obtained at high glucose concentration, which emphasizes the good retention capabilities of the alumina membrane. ConA leakage should indeed be favoured at high glucose concentration, when the network ConA-dextran is untied and as a result, ConA is free to diffuse through the nanoporous membrane. Moreover, the response time of the sensor did not increase with time, indicating that dextran and ConA did not clog the pores. The sensing principle worked well, glucose diffusing freely in and out of the sensor through the nanoporous membrane, whereas the sensitive fluid was completely confined inside the sensor.

For *in vivo* applications, the sensor has to properly operate at physiological temperature. We therefore evaluated the sensor at 37˚C, to check that the temperature increase does not impede the sensor function. Potential issues are mostly related to the microfluidic part, as evaporation and air bubble formation are favoured at higher temperature. The sensor functioned well at 37˚C, which demonstrates the robustness of the sensing principle.

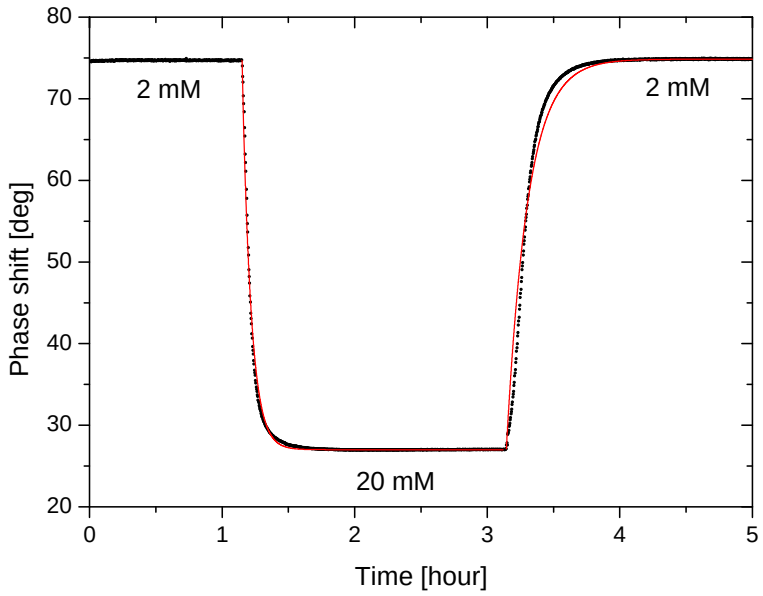

Figure 4.11: Sensor response to increasing and decreasing glucose concentrations fitted with an exponential model.

Finally, we observe that the degree of glucose-induced phase shift change is reduced by about 55% when the temperature increases. This was expected, since the sensitive fluid viscosity is highly temperature dependent. However, the reduced sensitivity at 37°C does not represent a practical limitation for the detection of the glucose concentration provided that some calibrations are carried out.

4.4.3 Sensor response dynamics

The sensor kinetics is mostly governed by the glucose diffusion through the nanoporous membrane and in the sensitive fluid. Both diffusion processes are free diffusions, approximately described by the diffusion in a semi-infinite slab whose solution is given by the error function (see section 3.5.5). The sensitive fluid is also mixed in the vicinity of the glass capillary by the alternative flow, which speeds up the sensor response compared to a purely diffusive process.

Experimentally, the diffusion of glucose in-outside of the sensor was well described by an exponential model (Fig. 4.11). The response time was determined by fitting the sensor response to glucose variations using an

exponential relationship given by

$$y = A(1 - e^{-\frac{t}{\tau}}) + B \tag{4.1}$$

where τ is the relaxation time. In sensor technology, the response time is commonly expressed as $\tau_{90\%}$, which is the response time of the sensor to reach 90% of the variation amplitude. For this exponential relationship (4.1), the response time is given by $\tau_{90\%} = \ln(10)\tau$.

The response time of the sensor was determined by fitting the sensor response to multiple glucose concentrations at 25 and 37˚C. The response time was averaged over 20 measurements for each temperature (Fig. 4.12). At 37˚C, the response time of the sensor was 3.6 ± 0.7 min when increasing glucose concentrations, and 12.8 ± 1.4 min for the decreasing case. The longer time constant related to decreasing glucose concentrations could be explained by a smaller mobility of glucose molecules in the viscous sensitive fluid with respect to the isotonic saline solution. This smaller mobility would increase the time required for glucose molecules to find a pore, consequently slowing down the diffusion process when glucose diffuse out of the sensor. Therefore, we expect that the porosity of the semi-permeable membrane affects more the glucose molecules leaving the sensor than glucose molecules entering the sensor.

The sensor kinetics was improved when increasing the temperature from 25 to 37˚C due to the reduction of the sensitive fluid viscosity. A stronger reduction of the response time was observed for increasing glucose concentration (51%) than for the decreasing case (16%). As the diffusion time in a solution is directly proportional to its viscosity, the response time reduction may be compared to the mean viscosity decrease of the sensitive fluid (38%). From these results, it seems that the glucose diffusion in the sensor directly depends on the sensitive fluid viscosity, whereas the diffusion out of the sensor is also limited by an other factor. Both diffusion in and out of the sensor were expected to strongly depend upon the viscosity and this difference is hardly explained. A hypothesis could be that the glucose diffusion out of the sensor is more importantly restricted by the membrane porosity.

The response time achieved by our device was slightly longer than our targeted 10 min response time required for a medical device. This response time may be shortened by reducing the sensor thickness since this would

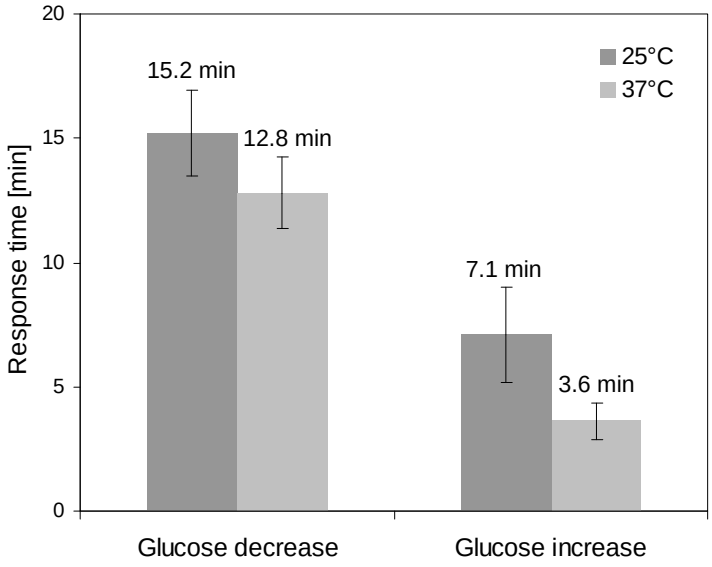

Figure 4.12: Response time of the sensor for increasing and decreasing glucose concentrations at 25 and 37˚C.

decrease the length for molecules to diffuse, and therefore would decrease the diffusion time. The relaxation time for diffusion is given by $\tau \propto L^2$, where L is the characteristic length. According to the above relation, a cavity thickness of 150 μm should achieve a response time less than 10 minutes. Such a dimension is quite standard in microengineering technologies.

4.4.4 Sensor accuracy and stability

For assessing reproducibility and stability, the sensor was tested in the most relevant physiologically glucose concentrations, namely 2 mM and 20 mM (Fig. 4.13). Seventeen full cycles performed without interruption during 70 hours demonstrated a high reversibility and stability of the sensor. The phase shift difference between 2 and 20 mM was constant throughout the measurements.

For each equilibrium value of glucose concentration, 400 measurements were averaged, leading to a mean standard deviation of 0.045 deg. The glucose sensitivity was 2.64 deg/mM, which combined with a 95% confidence interval of 0.09 deg (2σ), results in an accuracy of 0.034 mM. This value is comparable to the 1 mg/dl (0.056 mM) resolution of conventional glucose

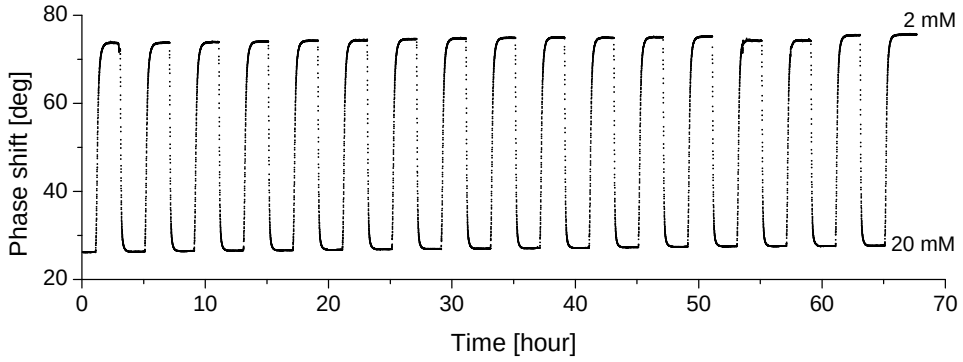

Figure 4.13: Phase shift response to seventeen full cycles of glucose concentrations (2 mM and 20 mM) in isotonic saline solution at 25˚C.

meters. In addition, when compared to a reference method, most of the glucose meters have an accuracy characterized by ∼95% of the readings in a ±20% deviation limit [90]. The sensor accuracy corresponds to a relative deviation of ±1.7% for a low hypoglycaemic value (2 mM), which confirms that the sensor resolution is accurate enough for patients monitoring. Moreover, no decrease in the sensor sensitivity was observed, demonstrating a high stability.

4.5 Conclusion

A glucose sensor demonstrator was developed and extensively tested in isotonic saline solution for physiological blood glucose concentrations between 2 and 20 mM. The quite high accuracy of ±1.7% in the hypoglycaemic range demonstrates the ability of this sensor for accurate glucose monitoring. A good degree of reversibility and stability of the sensor was also demonstrated for up to 3 days. Concerning its time response, we report a value of 12.8 min at 37˚C, which is only slightly above the 10 min required for medical applications. These results suggest that the combination of the ConA-based sensitive fluid and the microviscometer is a promising sensing principle for continuous glucose monitoring.

Chapter 5

Long term performance study of the sensor

5.1 Introduction

The sensor showed an excellent behaviour up to 3 days, which is promising for short term applications. Beside that, a long term implantable sensor is also highly desirable for diabetic patients. In this chapter, we therefore focus on the long term stability of the sensor, which is mandatory for such application.

The long term stability of the sensor was investigated by continuously cycling glucose concentrations at body temperature during 25 days. We also studied in detail the 2–4 nm nanoporous alumina membrane, which is a key for the long term stability since it has to confine the sensitive fluid whilst allowing fast glucose permeation. As ConA is a small protein, a defect-free membrane with a well defined pore size distribution is required for ensuring a perfect retention.

The size-selective diffusion in nanoporous alumina membranes was investigated using diffusion cells. ConA retention and glucose diffusion were measured using respectively ultraviolet absorption spectrometry and refractometry. In addition, the pores size distribution and the porosity were characterized using scanning electron microscopy. We also evaluated pores narrowing by atomic layer deposition as a mean to improve the retention properties of nanoporous alumina membranes.

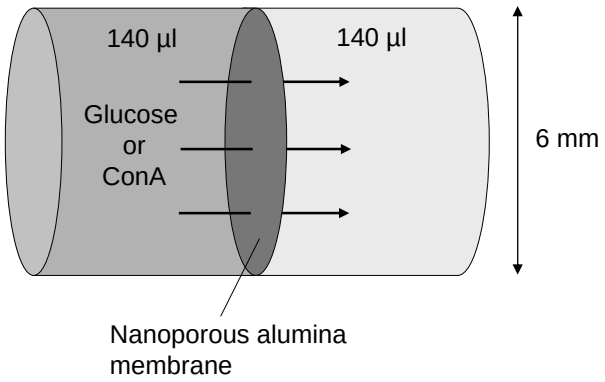

Figure 5.1: Glucose diffusion and ConA retention were evaluated using diffusion cells. The concentration of permeating molecules was monitored by refractometry or UV absorbance spectrometry during tests.

5.2 Experimental description

5.2.1 Diffusion cells

The ConA retention and glucose diffusion properties of 2–4 nm annealed nanoporous alumina membranes from Synkera Technologies were assessed using home-made diffusion cells fabricated in PMMA (poly(methyl methacrylate)) (Fig. 5.1). The two diffusion cells had a volume of 140 μl with a diffusing surface of about 28 mm^2. The two chambers were separated by the nanoporous membrane, which was glued using medical-grade adhesive epoxy (Loctite M-21HP) for ensuring leak-tight measurements. First, a solution with a given concentration of the solute was injected in the first cell while pure solvent was injected in the second one. Both cells could be stirred by standard PTFE (Teflon) magnetic stirrers. The solute diffusion was monitored by measuring the solute concentration by either refractometry or UV absorbance spectrometry.

5.2.2 Refractometry

The glucose concentration was determined by measuring the refractive index of the solution using a high precision refractometer (Bellingham and Stanley RFM 342). A volume as small as 60 μl is required for refractive index measurements carried out at the reference wavelength of 589.3 nm (the

sodium D line). The refractive index depends almost linearly on glucose concentration. An accuracy of $\sim 4 \times 10^{-4}$ is reported, which corresponds to 1.5 mM of glucose concentration.

For determining the glucose diffusion, the two diffusion cells were respectively filled with a 100 mM glucose solution and ultrapure water. Before each experiment, a two points calibration curve was performed by measuring the refractive index of the 100 mM glucose solution and ultrapure water. Both chambers were stirred during the whole experiment and measurements were recorded at regular intervals. A sample was withdrawn from the diffusion cell and placed on the refractometer crystal for the measurement, after what the solution was put back in the diffusion cell. The refractive index values were converted to glucose concentrations using the calibration curve.

5.2.3 UV absorbance spectrometry

UV absorbance spectrometry was used to quantify the concentration of ConA in solution. The tyrosine (274 nm) and tryptophan (280 nm) aromatic amino acids were detected as they are the most absorbing components of proteins. The UV light was transmitted via an optical fiber from the UV light source (DT-MINI-2-GS from Ocean Optics), then passed through the sample contained in a micro-cuvette (70 μl), and was collected by a spectrometer (USB4000-UV-VIS from Ocean Optics). The intensity of the transmitted UV light was measured by the spectrometer and a reference was used to determine the relative absorption induced by ConA. A calibration spectra was determined using isotonic saline solutions containing various ConA concentrations in the range of the sensitive fluid (0.01–0.1% [w/w]) (Fig. 5.2). A linear correlation was found between the ConA concentration and the relative absorbance at 280 nm, which was used to quantify ConA diffusion.

It is known that ConA is instable in solution and precipitates after a few hours. As its solubility is strongly increased in presence of dextran [91], the retention experiments were performed using the sensitive fluid. The two diffusion cells were respectively filled with the sensitive fluid and the isotonic saline solution. The glucose concentration of both solutions was 30 mM, a relatively high concentration where most ConA molecules are in their unbounded state, which favours their diffusion through the

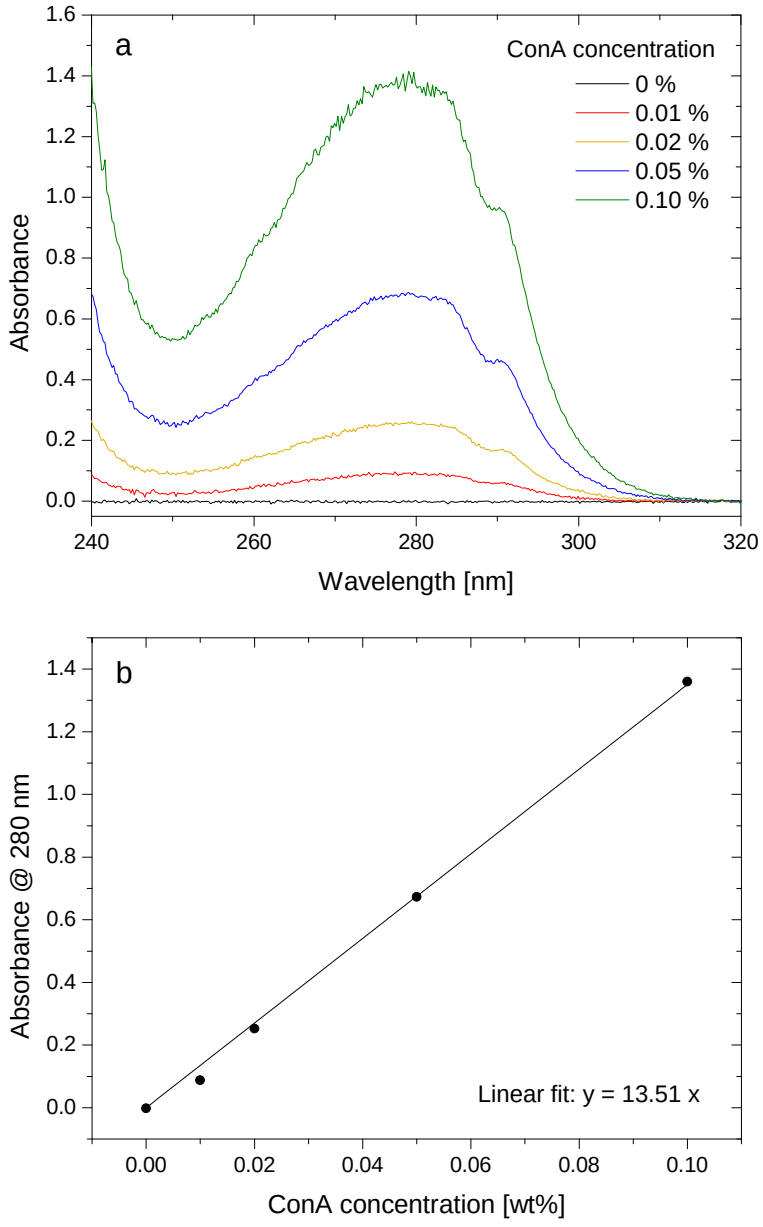

Figure 5.2: (a) UV absorbance spectra of various ConA concentrations in isotonic saline solution. (b) Calibration curve of the absorbance at 280 nm as a function of ConA concentration.

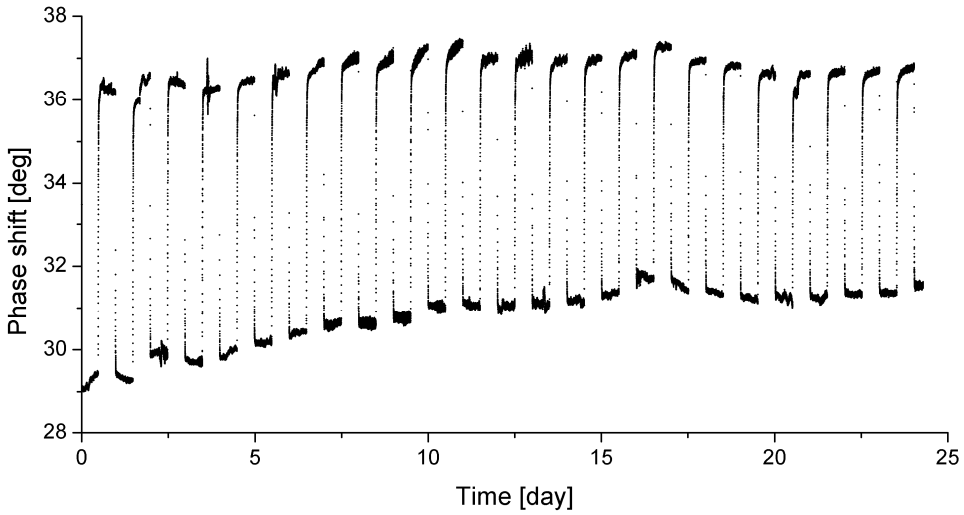

Figure 5.3: Long term measurement of glucose concentrations (2 mM and 12 mM) in isotonic saline solution at 37°C.

nanoporous membrane. For determining the ConA diffusion coefficient, a sample of isotonic saline solution was removed from the diffusion cell and placed in the micro-cuvette for recording the UV absorption spectrum. The ConA retention was evaluated by measuring its concentration in the isotonic saline solution every 24 hours, after what the solution was replaced by a fresh one.

5.3 Results and discussion

5.3.1 Long term stability of the sensor

The long term stability of the sensor at 37°C was investigated by varying glucose concentrations (2 and 12 mM) every 12 hours for a total of 25 days (Fig. 5.3). The sensor worked well during the whole experiment, glucose diffusing freely in and out of the sensor through the nanoporous membrane, whereas the sensitive fluid was still confined inside the sensor. This good behaviour throughout the experiment also demonstrates the excellent long term stability of the membrane in aqueous solution at 37°C. Moreover, the response time of the sensor did not increase with time, indicating neither dextran nor ConA clogged the pores. Beside these promising characteristics, the sensor sensitivity decreased linearly with a reduction

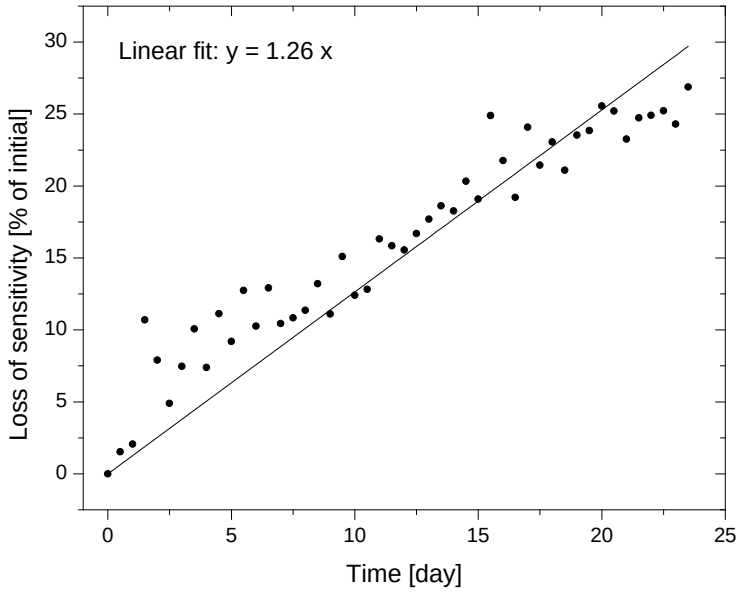

Figure 5.4: Loss of sensitivity of the long term measurement expressed as percentage of the initial sensitivity.

of 1.3% per day (Fig. 5.4). Multiple effects could account for the sensitivity reduction, as an incomplete confinement of the sensitive fluid, ConA deactivation, or mechanical fatigue of the piezoelectric diaphragms. However, the sensitive fluid showed a good stability, as it was stored at room temperature during several months without noticing any loss of sensitivity. In addition, piezoelectric diaphragms are generally used at higher frequencies, and thus the number of measuring cycles should not be an issue. Therefore, we hypothesize that the loss of sensitivity was mostly due to progressive ConA leakage through the nanoporous membrane. The ConA hydrodynamic radius (respectively 3.3 and 4.4 nm in dimer and tetramer configuration) is in fact close to the pores size distribution of the 2–4 nm nanoporous membrane.

5.3.2 Glucose diffusion in the nanoporous membrane

The glucose diffusion properties of the 2–4 nm nanoporous alumina membrane were characterized by measuring the glucose diffusion in 5 different membranes (Fig. 5.5). As expected from the diffusion cells model (see section 3.5.4), the dynamics of glucose diffusion is pretty well fitted by an

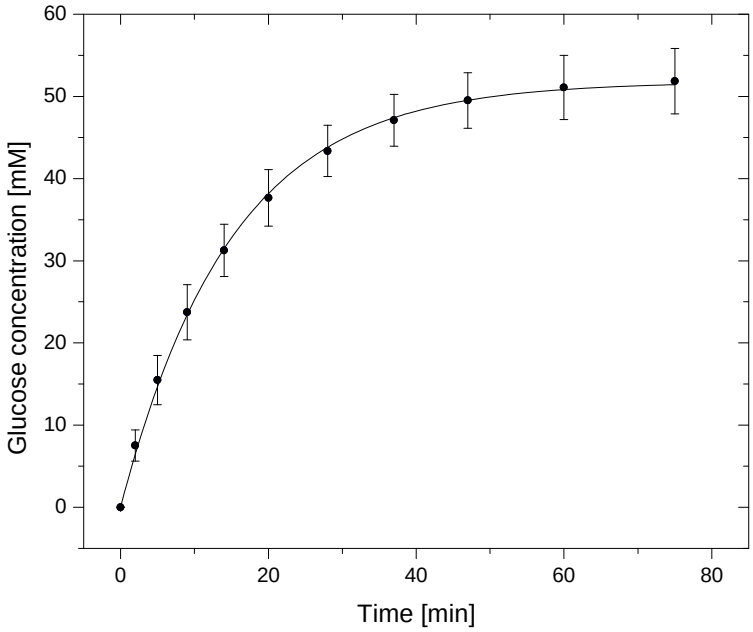

Figure 5.5: Dynamics of glucose diffusion through 5 different 2–4 nm nanoporous alumina membranes fitted by an exponential law.

exponential law. The relaxation time determined by best fitting gives a mean relaxation time of 15.3±3.5 min. The effective diffusion coefficient was calculated from the relaxation time following Eq. (3.27), which gives $(1.35 \pm 0.31) \times 10^{-4}$ mm^2/s. From these results, it comes out that the glucose diffusion coefficient in this membrane is only ∼5 times smaller than in water ($D = 6.73 \times 10^{-4}$ mm^2/s [16]). Considering the relative standard deviation of 23%, this value is of the same order of magnitude that the diffusion coefficient in a 20 nm asymmetric alumina membrane from Whatman (1.39×10^{-4} mm^2/s) and much higher than its value in a nanoporous polyethylene membrane (0.18×10^{-4} mm^2/s) [92]. This quite high diffusivity is remarkable when considering all possible effects impeding diffusion in nanoporous membranes. One important factor is the membrane porosity, which strongly reduces the active diffusing surface in nanoporous membranes. From SEM pictures, the porosity of the active layer with 13±2 nm alumina membranes was estimated to be 28.9%, which explains most of the reduction in diffusion. In addition, when moving to nanofiltration application, the free diffusion is progressively restricted when the dimensions of the pores become comparable with those of the diffusing molecules.

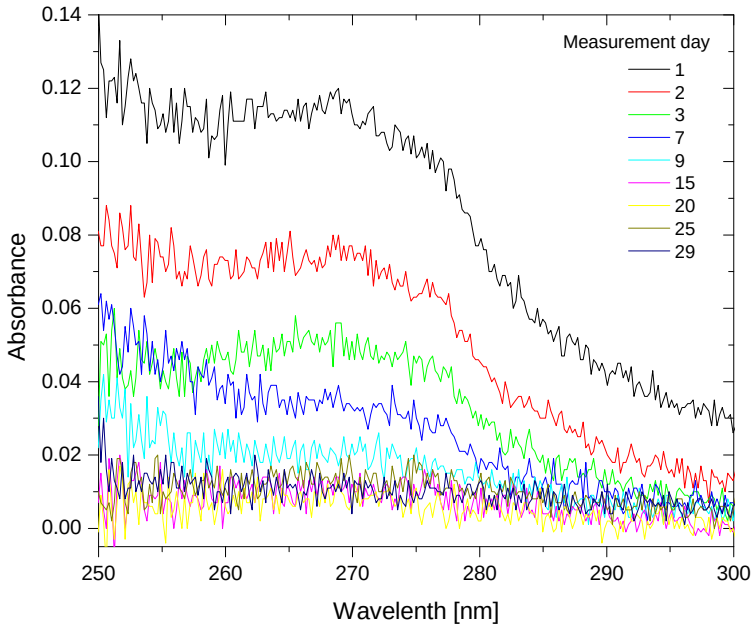

Figure 5.6: UV absorbance spectra of the retention test of the 2–4 nm alumina nanoporous membrane (unstirred solutions). Each spectrum characterizes the ConA permeation during 24 hours.

Factors explaining this limited diffusion may include an increased viscous drag in the pore, particle-pore wall interactions, as well as steric effects at the entrance of the pore [93]. With a factor of about 4 between the glucose hydrodynamic radius (0.365 nm [94]) and the pores size, we are typically in a situation where the high solute-to-pore ratio may restrict diffusion. This is confirmed by previous results which reported that glucose diffusion was already substantially reduced in a 7 nm nanoporous silicon nitride membrane [95]. However, from the quite good diffusion properties of the present membrane, it seems that the diffusion is only slightly affected, which is explained by the asymmetrical structure of the membrane. In fact, only a very thin active layer (0.5–1.5 μm) restricts diffusion whereas most of the diffusion takes place in the support layer (50 μm), which is characterized by larger pores (150–200 nm) which do not impede diffusion.

5.3.3 ConA retention by the nanoporous membrane

The ConA retention properties of 2–4 nm alumina membranes from Synkera Technologies were investigated during 35 days. We recorded the UV

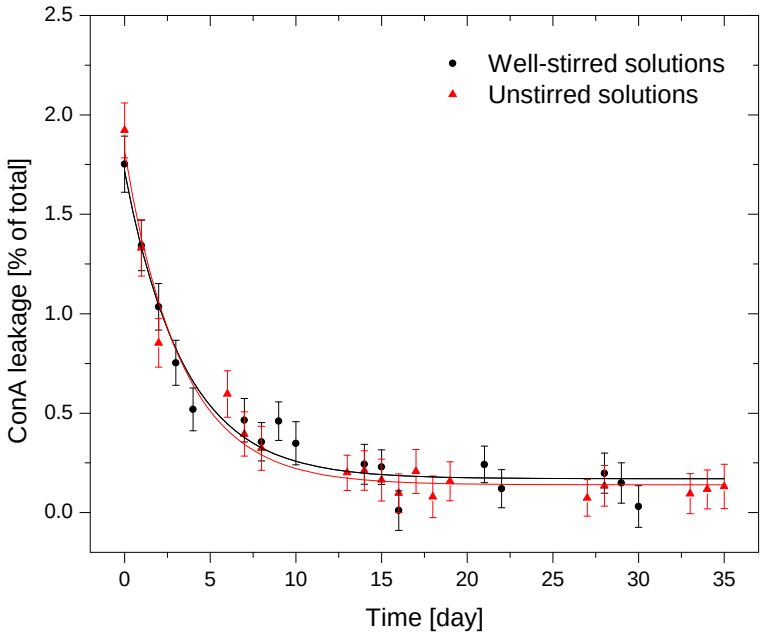

Figure 5.7: Long term ConA retention of two different 2–4 nm nanoporous alumina membranes fitted with an exponential law. ConA leakage is expressed in terms of percentage of the ConA concentration in the sensitive fluid.

absorbance spectrum of the isotonic saline solution which was in contact with the membrane during 24 hours (Fig. 5.6). A stronger absorbance is observed around a wavelength of 280 nm, indicating the presence of ConA. From these results, the ConA concentration was determined by averaging the absorbance over a 10 nm bandwidth around the peak absorbance. The error on the ConA concentration was estimated from the standard deviation of the mean absorbance and background noise. ConA leakage was finally expressed in terms of percentage of the ConA concentration in the sensitive fluid (Fig. 5.7). We performed ConA retention experiments with both well-stirred and unstirred solutions to confirm that stirring had no deleterious effect on ConA molecules (which could have eased ConA diffusion). A similar behaviour was observed for both well-stirred and unstirred solutions, which is explained by the constant quasi-equilibrium of the solutions (diffusion of a very small fraction of ConA) and the long time scale allowing diffusion in the cells. Therefore both retention experiments can be used to estimate the retention capabilities of the membrane.

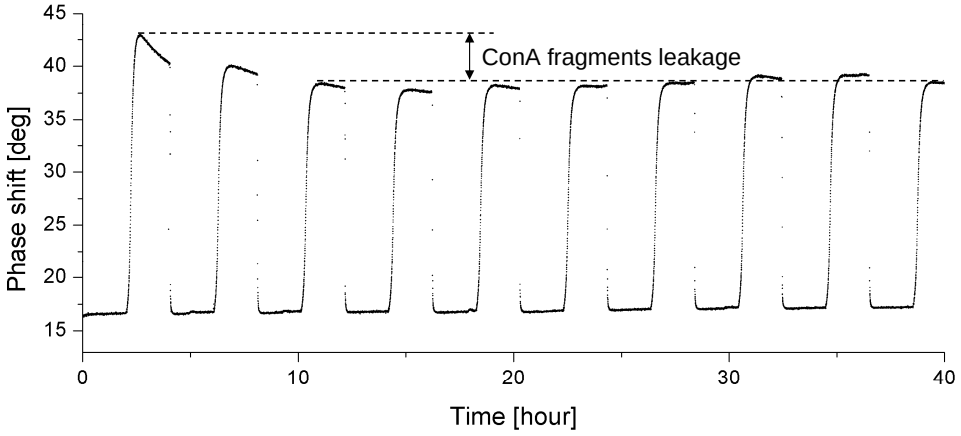

Figure 5.8: Initial sensitivity reduction of the sensor which may be due to ConA fragments leakage.

The ConA retention experiments showed a higher initial ConA leakage just after the beginning of the experiment. Then, after about 5–10 days the leakage stabilized at a lower level. In particular, ConA leakage was well described by an exponential model reaching a constant value. Initial higher leakage could be attributed to ConA fragments which are present in commercial ConA [96]. These fragments do not form tetramer and have a molecular weight 2–3 times smaller than the unaltered subunit. Due to their smaller size, ConA fragments could diffuse through the nanoporous membrane. An initial viscosity decrease of the sensitive fluid, which may be explained by leakage of ConA fragments, was also observed with the sensor. In fact, when the sensor was immersed for the first time in isotonic saline solution, the phase shift at low glucose concentration decreased during several measurements before reaching a stable value (Fig. 5.8). However, this should not affect the accuracy of the sensor and this process may be considered as a purification of the sensitive fluid. ConA could also be purified prior the preparation of the sensitive fluid if a better stability is required at the beginning of the measurement.

After that initial ConA leakage, a lower and stable value was observed with a mean leakage per day of $0.14 \pm 0.07\%$ of the initial concentration. As the measured ConA concentrations were small ($\pm 0.001\%$ [w/w]) and close to the resolution of the UV absorbance spectrometer, the error on the determination of ConA leakage was quite high. However, ConA leakage is in the same range for both experiments, thus validating the experimental

procedure despite the limited accuracy.

An almost complete retention was achieved by the membranes, which has to be emphasized given that ConA is a small protein (3.3 nm in dimer configuration). This also explains the good sensor stability observed for short-term measurements, as well as the reduction in sensitivity at large time scales. According to similar dimensions between the ConA molecules and the membrane pores size, we could have expected a complete retention. Several hypotheses could account for this small constant ConA diffusion, like a pore size distribution not as narrow as expected or some defects in the membrane structure. Therefore, ConA molecules would diffuse through a small fraction of pores outside the main distribution. The small leakage rate could also suggest that most of the ConA molecules are well confined by the nanoporous membrane. At physiological pH, the ConA tetramer configuration is highly prevailing whereas a small fraction of dimers remains. ConA tetramers would be confined by the membrane whereas dimers would freely diffuse in the isotonic saline solution. With a constant fraction of dimers and tetramers (determined by the chemical environment), the mechanism explaining constant ConA leakage would be a continuous dimer formation and diffusion.

Finally, the small constant diffusion also shows that the nanoporous membranes are close to achieve a complete retention of the sensitive fluid, which is emphasized by the much slower diffusion of ConA fragments than glucose out of the sensor (Fig. 5.8). The ConA fragments diffusion is slowed down by a reduced apparent porosity (small fraction of larger pores) and/or by interactions with the pores wall of the membrane (meaning that the pores are close to the confinement).

5.3.4 Pores size distribution

The nanoporous alumina membranes structure was investigated by scanning electron microscopy (SEM) (Fig. 5.9). These pictures confirm the highly ordered structure and well defined pores size that is expected for nanoporous alumina membranes. The 2–4 nm pores were close to the resolution of the microscope and thus we were not able to get well focused pictures. We therefore investigated the pores size distribution on a similar alumina membrane with larger pores (13 ± 2 nm from Synkera Technologies). The pores size distribution was experimentally determined using

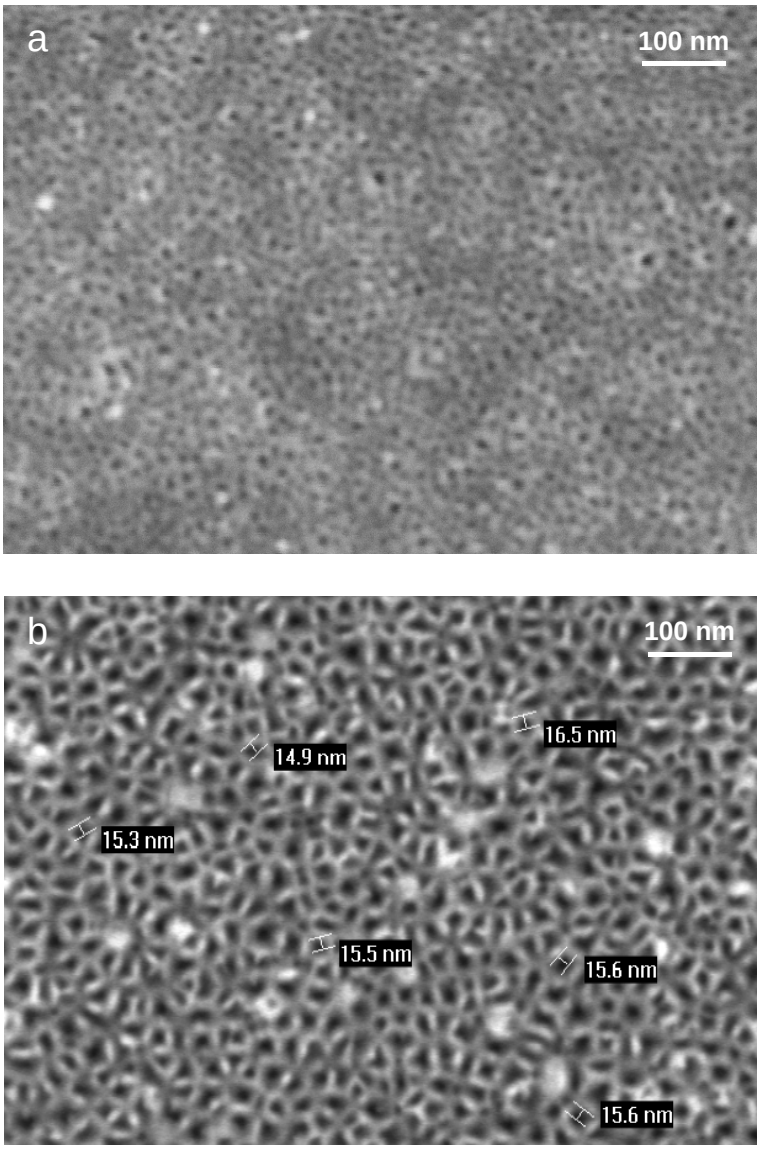

Figure 5.9: SEM pictures showing the active layer pores size of the nanoporous alumina membranes. (a) 2–4 nm membrane. (b) 13±2 nm membrane.

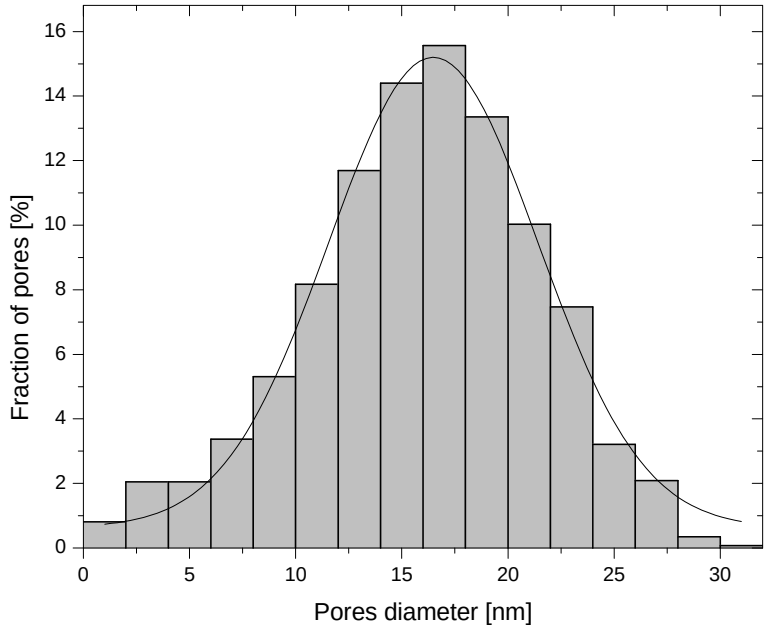

Figure 5.10: Experimental characterization (SEM pictures) of the pores size distribution of the 13 ± 2 nm membrane fitted with a Gaussian.

particles analysis. An area encompassing 2583 pores was measured on 5 SEM pictures (Fig. 5.10). The pores size distribution is well described by a Gaussian with a mean pores diameter of 16.49 nm and a standard deviation of 4.93 nm, confirming a regular pores size distribution. The mean porosity is 28.9$\pm$0.7%, which can be compared to the 37% reported for Whatman alumina membranes having a nominal pores size of 20 nm [23]. These measurements confirm that these alumina nanoporous membranes have a distribution not as narrow as expected, and as a consequence, a small fraction of pores is outside the main distribution with dimensions as large as 30 nm. The pores size distribution is also probably larger than expected for the 2-4 nm alumina membrane, which may explain the small ConA diffusion at large time scales.

5.3.5 Pores narrowing by atomic layer deposition

In numerous applications of nanofiltration in biotechnology and biomanufacturing, the precision and repeatability of the pores size of nanofiltration membranes is of high importance. Membrane manufacturing com-

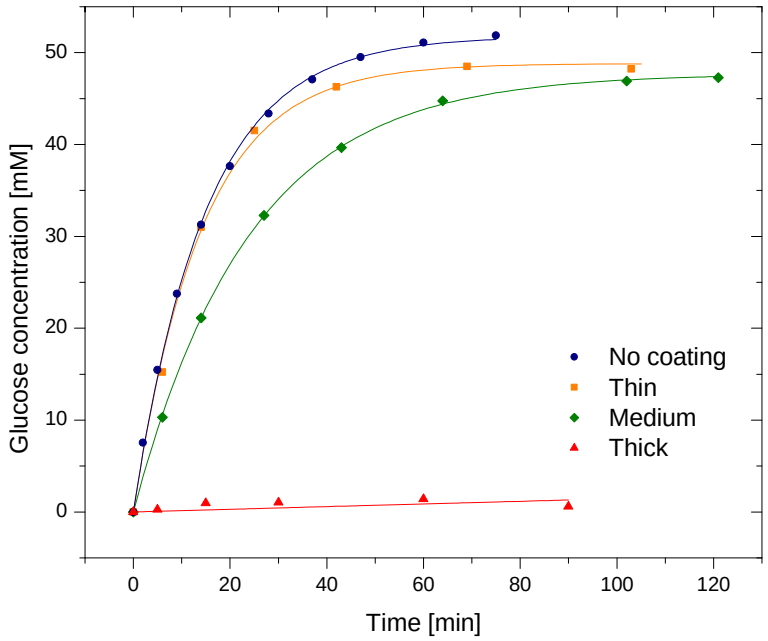

Figure 5.11: Glucose diffusion properties of 2–4 nm alumina nanoporous membranes coated with various thicknesses of Al_2O_3 using atomic layer deposition.

panies are therefore actively working on achieving precise pores size control below 2 nm while retaining narrow pore size distribution. With such membranes characteristics, we could expect a much better long term stability of the sensor in the future. For the moment, alternative solutions could be considered, like pores size reduction by atomic layer deposition. This is a gas-based, surface-driven deposition technique that is uniquely suited to coating ultrahigh aspect ratio structures such as nanopores in alumina membranes. Due to its characteristics, atomic layer deposition makes atomic scale deposition control possible, obtaining a resolution as fine as 0.1 Å per cycle.

We investigated this technology by coating the 2–4 nm membrane with Al_2O_3 (coating performed by Synkera Technologies). The coated membranes (3 different thicknesses) were characterized by their glucose diffusion properties and compared to the non-modified 2–4 nm membrane (Fig. 5.11). The thinner coating did not change the diffusion characteristics, the medium coating increased the diffusion time by 50%, and the thicker coating almost blocked the glucose diffusion. Even if the coating thickness

fine tuning was experimental, and that several iterations were required to arrive at a moderate pores size reduction, atomic layer deposition was effective in reducing the pores size. However, the major drawback of pores narrowing is the reduction of the porosity, which would significantly increase the response time of the sensor. The medium coating, which is characterized by an increase in the diffusion time of 50%, should correspond to a pores size of $\sim$1.6–3.2 nm. The pores size coating could therefore advantageously be used for small pores size adjustments but is more critical when large reductions are required.

5.4 Conclusion

The long term stability of the sensor was investigated, showing a loss of sensitivity of 1.3% per day during 25 days. As the nanoporous alumina membrane is a key for the sensor stability, its diffusion and retention properties were characterized in details. The very thin active layer of the membranes (0.5–1.5 μm) and quite high porosity (28.9%) gives remarkable diffusion properties, with only a 5-fold reduction compared to free diffusion in water. We also report an almost complete retention of ConA and a good stability in aqueous solution up to 35 days. However, a small ConA leakage remains, which could partly explain the reduction in sensitivity at large time scales. SEM pictures also confirm the highly ordered structure and well defined pores size that is expected for nanoporous alumina membranes. Finally, atomic layer deposition was effective in pores size reduction, but the porosity was strongly affected, which means that this technique can only be used for small pores size reduction. Therefore, these results confirm that nanoporous alumina membranes are well suited as size-selective interface for this sensor. However, improvements in membrane technology would be required for achieving a better long term stability.

Chapter 6

Determination of glucose in biological fluids

6.1 Introduction

The sensor is intended to be used in biological fluids such as blood or plasma, which are by far more complex than the physiological solution in which the measurements were demonstrated. Blood plasma essentially contains dissolved proteins, glucose, clotting factors, mineral ions, hormones and carbon dioxide. The small biomolecules present in blood plasma could diffuse into the sensor and potentially interfere with the measurement. In particular, small glycosylated biomolecules like peptides or lipids may compete with the binding of glucose to ConA. Moreover, the adhesion of biomolecules to surfaces could lead to biofouling of the semi-permeable membrane, which may hinder the glucose diffusion. In addition, Mn^{2+} which is used to activate one of the binding sites of ConA, only appears as trace element in blood, which could affect the stability of ConA. Checking the adequacy of our sensor for measurements in biological fluids is therefore not trivial.

In this chapter, the sensor performance in human blood serum and plasma is evaluated. The determination of glucose was first evaluated in serum, which has the advantage to contain no anticoagulant potentially interfering with the measurement. We also assessed the sensor in blood plasma containing two widely used anticoagulants, heparin and EDTA (ethylenediaminetetraacetic acid). Blood plasma is in fact more complete

than serum, still containing fibrinogens and other clotting proteins, and is therefore closer to the blood. It was also useful to assess the potential interferences with anticoagulants as an anticoagulant is added to the blood in hospital applications.

6.2 Experimental description

The sensor and experimental setup used for the measurements in human blood serum and plasma were as described in section 4.3.4. The sensor was filled with a sensitive fluid containing 2.25% [w/w] of dextran and 0.45% [w/w] of ConA. The actuating voltage and frequency were respectively 30 V and 2.5 Hz. Prior and after the measurement in serum and plasma, the sensor was exposed to the same glucose concentrations in isotonic saline solution. These reference measurements were used to assess the sensitivity and stability of the sensor in serum and plasma.

The human serum and plasma were stored frozen at -20°C. Before use, 0.1% sodium azide (NaN_3) was added as preservative, then the human serum was filtered (Millex HV 0.45 μm syringe filter) to remove aggregates which may clog the semi-permeable membrane. The blood serum and plasma samples were not dialyzed to keep all the small biomolecules which could potentially interfere with the measurement. The lower glucose concentration was therefore defined by the intrinsic concentration of serum and plasma, which was measured using a standard glucose meter (Accu-Chek). The intrinsic glucose concentration was in the physiological range (5 mM) and concentrated D-glucose (2 M) was added to increase the concentration to a hyperglycaemic value (20 mM).

6.3 Results and discussion

6.3.1 Measurements in human serum and plasma

The sensor was tested in human serum with glucose concentrations of 5 mM and 20 mM (Fig. 6.1). Nine changes of low and high glucose concentrations were performed during 17 hours. A good degree of reversibility and stability was observed, which is promising considering all possible issues arising in biological fluids. Moreover, the response time did not in-

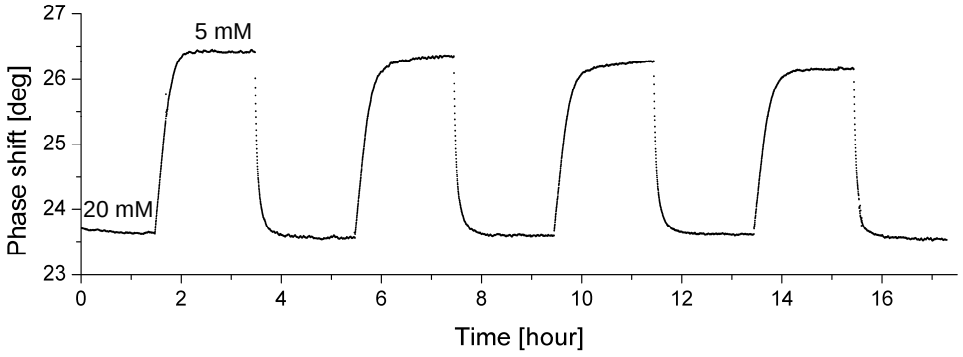

Figure 6.1: *In vitro* determination of glucose in human blood serum. Measurements carried out in original (5 mM) and glucose added (20 mM) serum at 25°C.

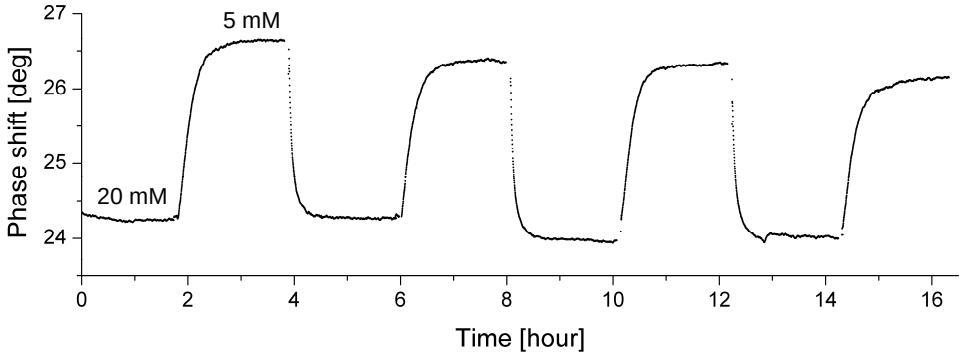

Figure 6.2: *In vitro* determination of glucose in human blood plasma containing heparin as anticoagulant.

crease with time, indicating that biofouling due to protein adsorption on the semi-permeable membrane, if any, was not an issue and that alumina nanoporous membranes are well-suited for biosensors size-selective interface in biological fluids.

In plasma containing heparin, a quite good reversibility was also observed during 16 hours (Fig. 6.2). The loss of sensitivity in plasma (heparin) is comparable to the loss of sensitivity in serum, suggesting that heparin does not interfere with the glucose determination. Heparin is a polysaccharide with multiple hydroxyl groups, which is characterized by a molecular weight ranging from 3 to 30 kDa. Therefore, heparin could diffuse

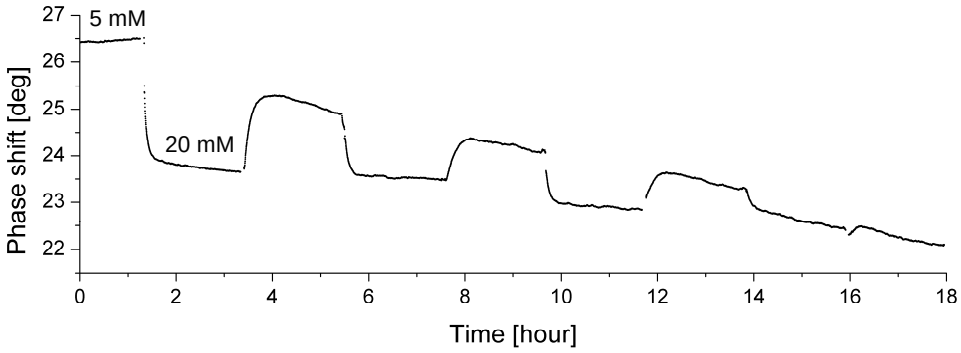

Figure 6.3: *In vitro* determination of glucose in human blood plasma containing EDTA as anticoagulant.

through the nanoporous membrane and potentially interfere with ConA. It was shown that heparin binds boronic acid moieties, which are also characterized by a high specific affinity for glucose [97]. A loss of sensitivity of 30% was reported in plasma containing heparin with a hydrogel-based glucose sensor. Fortunately, unlike boronic acid moieties, these results suggest that heparin does not interfere with ConA.

A progressive and high loss of sensitivity was observed in plasma containing EDTA (Fig. 6.3). The demonstrator did not recover its initial sensitivity when subsequently immersed in isotonic saline solution, suggesting that EDTA irreversibly altered the sensitive fluid. EDTA is known to be a strong chelating agent, sequestering metal ions such as Ca^{2+} and Fe^{3+}. After being bound by EDTA, metal ions remain in solution but exhibit a reduced reactivity. EDTA is therefore probably binding the two metal ions, Mn^{2+} and Ca^{2+}, which are used to activate the glucose binding sites of ConA. As a result, the protein undergoes a conformational change which strongly decreases its affinity for glucose. EDTA is therefore not compatible with this ConA-based measurement. However, this does not matter much, given that EDTA is used for blood samples but never in the human body. However, if required, a sensitive fluid based on boronic acid moieties could be used, as it was shown to measure glucose in plasma containing EDTA with a good sensitivity [97].

Table 6.1: Sensitivity in human blood serum and plasma compared to the sensitivity in isotonic saline solution.

Sensitivity compared to:	Serum	Plasma (heparin)
Solution before serum	74.2%	85.4%
Solution after serum	89.2%	97.7%

6.3.2 Molecular interference with sensitivity to glucose

From these measurements, it comes out that the sensor sensitivity in serum partly decreases compared to the sensitivity in isotonic saline solution. After evaluation of the glucose in serum, the sensor recovers its initial sensitivity for isotonic saline solution. Therefore the loss of sensitivity is reversible, suggesting that small biological molecules, most likely glycosylated peptides or lipids, may diffuse into the sensor and compete with the binding of glucose to ConA.

The loss of sensitivity due to molecular interferences was evaluated by averaging the sensor sensitivity in isotonic saline solution (prior and after the measurement in serum/plasma) and in serum/plasma (Tab. 6.1). With a reversible sensitivity reduction estimated to 10–20%, these measurements indicate that there is only a minimal amount of interferences with foreign species. Therefore, these experiments confirm that despite a slight loss in sensitivity, the sensitivity of the sensor in serum and plasma is still high enough for glucose monitoring.

6.3.3 Sensitive fluid stability in serum and plasma

Despite the quite good stability, a slight decrease of sensitivity was observed in serum, plasma and in isotonic saline solution. For determining whether the serum and plasma affect the measurement stability, the loss of sensitivity of the sensor was assessed in serum/plasma, and in isotonic saline solution prior and after the measurement in serum/plasma (Fig. 6.4). The loss of sensitivity was slightly higher in serum than in isotonic saline solution while it was comparable in plasma and isotonic saline solution. We can hardly conclude on the measurement stability in serum and plasma from these results. However, other results (data not shown) tend to show that the sensor is not as stable in serum/plasma as in isotonic saline solution.

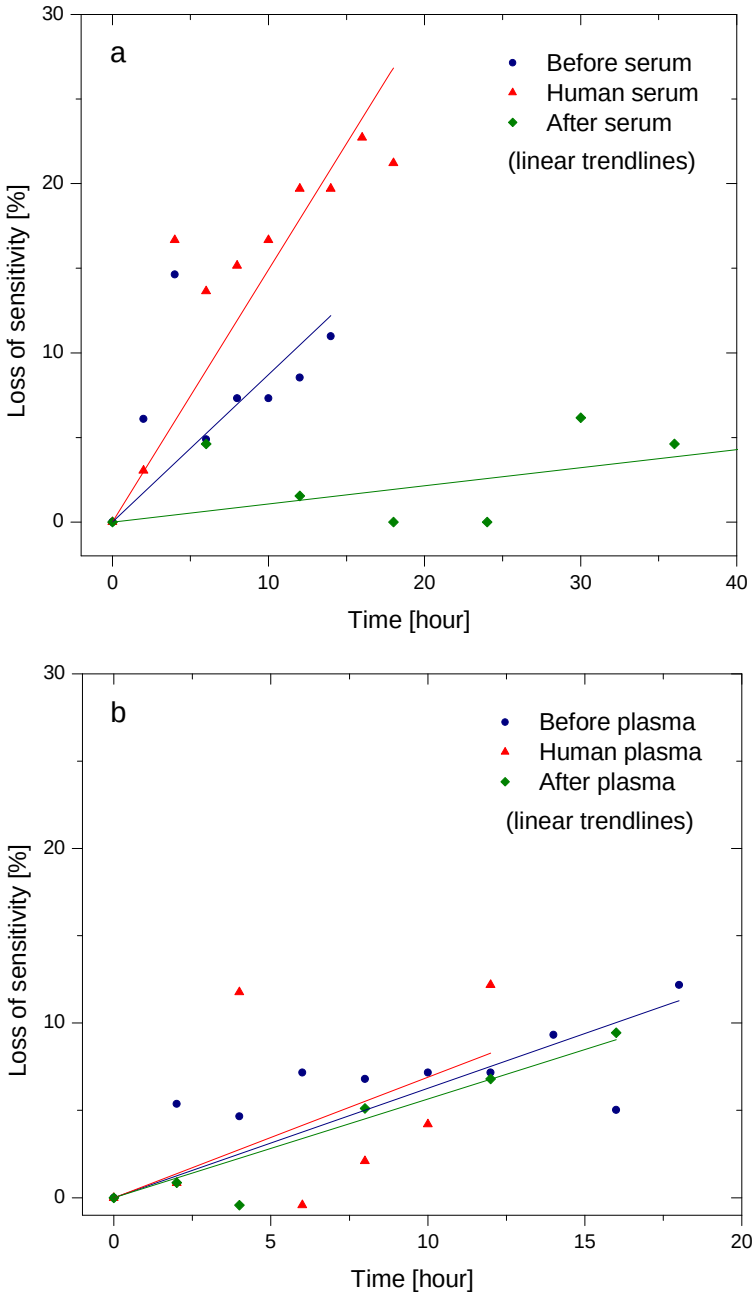

Figure 6.4: Loss of sensitivity of the sensor in human blood serum (a) and plasma (b) compared to isotonic saline solution (prior and after the measurement in serum/plasma).

Given the complexity of the serum/plasma composition, the lower stability in serum/plasma may have multiple origins. A hypothesis explaining this lower stability may be ConA deactivation. In isotonic saline solution, the two metal ions used to activate the glucose binding sites of ConA (Ca^{2+} and Mn^{2+}) are present, whereas in blood only Ca^{2+} appears in a significant concentration. Therefore, ConA stability in serum/plasma could be altered by the lack of Mn^{2+}. This hypothesis could be confirmed by testing the sensor in isotonic saline solution without Mn^{2+}, or alternatively by adding Mn^{2+} in serum/plasma. If this hypothesis proves to be correct, Ca^{2+} could be used for the two binding sites of ConA, which would have the advantage to be closer to *in vivo* conditions, and may therefore improve the sensor stability. Alternative hypotheses could include a favoured ConA leakage through the nanoporous membrane or a deleterious effect of small diffusing biomolecules on ConA. More testing would be required to fully characterize the stability of the sensitive fluid in biological fluids. However, although the stability seems lower in serum and plasma, it still remains good enough for short term monitoring.

6.4 Conclusion

The sensor was assessed in human blood serum and plasma, showing a quite good reversibility and stability. The response time did not increase with time, indicating that biofouling of the nanoporous membrane, if any, was not an issue. We report a reversible sensitivity reduction of 10–20% which is attributed to molecular interferences, most likely small glycosylated biomolecules. The sensor stability is also not as good in serum and plasma as in isotonic saline solution, which may be explained by the lack of Mn^{2+} in blood which could favour ConA deactivation. However, the sensitivity and stability is still high enough for short term monitoring, which is promising given the difficulty in measuring in biological fluids. The sensor is also compatible with heparin, which could be of high importance for hospital applications. Potential improvements include using Ca^{2+} for the two binding sites of ConA as Ca^{2+} is present in blood, and reducing the pores size of the nanoporous membrane to prevent most of interfering biomolecules from entering the sensor.

Chapter 7

Conclusion

A viscosity-dependent affinity sensor for continuous monitoring of glucose in biological fluids was developed using Concanavalin A in dextran as sensing fluid. A nanoporous alumina membrane was used as size-selective interface and the viscosity was detected using a flow-resisting microchannel. An analytical model was derived, showing that the relaxation time of the system is directly proportional to the liquid viscosity. The sensor was extensively tested in isotonic saline solution for physiological blood glucose concentrations between 2 and 20 mM, demonstrating an excellent reversibility and stability for up to 3 days. The quite low standard deviation of about 0.017 mM demonstrates the ability of this sensor for accurate glucose monitoring. Concerning its time response, we report a value of 12.8 min at 37 ˚C, which is in line with the 10 min required for medical applications.

The long term stability of the sensor was further investigated for evaluating its potential as an implantable glucose sensor. Despite the excellent short term stability, a progressive loss of sensitivity of about 1.3% per day was observed. Concanavalin A retention by the alumina nanoporous membrane was assessed by ultraviolet absorbance spectrometry. We measured Concanavalin A leakage of about 0.2% per day, which at least partly explains the long term sensitivity reduction of the sensor.

The sensor was finally evaluated in human blood serum and plasma, showing a good degree of reversibility and stability over 17 hours, meaning that the sensitive fluid remained chemically quite stable in presence of plasma and that biofouling of the alumina membrane, if any, was not an issue. A reversible decrease in sensitivity of 10–20% was observed, sug-

gesting that small biological molecules, most likely glycosylated peptides or lipids, may diffuse into the sensor and compete with the binding of glucose to ConA. However, these experiments confirm that despite a slight loss in sensitivity, the sensitivity of the sensor in blood plasma is still high enough for glucose monitoring.

In conclusion, these results suggest that the combination of the ConA-based sensitive fluid and the microviscometer is a promising sensing principle for continuous glucose monitoring in blood. The overall performance of the sensor still need to be improved, but technological solutions exit. Companies are actively working on nanofiltration membranes, which should increase the long term stability of the sensor by allowing a better retention of the sensitive fluid. In addition, a higher molecular weight sensitive fluid like a boronic acid based polymeric mixture could also be considered for improving the sensor stability. Finally, future research should address the sensor miniaturization using microfabrication technologies. Further work could also include extensive testing in human whole blood.

Bibliography

[1] D. M. Nathan. Long-term complications of diabetes mellitus. *The New England Journal of Medicine*, 328:1676–1685, 1993.

[2] C. D. Saudek, R. L. Derr, and R. R. Kalyani. Assessing glycemia in diabetes using self-monitoring blood glucose and hemoglobin A1c. *Journal of the American Medical Association*, 295:1688–1697, 2006.

[3] A. Barraud. *Molecular selective interface for an implantable glucose sensor based on the viscosity variation of a sensitive fluid containing dextran and concanavalin A*. PhD thesis, Ecole Polytechnique Fédérale de Lausanne, 2009.

[4] G. Reach and G. S. Wilson. Can continuous glucose monitoring be used for the treatment of diabetes. *Analytical Chemistry*, 64(6):381–386, 1992.

[5] D. C. Klonoff. Continuous glucose monitoring roadmap for 21st century diabetes therapy. *Diabetes Care*, 28(5):1231–1239, 2005.

[6] J. Wang. Electrochemical glucose biosensors. *Chemical Reviews*, 108(2):814–825, 2008.

[7] A. Heller and B. Feldman. Electrochemical glucose sensors and their applications in diabetes management. *Chemical Reviews*, 108(7):2482–2505, 2008.

[8] S. J. Finney, C. Zekveld, A. Elia, and T. W. Evans. Glucose control and mortality in critically ill patients. *Journal of the American Medical Association*, 290(15):2041–2047, 2003.

[9] G. Van den Bergue, P. Wouters, F. Weekers, C. Verwaest, F. Brunyninckx, M. Schetz, D. Vlasselaers, P. Ferdinande, P. Lauwers, and R. Bouillon. Intensive insulin therapy in critically ill patients. *The New England Journal of Medicine*, 345(19):1359–1367, 2001.

[10] J. S. Krinsley. Association between hyperglycemia and increased hospital mortality in a heterogeneous population of critically ill patients. *Mayo Clinic Proceedings*, 78:1471–1478, 2003.

[11] J. S. Krinsley. Effect of an intensive glucose management protocol on the mortality of critically ill adult patients. *Mayo Clinic Proceedings*, 79(8):992–1000, 2004.

[12] P. A. Goldberg, M. D. Siegel, R. R. Russell, R. S. Sherwin, J. I. Halickman, D. A. Cooper, J. D. Dziura, and S. E. Inzucchi. Experience with the Continuous Glucose Monitoring System® in a medical intensive care unit. *Diabetes Technology & Therapeutics*, 6(3):339–347, 2004.

[13] H. G. Piper, J. L. Alexander, A. Shukla, F. Pigula, J. M. Costello, P. C. Laussen, T. Jaksic, and M. S. D. Agus. Real-time continuous glucose monitoring in pediatric patients during and after cardiac surgery. *Pediatrics*, 118(3):1176–1184, 2006.

[14] U. Holzinger, J. Warszawska, R. Kitzberg, M. Wewalka, W. Miehsler, H. Herkner, and C. Mald. Real-time continuous glucose monitoring in critically ill patients a prospective randomized trial. *Diabetes Care*, 33(3):467–472, 2010.

[15] A. M. Corstjens, J. J. M. Ligtenberg, I. C. C. Van der Horst, R. Spanjersberg, J. S. W. Lind, J. E. Tulleken, J. H. J. M. Meertens, and J. G. Zijlstra. Accuracy and feasibility of point-of-care and continuous blood glucose analysis in critically ill ICU patients. *Critical Care*, 10(5):135–142, 2006.

[16] S. Kanji, J. Buffie, B. Hutton, P. Bunting, A. Singh, K. McDonald, D. Fergusson, L. McIntyre, and P. Hebert. Reliability of point-of-care testing for glucose measurement in critically ill adults. *Critical Care Medicine*, 33(12):2778–2785, 2005.

[17] D. Vlasselaers, L. Schaupp, I. Van den Heuvel, J. Mader, M. Bodenlenz, M. Suppan, P. Wouters, M. Ellmerer, and G. Van den Berghe. Monitoring blood glucose with microdialysis of interstitial fluid in critically ill children. *Clinical Chemistry*, 53:536–537, 2007.

[18] J. S. Schultz, S. Mansouri, and I. J. Goldstein. Affinity sensor: a new technique for developing implantable sensors for glucose and other metabolites. *Diabetes Care*, 5(3):245–253, 1982.

[19] R. Ballerstadt and R. Ehwald. Suitability of aqueous dispersions of dextran and concanavalin A for glucose sensing in different variants of the affinity sensor. *Biosensors and Bioelectronics*, 9(8):557–567, 1994.

[20] R. Ballerstadt, A. Polak, A. Beuhler, and J. Frye. In vitro long-term performance study of a near-infrared fluorescence affinity sensor for glucose monitoring. *Biosensors and Bioelectronics*, 19(8):905–914, 2004.

[21] R. Ballerstadt and J. S. Schultz. A fluorescence affinity hollow fiber sensor for continuous transdermal glucose monitoring. *Analytical Chemistry*, 72(17):4185–4192, 2000.

[22] S. Mansouri and J. S. Schultz. A miniature optical glucose sensor based on affinity binding. *Nature biotechnology*, 2:885–890, 1984.

[23] R. J. Russell and M. V. Pishko. A fluorescence-based glucose biosensor using concanavalin A and dextran encapsulated in a poly(ethylene glycol) hydrogel. *Analytical Chemistry*, 71(15):3126–3132, 1999.

[24] T. D. James, K. R. A. S. Sandanayake, and S. Shinkai. Saccharide sensing with molecular receptors based on boronic acid. *Angewandte Chemie International Edition in English*, 35:1910–1922, 1996.

[25] H. Fang, G. Kaur, and B. Wang. Progress in boronic acid-based fluorescent glucose sensors. *Journal of Fluorescence*, 14(5):481–489, 2004.

[26] S. Li, E. N. Davis, J. Anderson, Q. Lin, and Q. Wang. Development of boronic acid grafted random copolymer sensing fluid for continuous glucose monitoring. *Biomacromolecules*, 10(1):113–118, 2009.

[27] X. Huang, S. Li, J. S. Schultz, Q. Wang, and Q. Lin. A MEMS affinity glucose sensor using a biocompatible glucose-responsive polymer. *Sensors and Actuators B: Chemical*, 140(2):603–609, 2009.

[28] Y. Zhao, S. Li, A. Davidson, B. Yang, Q. Wang, and Q. Lin. A MEMS viscometric sensor for continuous glucose monitoring. *Journal of Micromechanics and Microengineering*, 17:2528–2537, 2007.

[29] U. Beyer, D. Schafer, A. Thomas, H. Aulich, U. Haueter, B. Reihl, and R. Ehwald. Recording of subcutaneous glucose dynamics by viscometric affinity sensor. *Diabetologia*, 44:416–423, 2001.

[30] P. Diem, L. Kalt, U. Haueter, L. Krinelke, R. Fajfr, B. Reihl, and U. Beyer. Clinical performance of a continuous viscometric affinity sensor for glucose. *Diabetes Technology & Therapeutics*, 6(6):790–799, 2004.

[31] K. O. Kyvik, J. Traulsen, B. Reinholdt, and A. Frøland. The exactech blood glucose testing system. *Diabetes Research and Clinical Practice*, 10(1):85–90, 1990.

[32] A. E. G. Cass, G. Davis, G. D. Francis, H. A. O. Hill, W. J. Aston, I. J. Higgins, E. V. Plotkin, D. L. Scott, and A. P. F. Turner. Ferrocene-mediated enzyme electrode for amperometric determination of glucose. *Analytical Chemistry*, 56(4):667–671, 1984.

[33] J. D. Newman and A. P. F. Turner. Home blood glucose biosensors: a commercial perspective. *Biosensors and Bioelectronics*, 20(12):2435–2453, 2005.

[34] Symposium on potentially implantable glucose sensors. *Diabetes Care*, 5:147–283, 1982.

[35] J. Mastrototaro. The Minimed continuous glucose monitoring system (CGMS). *Journal of Pediatric Endocrinology & Metabolism*, 12(Suppl 3):751–758, 1999.

[36] J. Mastrototaro. The Minimed continuous glucose monitoring system. *Diabetes Technology & Therapeutics*, 2(Suppl 1):S13–S18, 2000.

[37] J. S. Skyler. Continuous glucose monitoring: an overview of its development. *Diabetes Technology & Therapeutics*, 11(Suppl 1):S5–S10, 2009.

[38] K. J. Wientjes, P. Vonk, Y. Vonk-van Klei, A. J. M. Schoonen, and N. W. Kossen. Microdialysis of glucose in subcutaneous adipose tissue up to 3 weeks in healthy volunteers. *Diabetes Care*, 21(9):1481–1488, 1998.

[39] A. Maran, C. Crepaldi, A. Tiengo, G. Grassi, E. Vitali, G. Pagano, S. Bistoni, G. Calabrese, F. Santeusanio, F. Leonetti, M. Ribaudo,

U. Di Mario, G. Annuzzi, S. Genovese, G. Riccardi, M. Previti, D. Cucinotta, F. Giorgino, A. Bellomo, R. Giorgino, A. Poscia, and M. Varalli. Continuous subcutaneous glucose monitoring in diabetic patients. *Diabetes Care*, 25(2):347–352, 2002.

[40] T. Kubiak, B. Wörle, B. Kuhr, I. Nied, G. Gläsner, N. Hermanns, B. Kulzer, and T. Haak. Microdialysis-based 48-hour continuous glucose monitoring with glucoDay: Clinical performance and patients' acceptance. *Diabetes Technology & Therapeutics*, 8(5):570–575, 2006.

[41] A. Poscia, M. Mascini, D. Moscone, M. Luzzana, G. Caramenti, P. Cremonesi, F. Valgimigli, C. Bongiovanni, and M. Varalli. A microdialysis technique for continuous subcutaneous glucose monitoring in diabetic patients (part 1). *Biosensors and Bioelectronics*, 18(7):891–898, 2003.

[42] M. Varalli, G. Marelli, A. Maran, S. Bistoni, M. Luzzana, P. Cremonesi, G. Caramenti, F. Valgimigli, and A. Poscia. A microdialysis technique for continuous subcutaneous glucose monitoring in diabetic patients (part 2). *Biosensors and Bioelectronics*, 18(7):899–905, 2003.

[43] J. A. Tamada, N. J. V. Bohannon, and R. O. Potts. Measurement of glucose in diabetic subjects using noninvasive transdermal extraction. *Nature Medicine*, 1:1198–1201, 1995.

[44] M. J. Tierney, Y. J. Jayalakshmi, N. A. Parris, M. P. Reidy, C. Uhegbu, and P. Vijayakumar. Design of a biosensor for continual, transdermal glucose monitoring. *Clinical Chemistry*, 45:1681–1683, 1999.

[45] S. K. Garg, R. O. Potts, N. R. Ackerman, S. J. Fermi, J. A. Tamada, and H. P. Chase. Correlation of fingerstick blood glucose measurements with GlucoWatch biographer glucose results in young subjects with type 1 diabetes. *Diabetes Care*, 22(10):1708–1714, 1999.

[46] H. P. Chase, R. Beck, W. Tamborlane, B. Buckingham, N. Mauras, E. Tsalikian, T. Wysocki, S. Weinzimer, C. Kollman, K. Ruedy, and D. Xing. A randomized multicenter trial comparing the glucowatch biographer with standard glucose monitoring in children with type 1 diabetes. *Diabetes Care*, 28(5):1101–1106, 2005.

[47] A. Caduff, E. Hirt, Y. Feldman, Z. Ali, and L. Heinemann. First human experiments with a novel non-invasive, non-optical continuous glucose monitoring system. *Biosensors and Bioelectronics*, 19(3):209–217, 2003.

[48] A. Pfützner, A. Caduff, M. Larbig, T. Schrepfer, and T. Forst. Impact of posture and fixation technique on impedance spectroscopy used for continuous and noninvasive glucose monitoring. *Diabetes Technology & Therapeutics*, 6(4):435–441, 2004.

[49] I. M. E. Wenthold, J. B. Hoekstra, A. Zwart, and J. H. DeVries. Pendra goes dutch: lessons for the CE mark in Europe. *Diabetologia*, 48(6):1055–1058, 2005.

[50] G. McGarraugh. The chemistry of commercial continuous glucose monitors. *Diabetes Technology & Therapeutics*, 11:S17–S24, 2009.

[51] C. M. Girardin, C. Hulot, M. Gonthier, and D. Delvin. Continuous glucose monitoring: A review of biochemical perspectives and clinical use in type 1 diabetes. *Clinical Biochemistry*, 42(3):136–142, 2009.

[52] J. Brauker. Continuous glucose sensing: Future technology developments. *Diabetes Technology & Therapeutics*, 11(Suppl 1):S25–S36, 2009.

[53] J. Mastrototaro, J. Shin, A. Marcus, and G. Sulur. The accuracy and efficacy of real-time continuous glucose monitoring sensor in patients with type 1 diabetes. *Diabetes Technology & Therapeutics*, 10(5):385–390, 2008.

[54] I. J. Goldstein, C. E. Hollerman, and E. E. Smith. Protein-carbohydrate interaction. II. Inhibition studies on the interaction of concanavalin A with polysaccharides. *Biochemistry*, 4(5):876–883, 1965.

[55] D. Meadows and J. S. Schultz. Fiber-optic biosensors based on fluorescence energy transfer. *Talanta*, 35(2):145–150, 1988.

[56] D. L. Meadows and J. S. Schultz. Design, manufacture and characterization of an optical fiber glucose affinity sensor based on an homogeneous fluorescence energy transfer assay system. *Analytica Chimica Acta*, 280(1):21–30, 1993.

[57] R. Ballerstadt and J. S. Schultz. Competitive-binding assay method based on fluorescence quenching of ligands held in close proximity by a multivalent receptor. *Analytica Chimica Acta*, 345:203–212, 1997.

[58] G. H. McKenzie, W. H. Sawyer, and L. W. Nichol. The molecular weight and stability of concanavalin A. *Biochimica et Biophysica Acta (BBA) - Protein Structure*, 263(2):283–293, 1972.

[59] R. Ballerstadt, A. Gowda, and R. McNichols. Fluorescence resonance energy transfer-based near-infrared fluorescence sensor for glucose monitoring. *Diabetes Technology & Therapeutics*, 6(2):191–200, 2004.

[60] R. Ballerstadt, C. Evans, A. Gowda, and R. McNichols. In vivo performance evaluation of a transdermal near-infrared fluorescence resonance energy transfer affinity sensor for continuous glucose monitoring. *Diabetes Technology & Therapeutics*, 8(3):296–311, 2006.

[61] R. Ehwald, R. Ballerstadt, and H. Dautzenberg. Viscometric affinity assay. *Analytical biochemistry*, 234:1–8, 1996.

[62] U. Beyer, Ehwald R., and L.-G. Fleischer. Post-stress thickening of dextran/concanavalin A solutions used as sensitive fluids in a viscosimetric affinity assay for glucose. *Biotechnology Progress*, 13(6):722–726, 1997.

[63] X. Huang, S. Li, J. Schultz, Q. Wang, and Q. Lin. A capacitive MEMS viscometric sensor for affinity detection of glucose. *Journal of Microelectromechanical Systems*, 18(6):1246–1254, 2009.

[64] S. Kuenzi, E. Meurville, E. Grandjean, S. Straessler, and P. Ryser. Contactless rotational concentric microviscometer. *Sensors and Actuators A: Physical*, 167(2):194–203, 2011.

[65] S. Kuenzi. *Implantable glucose sensor: an approach based on a rotating microviscometer combined with a sensitive liquid containing dextran and concanavalin A*. PhD thesis, Ecole Polytechnique Fédérale de Lausanne, 2007.

[66] S. Kuenzi, E. Meurville, and P. Ryser. Automated characterization of dextran/concanavalin A mixtures–a study of sensitivity and temper-

ature dependence at low viscosity as basis for an implantable glucose sensor. *Sensors and Actuators B: Chemical*, 146(1):1–7, 2010.

[67] G. M. Edelman, B. A. Cunningham, G. N. Reeke, J. W. Becker, M. J. Waxdal, and J. L. Wang. The covalent and three-dimensional structure of concanavalin A. *Proceedings of the National Academy of Sciences of the United States of America*, 69(9):2580–2584, 1972.

[68] D. F. Senear and D. C. Teller. Effects of saccharide and salt binding on dimer-tetramer equilibrium of concanavalin A. *Biochemistry*, 20(11):3083–309, 1981.

[69] M. Huet. Factors affecting the molecular structure and the agglutinating ability of concanavalin A and other lectins. *European Journal of Biochemistry*, 59(2):627–632, 1975.

[70] G. M. Bradbrook, T. Gleichmann, S. J. Harrop, J. Habash, J. Raftery, J. Kalb, J. Yariv, I. H. Hillier, and J. R. Helliwell. X-ray and molecular dynamics studies of concanavalin A glucoside and mannoside complexes. relating structure to thermodynamics of binding. *Journal of the Chemical Society, Faraday Transactions*, 94(11):1603–1611, 1998.

[71] G. N. Reeke, J. W. Becker, and G. M. Edelman. The covalent and three-dimensional structure of concanavalin A. IV. Atomic coordinates, hydrogen bonding, and quaternary structure. *Journal of Biological Chemistry*, 250(4):1525–1547, 1975.

[72] S. H. Koenig, C. F. Brewer, and R. D. Brown. Conformation as the determinant of saccharide binding in concanavalin A: Ca^{2+}–concanavalin A complexes. *Biochemistry*, 17(20):4251–4260, 1978.

[73] C. E. Richardson and W. D. Behnke. Physical-chemical studies on role of metal-ions in concanavalin A. *Journal of Molecular Biology*, 102(3):441–451, 1976.

[74] R. D. Brown, C. F. Brewer, and S. H. Koenig. Conformation states of concanavalin A: Kinetics of transitions induced by interaction with Mn^{2+} and Ca^{2+} ions. *Biochemistry*, 16(17):3883–3896, 1977.

[75] J. Andersson, G. M. Edelman, G. Möller, and O. Sjöberg. Activation of B lymphocytes by locally concentrated concanavalin A. *European Journal of Immunology*, 2(3):233–235, 1972.

[76] G. R. Gunther, J. L. Wang, I. Yahara, B. A. Cunningham, and G. M. Edelman. Concanavalin A derivatives with altered biological activities. *Proceedings of the National Academy of Sciences of the United States of America*, 70(4):1012–1016, 1973.

[77] M. Leist and A. Wende. A novel mechanism of murine hepatocyte death inducible by concanavalin A. *Journal of Hepatology*, 25:948–959, 1996.

[78] R. Ballerstadt, C. Evans, R. McNichols, and A. Gowda. Concanavalin A for in vivo glucose sensing: A biotoxicity review. *Biosensors and Bioelectronics*, 22(2):275–284, 2006.

[79] N. S. Pujar and A. L. Zydney. Electrostatic and electrokinetic interactions during protein-transport through narrow pore membranes. *Industrial & Engineering Chemistry Research*, 33(10):2473–2482, 1994.

[80] M. Deshpande and L. Saggere. An analytical model and working equations for static deflections of a circular multi-layered diaphragm-type piezoelectric actuator. *Sensors and Actuators A: Physical*, 136(2):673–689, 2007.

[81] S. Uchida. The pulsating viscous flow superposed on the steady laminar motion of incompressible fluid in a circular pipe. *Zeitschrift für Angewandte Mathematik und Physik*, 7(5):403–422, 1956.

[82] C. Barnes. Diffusion through a membrane. *Journal of General and Applied Physics*, 5(1):4–8, 1934.

[83] J. Robinson and R. H. Stokes. *Electrolyte Solution*. Butterworths, 2nd edition, 1959.

[84] R. Collander. Über die durchlässigkeit der kupferferrozyanidniederschlagmembran für nichtelektrolyte. *Kolloid-Beihelfe*, 19:72–106, 1924.

[85] E. Manegold. Die dialyse durch kollodiummembranen und der zusammenhang zwischen dialyse, diffusion und membranstruktur. *Kolloid Zeitschrift*, 49:372–395, 1929.

[86] J. R. Pappenheimer. Passage of molecules through capillary walls. *Physiological Reviews*, 33:387–423, 1953.

[87] E. L. Cussler. *Diffusion. Mass Transfer in Fluid Systems*. Cambridge University Press, 3rd edition, 2007.

[88] P. Muralt. PZT thin films for microsensors and actuators: Where do we stand? *IEEE Transactions on Ultrasonics Ferroelectrics and Frequency Control*, 47(4):903–915, 2000.

[89] E. Hong, S. Trolier-McKinstry, R. L. Smith, S. V. Krishnaswamy, and C. B. Freidhoff. Design of MEMS PZT circular diaphragm actuators to generate large deflections. *Journal of Microelectromechanical Systems*, 15(4):832–839, 2006.

[90] G. A. Brunner, M. Ellmerer, G. Sendlhofer, A. Wutte, Z. Trajanoski, L. Schaupp, F. Quehenberger, P. Wach, G. J. Krejs, and T. R. Pieber. Validation of home blood glucose meters with respect to clinical and analytical approaches. *Diabetes Care*, 21(4):585–590, 1998.

[91] J. J. Kim and K. Park. Glucose-binding property of pegylated concanavalin A. *Pharmaceutical Research*, 18(6):794–799, 2001.

[92] H. Uehara, M. Kakiage, M. Sekiya, D. Sakuma, T. Yamonobe, N. Takano, A. Barraud, E. Meurville, and Ryser P. Size-selective diffusion in nanoporous but flexible membranes for glucose sensors. *ACS Nano*, 3(4):924–932, 2009.

[93] J. R. Pappenheimer, E. M. Renkin, and L. M. Borrero. Filtration, diffusion and molecular sieving through peripheral capillary membranes; a contribution to the pore theory of capillary permeability. *American Journal of Physiology*, 167:13–46, 1951.

[94] A. Bouchoux, H. Roux-de Balmann, and F. Lutin. Nanofiltration of glucose and sodium lactate solutions: Variations of retention between single- and mixed-solute solutions. *Journal of Membrane Science*, 258(1–2):123–132, 2005.

[95] L. Leoni, A. Boiarski, and T. A. Desai. Characterization of nanoporous membranes for immunoisolation: Diffusion properties and tissue effects. *Biomedical Microdevices*, 4(2):131–139, 2002.

[96] J. L. Wang, B. A. Cunningham, and G. M. Edelman. Unusual fragments in the subunit structure of concanavalin A. *Proceedings of the National Academy of Sciences of the United States of America*, 68(6):1130–1134, 1971.

[97] S. Tierney, B. Falch, D. Hjelme, and B. Stokke. Determination of glucose levels using a functionalized hydrogel optical fiber biosensor: Toward continuous monitoring of blood glucose in vivo. *Analytical Chemistry*, 81(9):3630–3636, 2009.

Curriculum Vitae

Christophe Boss
Les Chênes 17
1029 Villars-Ste-Croix
+41 78 738 50 23
christophe.boss@gmail.com

27 years old
Swiss citizen
Single

EDUCATION

2007–2012 **PhD in Microengineering**
Ecole Polytechnique Fédérale de Lausanne
Field of Biomedical Engineering
Development of a viscosity-dependent affinity sensor for continuous monitoring of glucose in biological fluids

2002–2007 **Master in Physics**
Ecole Polytechnique Fédérale de Lausanne
Orientation in Biophysics

PROFESSIONAL EXPERIENCES

2007–2012 **Research Assistant**
Laboratory of Microengineering for Manufacturing (EPFL)
Publication of 4 scientific articles as main author
Presentation of the research work at various international conferences
Direction of student projects on Master level

2010–2012 **Industrial collaboration with Baxter Healthcare**
Project of the Swiss Commission for Technology and Innovation (CTI) involving Baxter, the Univertiy Hospital of Lausanne (CHUV) and EPFL
Development of calcium, glucose and pH sensors for patient monitoring in the intensive care units of hospitals (patented technology)

RESEARCH PROJECT

2006–2007 **Master thesis in Biomechanics – Laboratory of Hemodynamics and Cardiovascular Technology (EPFL)**
Histology, imaging, mechanical tests and simulation of the arterial wall
Work published in *Journal of Biorheology*

CONTINUING EDUCATION

2008–2009 **Management of Technology and Innovation**, EPFL Technology Transfer Office

2008–2009 **Accounting and Finance**, EPFL Career Center

LANGUAGES

French	Mother tongue
English	Fluent
German	High school level

COMPUTER SKILLS

Office (MS Office), Data analysis (Origin), Computation (Mathematica, MATLAB), Design (SolidWorks), Instrumentation (LabVIEW)

INTERESTS AND ACTIVITIES

Medical technologies and biotechnologies (Member of the Swiss Society for Biomedical Engineering)
My hobbies are tennis, volleyball, skiing, and running

PUBLICATIONS

Peer-reviewed journals

C. Boss, E. Meurville, J. M. Sallese, and P. Ryser. Size-selective diffusion in nanoporous alumina membranes for a glucose affinity sensor, *Journal of Membrane Science*, doi:10.1016/j.memsci.2012.02.004, 2012.

C. Boss, E. Meurville, J. M. Sallese, and P. Ryser. A viscosity-dependent affinity sensor for continuous monitoring of glucose in biological fluids. *Biosensors and Bioelectronics*, 30(1):223–228, 2011.

S. Roy, **C. Boss**, R. Rezakhaniha, and N. Stergiopulos. Experimental characterization of the distribution of collagen fiber recruitment. *Journal of Biorheology*, 24(2):84–93, 2010.

Conference proceedings

C. Boss, E. Meurville, P. Ryser, F. Schmitt, L. Juillerat-Jeanneret, P. Dosil-Rosende, and D. De Souza. Multi-analyte detection for biological fluids: Towards continuous monitoring of glucose, ionized calcium and pH using a viscometric affinity biosensor. In *Proceedings of the International Conference on Biomedical Electronics and Devices*, pages 295–298, SciTePress, 2011.

C. Boss, E. Meurville, J. M. Sallese, and P. Ryser. Novel chemico-mechanical approach towards long-term implantable glucose sensing. In *Proceedings of the Eurosensors XXIII conference*, *Procedia Chemistry*, 1(1):313–316, 2009.